8-8-2007

Characterization of Oligosaccharides and Nanoparticles by MALDI-TOF Mass Spectrometry

Bing Guan
University of New Orleans

Characterization of Oligosaccharides and Nanoparticles by MALDI-TOF Mass Spectrometry

A Dissertation

Submitted to the Graduate Faculty of the
University of New Orleans
In partial fulfillment of the
Requirements for the degree of

Doctor of Philosophy
in
The Department of Chemistry

by

Bing Guan

B. S., Nanjing University, 1994
M. S., Institute of Chemistry, Chinese Academy of Sciences, 1998
M. S., Loyola University Chicago, 2001

August, 2007

ACKNOWLEDGEMENTS

I would like to express my greatest gratitude and appreciation to the following people for their supports extended to me during the pursuit of this dissertation.

My gratitude must go first to my advisor: Dr. Richard B. Cole, for all his support, guidance and advices. During the past five years, I really learned a lot from him. He's always encouraged me to hang in there when I got upset. Thanks very much for his deep understanding and huge support when I changed research projects after coming back after Hurricane Katrina. Thanks for his effort to improve my writing skills and presentation skills.

I would like to thank my committee members, Dr. Zeev Rosenzweig, Dr. Matthew A. Tarr and Dr. Guijun Wang, for their valuable advices and suggestions.

I would also like to thank Dr. Jiye Fang and Dr. Yang Cai for their initiative ideas that result in fruitful collaborations.

I am also extremely grateful for Columbia University Medical School. Thanks for accepting me as a visiting student during Hurricane Katrina. I really learned a lot from Dr. Wenzhu Zhang at the Institute of Cancer Genetics and had a wonderful time in New York City.

I can not put into words how much I appreciate my family. I would like to thank my parents for always believing in me. I would like to thank my parents-in-law for their greatest sacrifice and support. They can stop worrying about me now because I am finally finished. At last, I would like to thank my wife, Bing Leng, for giving me a reason to complete this venture. Her love, friendship and patience through this endeavor were unparalleled. This is also to my lovely daughter -- Rachel.

TABLE OF CONTENTS

LIST OF TABLES

LIST OF FIGURES

ABSTRACT

The possibilities of differentiating linkage positions and anomeric configurations of small oligosaccharides by negative ion mode MALDI using anion attachment followed by PSD are investigated. By careful initial adjustment of the focusing mirror ratios allowing acquisition of the peaks of interest within the same PSD segment, it is possible to obtain highly reproducible relative ion abundances. Discrimination of different linkage types is achieved by analysis of structurally-informative diagnostic peaks offered by PSD spectra of chloride adducts of oligosaccharides, whereas the relative peak intensities of selected diagnostic fragment pairs make differentiation of anomeric configuration possible. F^- and Ac^- cannot form anionic adducts with the oligosaccharides in significant yields. However, Br^-, I^- and NO_3^- anionic adducts consistently appear in higher abundances relative to $[M - H]^-$, just like Cl^-. Mildly acidic saccharides form both deprotonated molecules and anionic adducts, making it possible to simultaneously detect neutral and acidic oligosaccharides via anion attachment. PSD of $[oligosaccharide + Cl]^-$ yields structurally-informative fragment ions that retain the charge on the sugar molecule rather than solely forming Cl^-, whereas PSD of Br^-, I^- and NO_3^- adducts of oligosaccharides yield the respective anions as the main product ions without offering structural information concerning the sugar. PSD of the chloride adduct of saccharides containing 1-2 linkages also yields chlorine-containing fragment ions.

MALDI-TOF-MS and LDI-TOF-MS are shown to be useful for characterization of ultra-small titania nanoparticles. Peak maxima in MALDI-TOF mass spectra are found to correlate with nanoparticle size. The size distributions of TiO_2 nanoparticles, obtained from MALDI- and LDI-TOF-MS are in good agreement with parallel TEM observations. PSD analysis of inorganic

nanomaterials is performed and valuable information about the structure of analytes has been obtained.

A group of inorganic nitrate and perchlorate salts of forensic and health interest are investigated by LDI- and MALDI-TOF MS. In each case, a series of characteristic cluster ions are predominant in the negative-ion mode. The number and identity of metal atoms and anions in the recorded cluster ions can be positively identified by their m/z values, distinctive isotopic patterns and characteristic PSD fragmentation patterns.

Oligosaccharides, Nanoparticles, Mass Spectrometry, MALDI-TOF, Post-Source Decay

INRODUCTION

Almost a century ago, J. J. Thompson won the Nobel Prize for his pioneering research of mass spectrometry. The 2002 Nobel Prize for Chemistry was awarded to Koichi Tanaka and John Fenn for their development of "soft" ionization methods, i.e., matrix-assisted laser desorption/ionization (MALDI)[1, 2] and electrospray (ES)[3, 4], which allow detection and characterization of intact analytes, especially large nonvolatile and thermally-labile molecules. Mass spectrometry has become an interdisciplinary research methodology, impacting virtually every area of sciences, from physics to chemistry and biology, from materials research to environmental study and forensic analysis, from genomics to proteomics and glycomics projects.

Mass spectrometers are usually categorized by the types of ionization sources and mass analyzers employed. Mass spectrometers based on different ionization methods and analyzers often provide complementary information. The selection of appropriate ionization methods and mass analyzers is essential to a particular project.

Successful ionization of analytes is crucial for mass spectrometry. Ionizing large nonvolatile and thermally-labile molecules has been challenging for years until the successful development of matrix-assisted laser desorption/ionization (MALDI)[1, 2, 5, 6] and electrospray (ES)[3, 4].

In contrast to the extensive fragmentations commonly occurring in LDMS, it was found that the addition of matrixes to nonvolatile and thermally-labile samples increased the production of intact molecular ions. Developed almost simultaneously by Karas and Hillenkamp, and Tanaka in late 1980s[1, 2, 5, 6], MALDI revolutionized mass spectrometry since then. Tanaka and co-workers[1, 2] demonstrated the detection of lysozyme (MW 14,306) and carboxypeptidase-A

(m/z 34,529) molecular ions using inorganic matrixes (ultra fine cobalt powder in glycerol) to absorb the energy from a N_2 laser (λ = 337 nm). At about the same time, Karas and Hillenkamp, on the other hand, introduced organic matrixes for the analysis of large biomolecules using a Nd:YAG (neodymium-yttrium-garnet) laser (λ = 355 nm or λ = 266 nm)[6, 7]. Encouraged by the observation of $[M+H]^+$ ions of both strongly UV absorbing tryptophan and weakly UV absorbing alanine at laser powers well below that required to ionize alanine alone when a mixture of both amino acids was analyzed[7], use of highly UV absorbing nicotinic acid enabled successful detection of intact $[M+H]^+$ ions of bovine albumin (MW 67,000) by time-of-fight mass spectrometry (TOF-MS)[6]. After their milestone work, organic matrices quickly gained popularity and were more widely used in MALDI-MS analysis for a variety of large molecules such as nucleotides, peptides and proteins, carbohydrates, and synthetic polymers. Although Karas and Hillenkamp are generally recognized as the originators of MALDI, Tanaka won the Nobel Prize for his role in the development of MALDI.

In spite of the huge success and wide range applications of MALDI-MS, fundamental questions regarding mechanistic aspects have not all been answered[8-11]. One thing that is generally agreed is that matrix and sample preparation play key roles in the process[12, 13]. A high excess of matrix to sample is important, since a major role of the matrix in MALDI is the absorption of the UV radiation[14] which causes rapid localized heating of the matrix and analyte, and leads to rapid evaporation of the mixture into the gas phase. Additionally, the large excess of matrix effectively separates analyte molecules from one another spatially, reducing association between analyte molecules. The majority of the laser energy is absorbed by the matrix, leaving the analyte intact. The matrix also plays an important role in the ionization process although details of the ionization process in MALDI are still under debate. A number of mechanisms for

MALDI ion formation have been proposed[12, 13, 15], and it is generally accepted that the ionization process in MALDI is not a single one, but a collection of processes[8, 16, 17]. The immediate consequence is that the choice of matrix is still heavily analyte and sample preparation protocol dependent, since there is no universal matrix that works for all MALDI analyses.

Ion formation can be divided into two main categories, primary ion formation and secondary ion formation[8]. Preformed ions (ions in the condensed phase) and those ions produced during the initial desorption event are covered by primary ionization processes while all other ions formed after primary ionization processes are covered by secondary ion formation. Primary ionization mechanisms generally consider the formation of matrix-derived species, whereas secondary mechanisms generally correspond to the formation of analyte ions that are not directly generated by primary processes.

The most commonly observed types of ions in the positive mode MALDI experiments are: protonated pseudo-molecular ions, cationized pseudo-molecular ions and radical cations. Often singly-charged molecular ions are generated in the MALDI process without extensive fragmentation, which greatly facilitates the mass spectrometric molecular weight assignment of intact molecules.

Coulomb energy is considerably reduced by dielectric screening provided by residual solvent, matrix, or polar parts of large molecules. Multiphoton ionization mechanisms are also responsible for formation of matrix ions[18]. After laser excitation, a matrix radical cation is formed:

$$M + n(h\nu) \rightarrow M^{+\cdot} + e^{-}$$

Matrix ions can also be produced during collisions with electronically excited matrix molecules[5]:

$$M^{*} + M \rightarrow MH^{+} + (M - H)^{-}$$

Since the plume formed during desorption is dense, many molecule-molecule and ion-molecule collisions occur[18-20]. The analyte ions can be formed through gas-phase proton transfer reaction[21].

$$MH^+ + A \rightarrow M + AH^+$$

In the early days of mass spectrometry, magnetic fields were used to separate ions according to their mass-to-charge ratios until techniques based on time of flight were developed in the 1940s[22, 23]. The pulsed nature of ion generation in MALDI favors coupling with a time-of-flight mass analyzer[24, 25] which is capable of recording complete mass spectra for every laser shot.

TOF is considered to be the fastest MS analyzer with the theoretically unlimited mass/charge range and ion transmission approaching 100% (almost all ions generated in the source can reach the detector). These features make it the best choice for the detection of some very large singly-charged MALDI ions, which may be challenging for other mass analyzers.

In MALDI-TOF, the m/z of an ion is determined by measuring the flight time of the ion through a field free tube having a fixed length under high vacuum. The ions in the MALDI source are accelerated to the same kinetic energy before they enter into the flight tube, thus ions with different m/z will have different velocities which are proportional to their $(m/z)^{-1/2}$. So ions with smaller m/z will travel at a higher velocities and reach the detector earlier, and ions with larger m/z will move more slowly and reach the detector later.

However, the ions leaving the MALDI source and entering the TOF analyzer under continuous extraction mode do not have exactly the same kinetic energy because of the initial kinetic energy distribution. To compensate for the initial kinetic energy difference, a delayed pulse[26] for acceleration is used to enable the ions to first form in the absence of an electric field,

and disperse in the source region since their position in the ion source is correlated with their initial velocity. Then after the extraction field is applied, initially slower ions experience more from the extraction field and gain slightly higher energy from the accelerating field than initially faster ions. The delay time can be fine tuned together with the extraction field so slow and fast ions of the same mass reach the detector plane at the same time, thus improving mass resolution. This is referred to as "velocity focusing" through delayed extraction.

Another approach to improve mass resolution in MALDI-TOF MS is to use a reflectron[27], a device in which ions pass through an ion mirror and their flight direction is reversed. For ions of the same m/z, the reflectron allows ions with greater kinetic energies to penetrate deeper into the electric field of the ion mirror than ions with smaller kinetic energies. The ions that penetrate deeper will take longer to return to the reflectron detector while those penetrating lower take a shorter time to fly back. In this case, the ions of the same m/z will arrive at the detector at about the same time. Thus the reflectron effectively decreases the spread in the ion flight times due to an initial kinetic energy spread. The electrostatic mirror also increases the flight path length of the mass spectrometer, thus providing a focusing effect. Therefore, the introduction of reflectron greatly improves the mass resolution of the TOF mass spectrometer.

Although not commonly used for MS/MS experiments due to the limited precursor-ion selectivity, post-source decay (PSD)[28, 29] can provide valuable structural information for the selected precursor ions. At elevated laser intensities, some molecular ions decompose into PSD fragment ions in the field-free flight tube of a TOF mass analyzer after they leave the ion source (the post-source decay process). The introduction of the reflectron facilitates the analysis of PSD of metastable precursor ions and the reflectron acts as an energy analyzer for the product ions. When metastable precursor ions decompose in the field-free flight tube, the product ions will

maintain the same velocity as the precursor ions, but only portions of the kinetic energies of the precursor ions because of the mass loss during fragmentation. One problem frequently encountered in PSD studies is that not all product ions can be focused simultaneously onto the reflectron detector in a linear reflectron, and only a portion of product ions with a lower energy than that of the precursor ion can be recorded in a PSD segment. Fragment ions with even lower energy have to be focused by lowering the voltage applied to the mirror sequentially. Afterwards, all the PSD segments are stitched together to generate the full PSD mass spectrum. A TOF mass spectrometer equipped with non-linear "curved-field"[30] reflectron allows the acquisition of the full PSD spectrum of a precursor ion all at once without the need to step down the mirror ratios; however, sensitivity and mass resolution are sacrificed.

Sample preparation is critical to a successful MALDI analysis. MALDI involves mixing the analyte of interest with a strongly UV-absorbing compound, depositing the mixture onto the surface of a sample plate and allowing it to dry before inserting it into the mass spectrometer. Typical matrix compounds used in MALDI experiments are 2,5-dihydroxybenzoic acid (DHB), 3,5-dimethoxy-4-hydroxy-trans-cinnamic acid (sinapic or sinapinic acid), and α-cyano-4-hydroxy-trans-cinnamic acid (α-CHCA). The "dried droplet"[6, 31] method and the "thin film"[32, 33] method are the two most commonly used MALDI sample preparation techniques. Gold coated or stainless steel plates are generally used as solid substrates in MALDI sample preparation while other types of substrates, such as nylon[34], poly-(vinylidine difluoride)[35], nitrocellulose[36, 37] and polyethylene[38], were also explored.

Ionic adducts are noteworthy in MALDI mass spectrometry of the positive-ion mode as well as negative-ion mode. Compared to extensive studies on cationic adducts, the formation of anionic adducts have not been extensively investigated. The first objective of this work is to

develop a novel MALDI linear-field reflectron TOF approach so that selected PSD diagnostic fragment ions could be focused within the same acquisition segment where ionization conditions are constant and stable relative diagnostic peak intensities could be obtained; the second objective is to develop an anionic attachment PSD approach for differentiation of structurally similar disaccharides and oligosaccharides, i.e., those that differ only by linkage type and anomeric configuration; the third objective is to explore the possibility of using mass spectrometric method to characterize synthesized ultra small titanium oxides nanoparticles; lastly, the final objective of this study is to characterize inorganic nitrate and perchlorate compounds by negative MALDI-TOF MS and PSD.

References:

1. Tanaka, K.; Waki, H.; Ido, Y.; Akita, S.; Yoshida, Y.; Yoshida, T., Protein and polymer analyses up to <I>m/z</I> 100 000 by laser ionization time-of-flight mass spectrometry. *Rapid Communications in Mass Spectrometry* **1988,** 2, (8), 151-153.
2. Tanaka, K.; Ido, Y.; Akita, S.; Yoshida, Y.; Yoshida, T. In the Second Japan-China Joint Symposium on Mass Spectrometry (abstract), Osaka, Japan, Sept. 15-18, 1987; Osaka, Japan, 1987.
3. Yamashita, M.; Fenn, J. B., Electrospray Ion-Source - Another Variation on the Free-Jet Theme. *Journal of Physical Chemistry* **1984,** 88, (20), 4451-4459.
4. Yamashita, M.; Fenn, J. B., Negative-Ion Production with the Electrospray Ion-Source. *Journal of Physical Chemistry* **1984,** 88, (20), 4671-4675.
5. Karas, M.; Bachmann, D.; Bahr, U.; Hillenkamp, F., Matrix-Assisted Ultraviolet-Laser Desorption of Nonvolatile Compounds. *International Journal of Mass Spectrometry and Ion Processes* **1987,** 78, 53-68.
6. Karas, M.; Hillenkamp, F., Laser Desorption Ionization of Proteins with Molecular Masses Exceeding 10000 Daltons. *Analytical Chemistry* **1988,** 60, (20), 2299-2301.
7. Karas, M.; Bachmann, D.; Hillenkamp, F., Influence of the Wavelength in High-Irradiance Ultraviolet-Laser Desorption Mass-Spectrometry of Organic-Molecules. *Analytical Chemistry* **1985,** 57, (14), 2935-2939.
8. Zenobi, R.; Knochenmuss, R., Ion formation in MALDI mass spectrometry. *Mass Spectrometry Reviews* **1998,** 17, (5), 337-366.

9. Knochenmuss, R.; Zenobi, R., MALDI ionization: The role of in-plume processes. *Chemical Reviews* **2003,** 103, (2), 441-452.
10. Karas, M.; Gluckmann, M.; Schafer, J., Ionization in matrix-assisted laser desorption/ionization: singly charged molecular ions are the lucky survivors. *Journal of Mass Spectrometry* **2000,** 35, (1), 1-12.
11. Karas, M.; Kruger, R., Ion formation in MALDI: The cluster ionization mechanism. *Chemical Reviews* **2003,** 103, (2), 427-439.
12. Vertes, A.; Gijbels, R.; Levine, R. D., Homogeneous Bottleneck Model of Matrix-Assisted Ultraviolet-Laser Desorption of Large Molecules. *Rapid Communications in Mass Spectrometry* **1990,** 4, (6), 228-233.
13. Vertes, A.; Irinyi, G.; Gijbels, R., Hydrodynamic Model of Matrix-Assisted Laser-Desorption Mass-Spectrometry. *Analytical Chemistry* **1993,** 65, (17), 2389-2393.
14. Allwood, D. A.; Dreyfus, R. W.; Perera, I. K.; Dyer, P. E., UV optical absorption of matrices used for matrix-assisted laser desorption/ionization. *Rapid Communications in Mass Spectrometry* **1996,** 10, (13), 1575-1578.
15. Zare, R. N.; Levine, R. D., Mechanism for Bond-Selective Processes in Laser Desorption. *Chemical Physics Letters* **1987,** 136, (6), 593-599.
16. Spengler, B.; Karas, M.; Bahr, U.; Hillenkamp, F., Excimer Laser Desorption Mass-Spectrometry of Biomolecules at 248 and 193 Nm. *Journal of Physical Chemistry* **1987,** 91, (26), 6502-6506.
17. Allwood, D. A.; Dyer, P. E.; Dreyfus, R. W., Ionization modelling of matrix molecules in ultraviolet matrix-assisted laser desorption/ionization. *Rapid Communications in Mass Spectrometry* **1997,** 11, (5), 499-503.
18. Ehring, H.; Karas, M.; Hillenkamp, F., Role of Photoionization and Photochemistry in Ionization Processes of Organic-Molecules and Relevance for Matrix-Assisted Laser Desorption Ionization Mass-Spectrometry. *Organic Mass Spectrometry* **1992,** 27, (4), 472-480.
19. Harrison, A. G., The gas-phase basicities and proton affinities of amino acids and peptides. *Mass Spectrometry Reviews* **1997,** 16, (4), 201-217.
20. Sunner, J., Ionization in Liquid Secondary-Ion Mass-Spectrometry (Lsims). *Organic Mass Spectrometry* **1993,** 28, (8), 805-823.
21. Scott, C. T. J.; Kosmidis, C.; Jia, W. J.; Ledingham, K. W. D.; Singhal, R. P., Formation of Atomic-Hydrogen in Matrix-Assisted Laser-Desorption Ionization. *Rapid Communications in Mass Spectrometry* **1994,** 8, (10), 829-832.
22. Cameron, A. E.; Eggers, D. F., Jr., *Review of Scientific Instruments* **1948,** 18, (9), 605-607.
23. Stephens, W. E. US Patent 2,612,607, 1952.
24. Hillenkamp, F.; Unsold, E.; Kaufmann, R.; Nitsche, R., High-Sensitivity Laser Microprobe Mass Analyzer. *Applied Physics* **1975,** 8, (4), 341-348.
25. Vanbreemen, R. B.; Snow, M.; Cotter, R. J., Time-Resolved Laser Desorption Mass-Spectrometry .1. Desorption of Preformed Ions. *International Journal of Mass Spectrometry and Ion Processes* **1983,** 49, (1), 35-50.
26. Wiley, W. C.; McLaren, I. H., *Review of Scientific Instruments* **1955,** 26, 1150-1157.
27. Mamyrin, B. A.; Karataev, V. I.; Shmikk, D. V.; Zagulin, V. A., *Sov. Phys. JETP* **1973,** 37, 45.

28. Spengler, B.; Kirsch, D.; Kaufmann, R., Metastable Decay of Peptides and Proteins in Matrix-Assisted Laser-Desorption Mass-Spectrometry. *Rapid Communications in Mass Spectrometry* **1991,** 5, (4), 198-202.
29. Spengler, B.; Kirsch, D.; Kaufmann, R.; Jaeger, E., Peptide Sequencing by Matrix-Assisted Laser-Desorption Mass-Spectrometry. *Rapid Communications in Mass Spectrometry* **1992,** 6, (2), 105-108.
30. Fabris, D.; Vestling, M. M.; Cordero, M. M.; Doroshenko, V. M.; Cotter, R. J.; Fenselau, C., Sequencing Electroblotted Proteins by Tandem Mass-Spectrometry. *Rapid Communications in Mass Spectrometry* **1995,** 9, (11), 1051-1055.
31. Fan, X.; Beavis, R. C., Growing Protein-Doped Sinapic Acid Crystals for Laser-Desorption - an Alternative Preparation Method for Difficult Samples. *Organic Mass Spectrometry* **1993,** 28, (12), 1424-1429.
32. Xiang, F.; Beavis, R. C., A Method to Increase Contaminant Tolerance in Protein Matrix-Assisted Laser-Desorption Ionization by the Fabrication of Thin Protein-Doped Polycrystalline Films. *Rapid Communications in Mass Spectrometry* **1994,** 8, (2), 199-204.
33. Vorm, O.; Roepstorff, P.; Mann, M., Improved Resolution and Very High-Sensitivity in Maldi Tof of Matrix Surfaces Made by Fast Evaporation. *Analytical Chemistry* **1994,** 66, (19), 3281-3287.
34. Zaluzec, E. J.; Gage, D. A.; Allison, J.; Watson, J. T., Direct Matrix-Assisted Laser-Desorption Ionization Mass-Spectrometric Analysis of Proteins Immobilized on Nylon-Based Membranes. *Journal of the American Society for Mass Spectrometry* **1994,** 5, (4), 230-237.
35. Vestling, M. M.; Fenselau, C., Surfaces for interfacing protein gel electrophoresis directly with mass spectrometry. *Mass Spectrometry Reviews* **1995,** 14, (3), 169-178.
36. Preston, L. M.; Murray, K. K.; Russell, D. H., Reproducibility and Quantitation of Matrix-Assisted Laser-Desorption Ionization Mass-Spectrometry - Effects of Nitrocellulose on Peptide Ion Yields. *Biological Mass Spectrometry* **1993,** 22, (9), 544-550.
37. Liu, Y. H.; Bai, J.; Liang, X. O.; Lubman, D. M.; Venta, P. J., Use of a Nitrocellulose Film Substrate in Matrix-Assisted Laser Desorption/Ionization Mass-Spectrometry for DNA Mapping and Screening. *Analytical Chemistry* **1995,** 67, (19), 3482-3490.
38. Blackledge, J. A.; Alexander, A. J., Polyethylene Membrane as a Sample Support for Direct Matrix-Assisted Laser-Desorption Ionization Mass-Spectrometric Analysis of High-Mass Proteins. *Analytical Chemistry* **1995,** 67, (5), 843-848.

Chapter 1: Differentiation of Both Linkage Position and Anomeric Configuration in Underivatized Glucopyranosyl Disaccharides by Anion Attachment with Post-Source Decay in MALDI Linear-Field Reflectron TOFMS

1.1 Introduction

Understanding oligosaccharide expression patterns in cells and correlating oligosaccharide structures with their functions necessarily requires structural characterization of the relevant carbohydrates[1]. However, gaining unambiguous information for linkage positions and anomeric configurations between monosaccharide units represents a challenging aspect of structural elucidation of carbohydrates.

Matrix-assisted laser desorption/ionization time-of-flight mass spectrometry (MALDI-TOF MS) has become established as a powerful tool to analyze biological molecules such as peptides, proteins, nucleotides and lipids, as well as carbohydrates[2-4]. After ion extraction, metastable decay can take place in the first field-free region of a reflectron TOF mass spectrometer, especially at elevated laser intensities. Although not truly tandem MS, this so-called post-source decay (PSD) can provide valuable information about the structures of gas-phase ions generated by MALDI[5, 6]. The fragment ions resulting from this unimolecular decay retain only a fraction of the precursor ion's kinetic energy (proportional to fragment ion masses), and the fragment ions continue to travel at the same velocity as the precursor ion (ignoring adjustments attributable to the energy of dissociation). Portions of the mass spectrum containing fragment ions falling within a specified energy "window" can be focused and detected. Fragment ions falling within other (lower) energy "windows" are subsequently detected by stepping down the reflectron (ion mirror) voltage to match the respective kinetic energies of the charged

fragments in a sequential manner. The full composite PSD spectrum can then be reconstructed by assembling or "stitching" together the different PSD segments.

Normally, it is difficult to compare relative ion abundances in PSD spectra when these spectra are acquired in several different "stitched" segments[2], because the precursor signal intensity may change substantially in successive irradiation events owing especially to particularities of the matrix crystal. Yamagaki et al.[7-14] circumvented this problem by using a MALDI-TOF MS equipped with a curved-field reflectron that allows focused collection of all PSD fragment ions in a single spectrum under the same conditions. The curved-field reflectron thus eliminates the need to sequentially step the reflectron voltage, and the relative ion abundances in PSD spectra were found to be reliably reproducible. This reproducibility implies that even though the precursor absolute abundance may vary substantially from shot–to-shot, relative PSD fragment ion abundances do not.

When subjected to PSD fragmentation in the positive ion mode, saccharides are frequently cleaved at the glycosyl linkages. It has been found that linkage isomers of saccharides are not readily distinguished based upon the PSD spectral patterns because cross-ring cleavage ions that are more specific to providing clues concerning linkage position are often rather weak in positive mode PSD[2, 15, 16].

Negative ion MALDI-TOF MS analysis of neutral oligosaccharides has been recently gaining popularity ever since Nonami et al.[17-19] introduced a series of β-carboline compounds, e.g., harmane, norharmane and harmine, which can be used as efficient matrixes. Anion attachment represents a promising alternative to deprotonation as a means to charge neutral saccharides in negative-ion MALDI MS. Wong et al.[20] were able to charge neutral saccharides via bisulfate anion attachment using harmane as the MALDI matrix (gave strongest signal and

cleanest spectrum) along with other more conventional matrixes. Bisulfate adducts, $[M + HSO_4]^-$ along with $[M + HSO_4 - H_2O]^-$ were observed, but only $[M + HSO_4 - H_2O]^-$ gave structural information upon collision induced dissociation (CID). Cai et al.[21] found that chloride anions formed stable anionic adducts with neutral oligosaccharides using harmine as the matrix in MALDI-TOF MS and NH_4Cl as the chloride ion source. It was shown that direct decompositions of these chloride adducts produced abundant oligosaccharide fragments that offered a wealth of structural information[21].

MALDI-PSD fragmentation in the negative-ion mode has emerged as a means to study oligosaccharides, and it has shown some success for differentiation of linkage positions as well as anomeric configurations in oligosaccharides[21-27]. PSD of anionic adducts of oligosaccharides has also been performed[21, 25-27]. Cai et al.[21] observed cross-ring cleavage ions in negative MALDI-PSD of $[turanose + Cl]^-$. Yamagaki et al.[25] also observed extensive cross-ring cleavage ions produced by PSD of oligosaccharide chloride adducts employing a curved-field reflectron in negative ion MALDI-PSD, and the relative abundance difference of the $[M - C_2H_4O_2 - H_2O - HCl]^-$ ions and the $[M - C_4H_8O_4 - HCl]^-$ ions could be used to differentiate between the α- and β-configuration in the 1-4 glycosyl linkages. But they found it difficult to distinguish between the α- and β-configuration in the 1-6 glycosyl linkages, and differentiation between the α- and β-configuration in 1-3 linkages was not discussed.

Even without a curved-field reflectron mass spectrometer that allows acquisition of an entire PSD spectrum for each laser shot, we sought to maximize the potential of our MALDI linear-field reflectron TOF mass spectrometer by employing a novel approach. By manually adjusting the mirror ratios so that selected fragment ions of interest could be focused, offering relatively narrow peaks that appear within the same acquisition segment where ionization

conditions (including laser intensity) would be constant, it is possible to obtain stable relative peak intensities to allow comparison of structurally similar disaccharides. Here we demonstrate that by comparing specific relative ion abundances of PSD peaks which we have deemed to be diagnostic, the anomeric configurations of disaccharides can be differentiated. Three pairs of glucopyranosyl-glucose disaccharides were examined: gentiobiose (Glcβ1-6Glc) and isomaltose (Glcα1-6Glc), cellobiose (Glcβ1-4Glc) and maltose (Glcα1-4Glc), and laminaribiose (Glcβ1-3Glc) and nigerose (Glcα1-3Glc). These three groups of stereoisomeric pairs differ from one another only in the linkage position between the glucose rings. Within each pair, the only structural difference is the anomeric configuration at the glycosidic bond.

1.2 Experimental

Negative MALDI-TOF (Voyager Elite, Applied Biosystems, Framingham, MA) PSD experiments were performed using harmine as the matrix.

1.3 Results and Discussions

PSD of chloride adducts $[disaccharide + Cl]^-$ at m/z 377 (and 379) produces the product ions shown in Figures 1.1-1.3. Deprotonated molecules, i.e., $[disaccharide - H]^-$ at m/z 341 were consistently observed in all PSD studies of $[disaccharide + Cl]^-$, although the intensity varied substantially. Owing to the complete absence of chloride-containing product ions, it appears that upon PSD, $[disaccharide + Cl]^-$ precursors initially lose HCl, leaving $[disaccharide - H]^-$ that undergo subsequent consecutive decompositions which is consistent with our previous CID studies of electrospray (ES) generated chloride adducts of oligosaccharides[28]. Also, the peak at m/z 179, corresponding to the loss of a glucose unit, is observed for all disaccharides, which

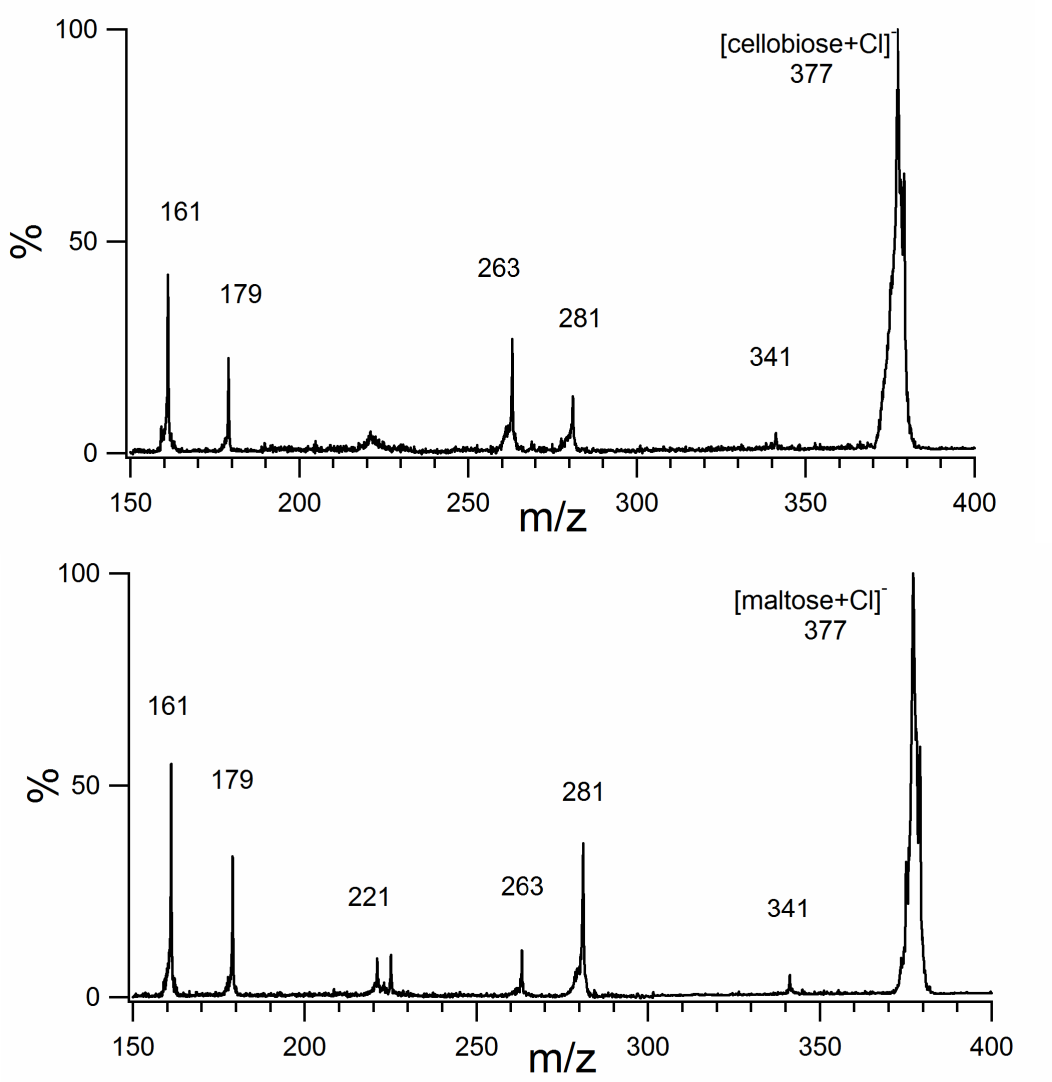

Figure 1.1. Negative ion PSD of chloride adducts of cellobiose (Glcβ1-4Glc) (top) and maltose (Glcα1-4Glc) (bottom).

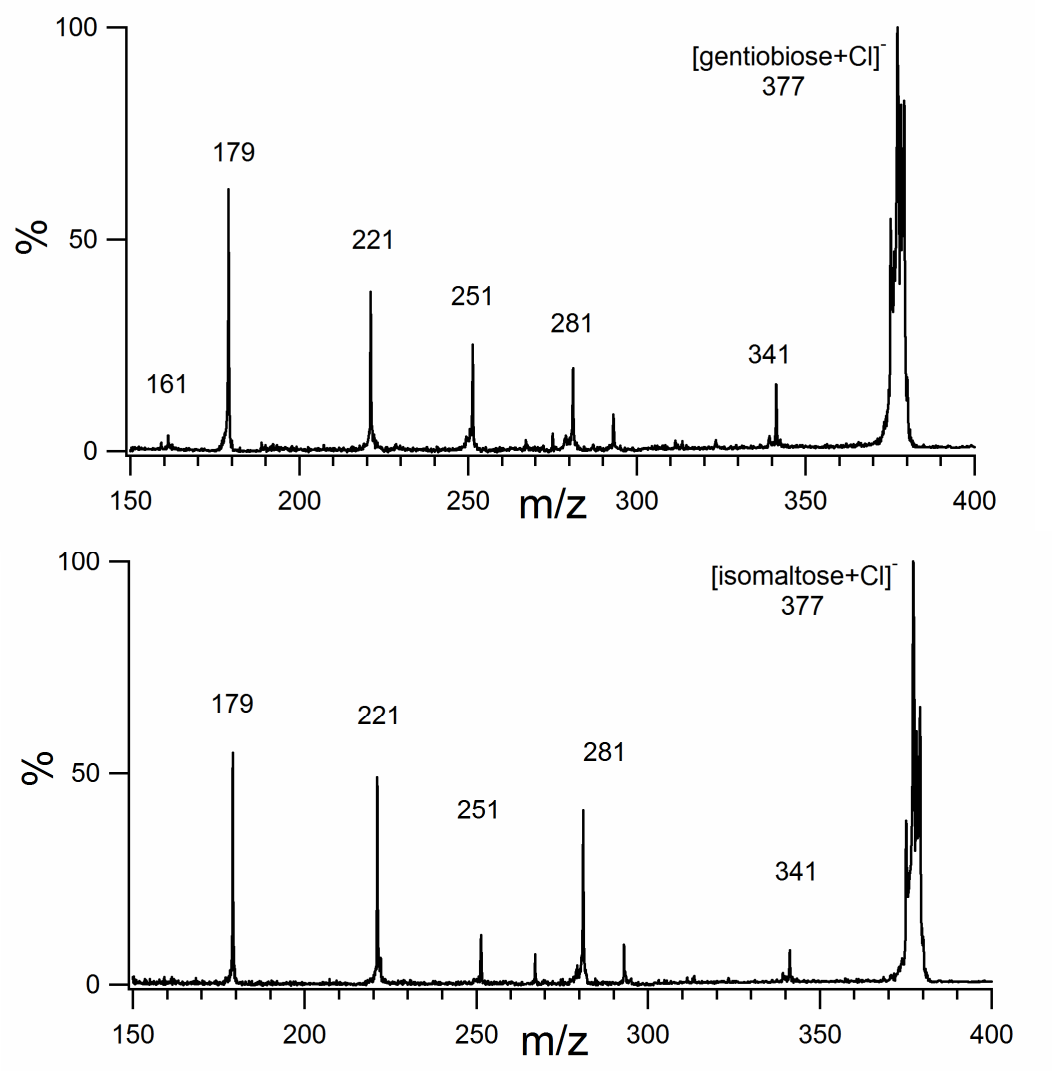

Figure 1.2. Negative ion PSD of chloride adduct of gentiobiose (Glcβ1-6Glc) (top) and isomaltose (Glcα1-6Glc) (bottom).

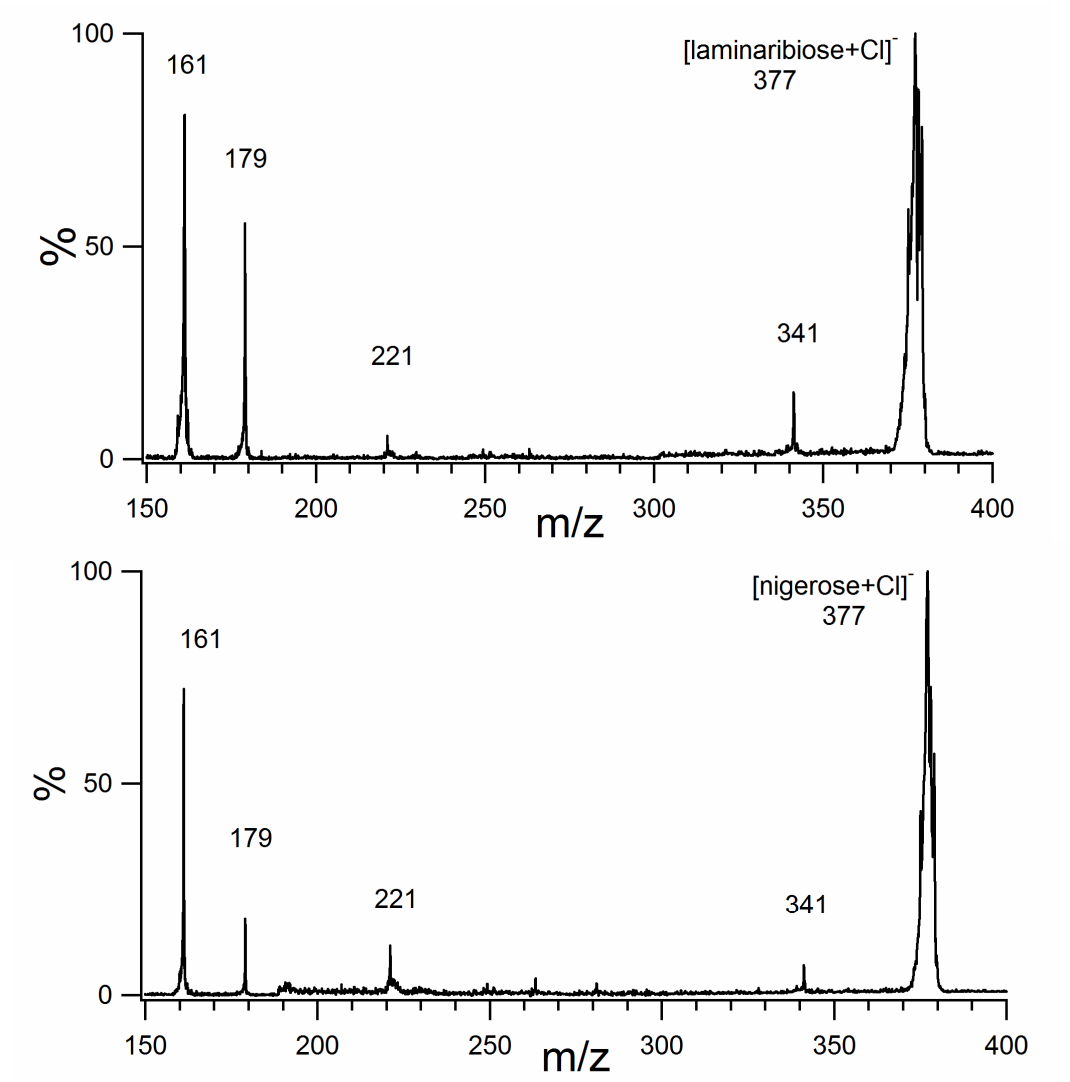

Figure 1.3. Negative ion PSD of chloride adducts of laminaribiose (Glcβ1-3Glc) (top) and nigerose (Glcα1-3Glc) (bottom).

shows great similarity to the decomposition pattern reported in a LSIMS study[29] and a FAB-MS/MS study[30], but differs somewhat from a previous FAB-MS/MS study[31].

Certain fragment ions observed in PSD spectra are found to be diagnostic indicators of the glycosidic linkage positions between adjacent monosaccharide units. It appears that negative ion PSD fragmentation patterns are mainly determined by the linkage positions between the monosaccharide rings, with only subtle differences in relative peak intensities occurring for different anomeric configurations. The appearance of product ions at m/z 161, 179, 263 and 281 with the absence of m/z 251 appears to be characteristic of the 1-4 linked disaccharides (Figure 1.1); observation of product ions at m/z 179, 221, 251, and 281 with the absence of m/z 263 appears to be characteristic of the 1-6 linked disaccharides (Figure 1.2); while observation of glycosidic bond cleavages yielding m/z 161 or 179, as well as the weak cross-ring cleavage peak at m/z 221, appears to be characteristic of the 1-3 linked disaccharides (Figure 1.3).

The negative ion PSD mass spectra of the 1-6 linked isomers (Figure 1.2) show strong peaks at m/z 179 while m/z 161 is barely detectable, which is quite different from that of 1-4 (Figure 1.1) and 1-3 (Figure 1.3) linked disaccharides where m/z 161 peaks appear in higher abundances than those of m/z 179. This distinction appears to be a potential indicator to distinguish the 1-6 linkage from the 1-4 and 1-3 linkages[29] along with other diagnostic peaks (Figures 1.1-1.3).

In our study, a clear-cut differentiation between the α- (maltose) and β-configuration (cellobiose) in 1-4 linked glucopyranosyl disaccharides can be made by simply checking whether the relative abundance ratio of m/z 263:281 is larger than unity (β isomer) or smaller than unity (α isomer) (Figures 1.1 and 1.4). Moreover, the 1-6 linked anomers which were not previously distinguished by MALDI-PSD-MS[25], can also be readily differentiated by examining whether the

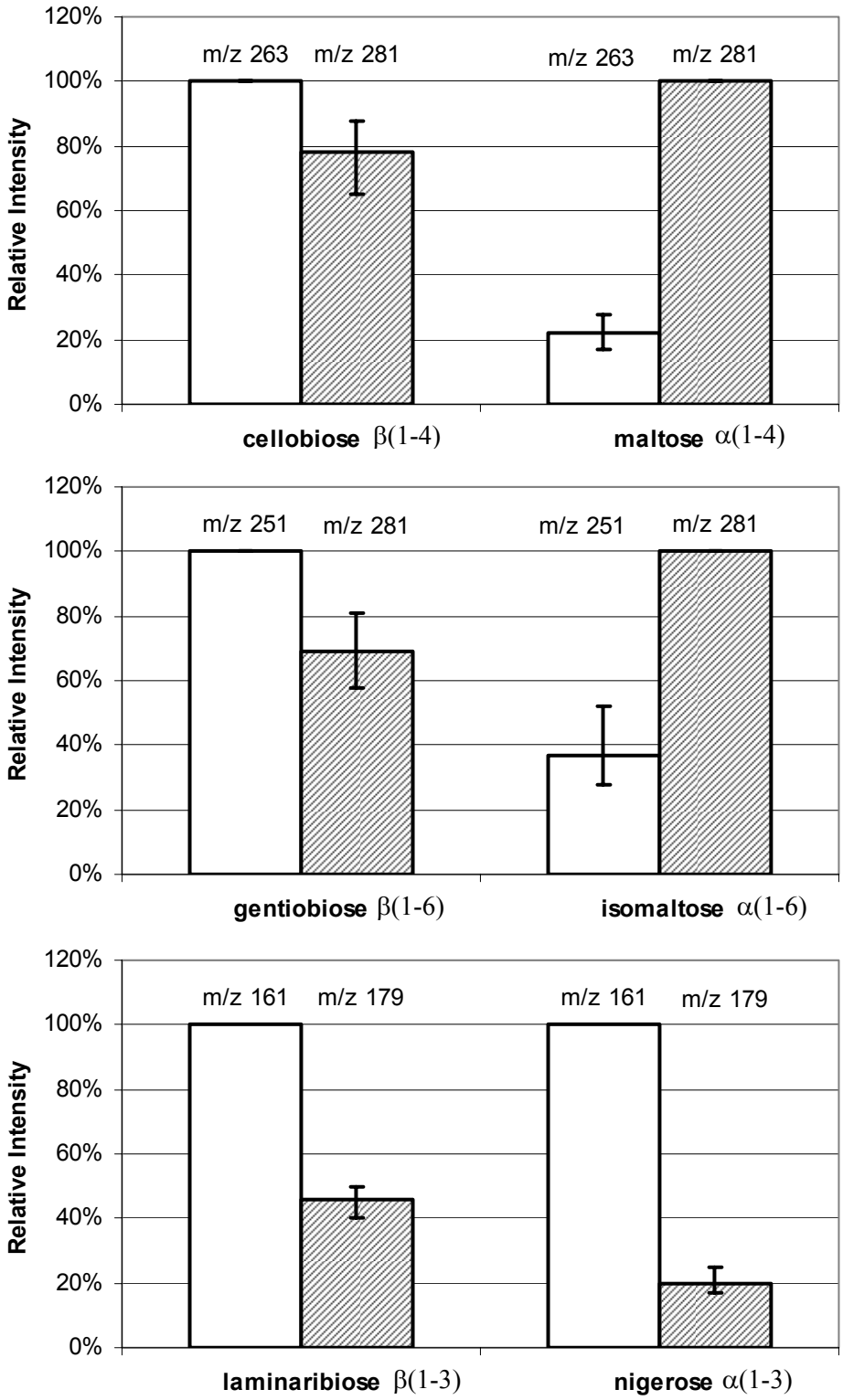

Figure 1.4. Relative peak intensities of diagnostic fragments of 1-4 (top), 1-6 (middle) and 1-3 (bottom) linked disaccharides. Each pair was acquired in the same MALDI-PSD segment in eight replicate runs.

relative abundance ratio of m/z 251:281 is larger than unity (β isomer) or smaller than unity (α isomer) to unambiguously differentiate between the α- (isomaltose) and β-configuration (gentiobiose) (Figures 1.2 and 1.4). On the other hand, for the 1-3 glycosyl linkages, the relative abundances of m/z 161:179 is consistently lower for the α isomer (nigerose) than for the β isomer (laminaribiose) (Figures 1.3 and 1.4). The fact that the m/z 161:179 ratio is larger than unity for both 1,3-linked anomers, combined with the fact that both products ions are formed as a result of glycosidic bond cleavages rather than more specific cross-ring fragmentations renders this last differentiation less obvious than the previous two anomeric pairs. Nevertheless, the relative abundances of these diagnostic peaks are still sufficiently different to permit distinction between the α- and β-configurations in the 1-3 linked disaccharides.

The reproducibility of the relative peak intensities of the above pairs of diagnostic peaks obtained within the same MALDI-PSD segment was checked in eight measurements taken under the same conditions. In each comparison, the intensity of the higher peak in each pair was normalized to 100%, then the relative intensity of the lower peak was calculated (Fig. 1.4). Because there is no overlap in the error bars obtained for any pair, the anomeric configurations can be unambiguously distinguished.

1.4 Conclusions

In conclusion, contrary to the often encountered view that relative peak intensities are not generally reliable in PSD, we demonstrate that even without a curved-field reflectron, it is possible to get rather stable relative peak intensities for mass spectral fragments whose m/z values do not widely differ. Reproducibility improves when these peaks are intentionally acquired within the same PSD segment with the laser intensity held constant, even if the target

crystals vary substantially in shape and quality. Thus, not only is it possible to differentiate linkage position by MALDI-PSD analysis of [disaccharide + Cl]$^-$ ions using negative ion PSD of chloride adducts on a linear-field reflectron MALDI-TOF MS, but it is also established that differentiating *anomeric* configurations is viable by comparing relative peak intensities of diagnostic fragments. Carbohydrates seem particularly amenable to this methodology because, often, the fragment ions serendipitously fall within a narrow m/z range. The fragmentation profiles and relative peak abundances in PSD spectra are expected to present important hints for determining the glycosidic linkage types and anomeric configurations of even more complex glycoconjugates.

1.5 References

1. Bertozzi, C. R.; Kiessling, L. L., Chemical glycobiology. *Science* **2001,** 291, (5512), 2357-2364.
2. Harvey, D. J., Matrix-assisted laser desorption/ionization mass spectrometry of carbohydrates. *Mass Spectrometry Reviews* **1999,** 18, (6), 349-450.
3. Dell, A.; Morris, H. R., Glycoprotein structure determination mass spectrometry. *Science* **2001,** 291, (5512), 2351-2356.
4. Zaia, J., Mass spectrometry of oligosaccharides. *Mass Spectrometry Reviews* **2004,** 23, (3), 161-227.
5. Spengler, B.; Kirsch, D.; Kaufmann, R., Metastable Decay of Peptides and Proteins in Matrix-Assisted Laser-Desorption Mass-Spectrometry. *Rapid Communications in Mass Spectrometry* **1991,** 5, (4), 198-202.
6. Spengler, B.; Kirsch, D.; Kaufmann, R.; Jaeger, E., Peptide Sequencing by Matrix-Assisted Laser-Desorption Mass-Spectrometry. *Rapid Communications in Mass Spectrometry* **1992,** 6, (2), 105-108.
7. Yamagaki, T.; Nakanishi, H., Distinguishing of linkage isomers of lactotetra oligosaccharides by using the relative ion intensity analysis of post-source decay fragment ions in curved-field reflectron matrix-assisted laser desorption/ionization time-of-flight mass spectrometry. *Analytical Sciences* **2001,** 17, (1), 83-87.
8. Yamagaki, T.; Nakanishi, H., Ion intensity analysis of post-source decay fragmentation in curved-field reflectron matrix-assisted laser desorption/ionization time-of-flight mass spectrometry of carbohydrates: For structural characterization of glycosylation in proteome analysis. *Proteomics* **2001,** 1, (2), 329-339.

9. Yamagaki, T.; Nakanishi, H., Post-source decay fragmentation analyses of linkage isomers of Lewis-type oligosaccharides in curved-field reflectron matrix-assisted laser desorption/ionization time-of-flight mass spectrometry: combined in-source decay/post-source decay experiments and relative ion abundance analysis. *Journal of Mass Spectrometry* **2000,** 35, (11), 1300-1307.
10. Yamagaki, T.; Nakanishi, H., Influence of acceleration voltages on relative ion intensities in the post-source decay fragmentation of isomeric cyclic oligosaccharides by matrix-assisted laser desorption/ionization time-of-flight mass spectrometry. *Rapid Communications in Mass Spectrometry* **1999,** 13, (21), 2199-2203.
11. Yamagaki, T.; Nakanishi, H., Influence of stereoisomeric glucose, galactose and mannose residues on fragmentation at their glycosidic linkages in post-source decay fragment analyses for oligosaccharides using matrix-assisted laser desorption/ionization time-of-flight mass spectrometry. *Rapid Communications in Mass Spectrometry* **1998,** 12, (16), 1069-1074.
12. Yamagaki, T.; Mitsuishi, Y.; Nakanishi, H., Influence of different glycosidic linkages on relative ion intensities in post-source decay fragmentation of a xyloglucan heptaoligosaccharide using matrix-assisted laser desorption/ionization time-of-flight mass spectrometry. *Rapid Communications in Mass Spectrometry* **1998,** 12, (6), 307-311.
13. Yamagaki, T.; Ishizuka, Y.; Kawabata, S.; Nakanishi, H., Analysis of glycosidic linkages in saccharide compounds by post-source decay fragment methods in matrix-assisted laser desorption/ionization time-of-flight mass spectroscopy. *Rapid Communications in Mass Spectrometry* **1997,** 11, (5), 527-531.
14. Yamagaki, T.; Ishizuka, Y.; Kawabata, S.; Nakanishi, H., Post-source decay fragment spectra of cyclomalto-octaose and branched cyclomalto-hexaose by matrix-assisted laser desorption/ionization time-of-flight mass spectrometry. *Rapid Communications in Mass Spectrometry* **1996,** 10, (15), 1887-1890.
15. Harvey, D. J.; Naven, T. J. P.; Kuster, B.; Bateman, R. H.; Green, M. R.; Critchley, G., Comparison of fragmentation modes for the structural determination of complex oligosaccharides ionized by matrix-assisted laser desorption/ionization mass spectrometry. *Rapid Communications in Mass Spectrometry* **1995,** 9, (15), 1556-1561.
16. Spengler, B.; Kirsch, D.; Kaufmann, R.; Lemoine, J., Structure-Analysis of Branched Oligosaccharides Using Post-Source Decay in Matrix-Assisted Laser-Desorption Ionization Mass-Spectrometry. *Organic Mass Spectrometry* **1994,** 29, (12), 782-787.
17. Nonami, H.; Fukui, S.; ErraBalsells, R., beta-carboline alkaloids as matrices for matrix-assisted ultraviolet laser desorption time-of-flight mass spectrometry of proteins and sulfated oligosaccharides: A comparative study using phenylcarbonyl compounds, carbazoles and classical matrices. *Journal of Mass Spectrometry* **1997,** 32, (3), 287-296.
18. Nonami, H.; Tanaka, K.; Fukuyama, Y.; Erra-Balsells, R., beta-carboline alkaloids as matrices for UV-matrix-assisted laser desorption/ionization time-of-flight mass spectrometry in positive and negative ion modes. Analysis of proteins of high molecular mass, and of cyclic and acyclic oligosaccharides. *Rapid Communications in Mass Spectrometry* **1998,** 12, (6), 285-296.
19. Nonami, H.; Wu, F. Y.; Thummel, R. P.; Fukuyama, Y.; Yamaoka, H.; Erra-Balsells, R., Evaluation of pyridoindoles, pyridylindoles and pyridylpyridoindoles as matrices for ultraviolet matrix- assisted laser desorption/ionization time-of-flight mass spectrometry. *Rapid Communications in Mass Spectrometry* **2001,** 15, (23), 2354-2373.

20. Wong, A. W.; Cancilla, M. T.; Voss, L. R.; Lebrilla, C. B., Anion dopant for oligosaccharides in matrix-assisted laser desorption/ionization mass spectrometry. *Analytical Chemistry* **1999,** 71, (1), 205-211.
21. Cai, Y.; Jiang, Y. J.; Cole, R. B., Anionic adducts of oligosaccharides by matrix-assisted laser desorption/ionization time-of-flight mass spectrometry. *Analytical Chemistry* **2003,** 75, (7), 1638-1644.
22. Talbo, G.; Mann, M., Aspects of the sequencing of carbohydrates and oligonucleotides by matrix-assisted laser desorption/ionization post-source decay. *Rapid Communications in Mass Spectrometry* **1996,** 10, (1), 100-103.
23. Gibson, B. W.; Engstrom, J. J.; John, C. M.; Hines, W.; Falick, A. M., Characterization of bacterial lipooligosaccharides by delayed extraction matrix-assisted laser desorption ionization time-of-flight mass spectrometry. *Journal of the American Society for Mass Spectrometry* **1997,** 8, (6), 645-658.
24. Fukuyama, Y.; Ciancia, M.; Nonami, H.; Cerezo, A. S.; Erra-Balsells, R.; Matulewicz, M. C., Matrix-assisted ultraviolet laser-desorption ionization and electrospray-ionization time-of-flight mass spectrometry of sulfated neocarrabiose oligosaccharides. *Carbohydrate Research* **2002,** 337, (17), 1553-1562.
25. Yamagaki, T.; Suzuki, H.; Tachibana, K., In-source and postsource decay in negative-ion matrix-assisted laser desorption/ionization time-of-flight mass spectrometry of neutral oligosaccharides. *Analytical Chemistry* **2005,** 77, (6), 1701-1707.
26. Yamagaki, T.; Suzuki, H.; Tachibana, K., Semiquantitative analysis of isomeric oligosaccharides by negative-ion mode UV-MALDI TOF postsource decay mass spectrometry and their fragmentation mechanism study at N-acetylhexosamine. *Journal of Mass Spectrometry* **2006,** 41, (4), 454-462.
27. Yamagaki, T.; Suzuki, H.; Tachibana, K., A comparative study of the fragmentation of neutral lactooligosaccharides in negative-ion mode by UV-MALDI-TOF and UV-MALDI ion-trap/TOF mass spectrometry. *Journal of the American Society for Mass Spectrometry* **2006,** 17, (1), 67-74.
28. Zhu, J. H.; Cole, R. B., Ranking of gas-phase acidities and chloride affinities of monosaccharides and linkage specificity in collision-induced decompositions of negative ion electrospray-generated chloride adducts of oligosaccharides. *Journal of the American Society for Mass Spectrometry* **2001,** 12, (11), 1193-1204.
29. Carroll, J. A.; Ngoka, L.; Beggs, C. G.; Lebrilla, C. B., Liquid Secondary-Ion Mass-Spectrometry Fourier-Transform Mass-Spectrometry of Oligosaccharide Anions. *Analytical Chemistry* **1993,** 65, (11), 1582-1587.
30. Dallinga, J. W.; Heerma, W., Reaction-Mechanism and Fragment Ion Structure Determination of Deprotonated Small Oligosaccharides, Studied by Negative-Ion Fast-Atom-Bombardment (Tandem) Mass-Spectrometry. *Biological Mass Spectrometry* **1991,** 20, (4), 215-231.
31. Garozzo, D.; Giuffrida, M.; Impallomeni, G.; Ballistreri, A.; Montaudo, G., Determination of Linkage Position and Identification of the Reducing End in Linear Oligosaccharides by Negative-Ion Fast Atom Bombardment Mass-Spectrometry. *Analytical Chemistry* **1990,** 62, (3), 279-286.

Chpater 2: MALDI Linear-Field rTOF Post-Source Decay Analysis of Glycosidic Linkages and Anomeric Configurations in Underivatized Oligosaccharides

2.1 Introduction

Following the advances in proteomics, there is a growing interest in the importance of glycomics, i.e., the study of the breadth of sugar forms (structure and function of glycans) in biological organisms. Carbohydrates or saccharides are the most abundant biological compounds found on earth. They are well known as energy reservoirs and structural materials in cell walls. However, it has become clear that oligosaccharides and glycoconjugates (e.g., glycoproteins and glycolipids) serve as crucial mediators for a wide variety of complex cellular events[1]. Carbohydrates also play an important role in specific molecular recognition, protein folding, stability, and pharmacokinetics due to their great structural diversity. Moreover, glycosylation is a ubiquitous form of post-translational modification to both proteins and lipids.

Gaining a clear understanding of the crucial biological roles of oligosaccharides requires complete structural characterization of carbohydrates or glycoconjugates which includes determinations of the numbers and types of monosaccharide units, ring substituents, sequences, branching, linkage positions and anomeric configurations between adjacent monosaccharide units. In most cases, merely knowing the monosaccharide sequence is inadequate, thus, unambiguous differentiation of both linkage positions and anomeric configurations represents an essential aspect of the fine stereochemical analysis of oligosaccharides.

Although permethylation is a well established method for linkage determination in oligosaccharides, the analysis involving gas chromatography-mass spectrometry (GC-MS) is labor intensive and time consuming[2]. NMR is a powerful technique which allows unambiguous

determination of the linkage positions and anomeric configurations of oligosaccharides[3]. The major disadvantages are that relatively large quantities (micromolar level) of highly purified sample and long acquisition times are required.

Mass spectrometry (MS) has emerged as an important technique for structural analysis of oligosaccharides[4], offering certain advantages such as lower sample consumption, higher sensitivity, shorter acquisition times, and less stringent sample purity requirements. Anomers and linkage isomers which have identical masses cannot be easily distinguished in mass spectrometry, but to aid in this endeavor, separation steps are often performed prior to mass spectrometric identification. Nevertheless, MS does have the capability to differentiate underivatized saccharide stereoisomers as demonstrated when coupled with several different desorption/ionization techniques such as field desorption (FD)[5, 6], laser desorption (LD)[7, 8] and fast atom bombardment (FAB)[9, 10].

FD-MS has been used primarily for molecular mass determination of the protonated molecular ion and component monosaccharide units because the glycosidic bond cleavages are usually not prominent and the cross-ring fragmentations are often minor[5, 6]. Both glycosidic bond cleavages and cross-ring fragmentations are produced in LD-MS, from which complete sequence information can be deduced, but only tentative information concerning linkage positions is provided[7, 8].

Coupled with collision-induced dissociation (CID) or metastable decay, FAB-MS has demonstrated great potential for linkage determination of oligosaccharides, although derivatization has been involved in many cases[11]. In the positive ion mode, different fragment ion abundances were obtained by CID of FAB-generated $[M + glycerol + H]^+$ precursors for a series of underivatized disaccharides[12]. But the possibility to differentiate both linkage positions

and anomeric configurations of oligosaccharides was greatly limited because the spectral differences between these positive-ion CID spectra were minor[12].

Metal cationization has been widely used in MS[13]; it has been shown that the fragments obtained in the CID spectra of mono- and di-lithiated quasi-molecular ions of disaccharides and small oligosaccharides can be used to differentiate linkage position isomers[14-16]. Cobalt complexes have also been used to differentiate the anomeric configuration of 1-3, 1-4 and 1-6 glucosyl-glucose disaccharides by measuring the kinetic energy release for the metastable decay of $[Co^{3+}(acac)_2/disaccharide]^+$ [17]. It was shown that complexes possessing α-linked disaccharides consistently displayed greater kinetic energy release values than those possessing β-linked disaccharides.

In the negative mode, FAB-MS together with CID and metastable fragmentation tends to produce more abundant ring cleavages of underivatized oligosaccharides which allows linkage position analyses[18, 19]. Assignment of anomeric configurations was also attempted for glucosyl-glucose disaccharides based on the relative CID fragment abundances of the m/z 221 precursor[19]. But the differences between the anomers were not always pronounced enough for unambiguous identification. Linkage determination has also been achieved by liquid secondary ion mass spectrometry/fourier transform mass spectrometry (LSIMS/FT-MS) in the negative mode[20, 21].

Electrospray tandem mass spectrometry (ES-MS/MS) has been used to differentiate the Ca^{2+}- and Mg^{2+}-coordinated branched trisaccharide isomers[22]. In the negative mode, ES-MS/MS has been used for linkage determination of underivatized oligosaccharides[23]. Later, an attempt was made to determine directly both linkage positions and anomeric configurations for all underivatized isomers in a glucopyranosyl disaccharide series based on characteristic fragments and abundances of ES in-source CID mass spectra[24]. Decomposition of anionic

adducts has also been investigated for differentiation of linkage positions[25, 26] and anomeric configurations[26] of disaccharides in the negative ion mode using ESI-MS/MS. Molecular orbital calculations performed on deprotonated glucopyranosyl disaccharides showed that the anomeric configurations and the stereochemistry at the 2-position of the non-reducing ring might have a significant effect on disaccharide fragmentation[27].

Matrix-assisted laser desorption/ionization mass spectrometry (MALDI-MS) has become established as a powerful tool to characterize carbohydrates[28-30]. Although the vast majority of mass spectral analyses of neutral saccharides are performed in the positive mode via adduct formation with H^+ or with metal cations, a potential limitation for positive ion MALDI analysis is that facile decomposition and nonspecific cleavages are often induced for certain unstable alkali metal ion adducts[31, 32]. Moreover, the inability to simultaneously analyze neutral and acidic oligosaccharides for MALDI in the positive ion mode is also a noteworthy drawback.

The above limitations potentially can be resolved by using negative ion mode MALDI MS analysis of oligosaccharides which has been gaining popularity after a series of β-carboline compounds, e.g., harmane, non-harmane and harmine, were introduced as efficient MALDI matrixes[33-35]. The tendencies for fucosylated oligosaccharides to lose fucose and for sialylated oligosaccharides to lose sialic acid as seen in most positive ion MALDI spectra are not as apparent in negative ion mode analysis[36]. In addition, the acidic oligosaccharides, which readily ionize as $[M - H]^-$ anions, can be far more amenable to detection in negative mode MALDI analysis than in positive mode. However, unlike acidic oligosaccharides, neutral oligosaccharides exhibit a much lower tendency to deprotonate, rendering the $[M - H]^-$ signal intensity generally weaker.

Anion attachment represents a promising alternative method to charge neutral saccharides in negative ion MALDI-MS using β-carboline compounds as the MALDI matrix and structurally-informative fragments were readily produced after decompositions of $[M + HSO_4 - H_2O]^-$[36] and $[M + Cl]^-$[37-40]. Although not truly tandem MS, post-source decay (PSD) can provide valuable information about the structures of gas-phase ions generated by MALDI[41, 42]. When subjected to PSD fragmentation in the positive ion mode, linkage isomers of saccharides are not readily distinguished based upon the PSD spectral patterns because saccharides are frequently cleaved at the glycosyl linkages and more specific cross-ring cleavage ions are often rather weak in positive mode PSD[29, 43, 44]. On the contrary, when subjected to PSD fragmentation in the negative ion mode, prominent cross-ring cleavages are usually produced along with glycosyl bond cleavages. PSD of both deprotonated molecules and anionic adducts of oligosaccharides has been performed and some success for differentiation of linkage positions as well as anomeric configurations in oligosaccharides has been shown[37-40, 45-47] .

Recent studies in negative ES-MS have established that more than a dozen stable anionic adducts of carbohydrates (anion attachment) can be observed in the gas phase and some of these anionic adducts could offer structural information upon CID[26, 48-53]. But the corresponding studies of anion attachment of oligosaccharides in negative ion mode *MALDI-MS* have not been systematically exploited[36-40]. The current study focuses on studying the PSD fragmentation patterns of MALDI-generated anionic adducts of oligosaccharides. The current study compares different anions for their ability to form anionic adducts with saccharides of varying sizes in MALDI-rTOF MS and evaluates their PSD patterns for the possibility of yielding structurally-informative fragments. Our goal is to document the effects of linkage positions and anomeric configurations of neutral oligosaccharides on the PSD patterns of their anionic adducts. We

evaluate the application of anion attachment with PSD in MALDI linear-field reflectron TOF MS not only as a technique to determine linkage positions, but also to differentiate anomeric configurations in underivatized oligosaccharides.

2.2 Experimental

2.2.1 Chemicals

All neutral oligosaccharides were purchased from Sigma Chemical Co. (St. Louis, MO) and prepared at 1 mM in a solution of 4:1 methanol/water. D-Glucuronic acid was purchased from Aldrich (Milwaukee, WI) and prepared at 1 mM in a 4:1 solution of methanol/water. Hydrochloric acid, acetic acid, ammonium nitrate, ammonium fluoride, ammonium chloride, ammonium bromide, ammonium iodide and ammonium acetate were obtained from Aldrich (Milwaukee, WI) and were prepared at 1 mM in a solution of 4:1 methanol/water. Harmine and harmine hydrochloride were purchased from Aldrich (Milwaukee, WI). Both matrixes were prepared at 20 mg/mL in a solution of 4:1 methanol/water. All chemicals were used as received without further purification.

2.2.2 Mass Spectrometry

Mass spectra were acquired on an Applied Biosystems Voyager Elite MALDI-TOF mass spectrometer equipped with delayed extraction (Applied Biosystems, Framingham, MA) and a pulsed N_2 laser (λ = 337 nm). An extraction voltage of 20 kV was typically employed. All mass spectra were acquired in the negative reflectron mode employing delayed extraction. Laser intensity was adjusted to just above the threshold energy for appearance of oligosaccharide anionic adducts. When acquiring PSD spectra, laser intensity was adjusted to 10-30% above this threshold, and the mirror ratios in the PSD segment list were manually calculated and specified

such that the targeted ions in question would be focused and collected within the same PSD segment. All mass spectra and PSD spectra consist of an average of 50-100 laser shots. Reported m/z values show nominal masses only (i.e., values after the decimal places have been truncated). The instrument was externally calibrated by monoisotopic peaks of anionic dopants, harmine matrix and oligosaccharides. Data processing was performed using IGOR Pro 4.07 (Wave Metrics Inc., Lake Oswego, OR).

MALDI samples were prepared using an optimized "thin-layer" method. Corresponding ammonium salts were used when investigating six different anionic species, i.e., acetate, fluoride, chloride, bromide, iodide and nitrate anions, for their abilities to yield anionic adducts of oligosaccharides in MALDI. First, 2 μL of 1 mM ammonium salt solution, 2 μL of 1 mM acid and 4 μL of harmine matrix solution (all in 4:1 methanol/water) were mixed. Next, a 0.5 μL aliquot of this final matrix solution was deposited onto a sample plate and dried to form the matrix layer. 0.5 μL of disaccharide solution was then deposited on top of the matrix layer and allowed to dry. 1 mM HCl in a 4:1 solution of methanol/water was sued when testing chloride anion whereas 1 mM HNO_3 was used when testing nitrate anion (no introduction of other anions). For all the other ions, i.e., acetate, fluoride, bromide and iodide anions, 5% acetic acid in a 4:1 solution of methanol/water was used during sample preparation. Acetic acid was chosen because it does not form acetate adducts with the tested oligosaccharides (see results below) which might complicate the interpretation of results. Acidic condition is preferred since harmine as MALDI matrix works best at low pH[36]. PSD experiments were performed on stable anionic adducts (Cl^-, Br^-, I^- and NO_3^-) of oligosaccharides.

2.3 Results and Discussion

2.3.1 Anion Comparison and Anion Adducts of Neutral and Acidic Oligosaccharides

Employing the thin-layer sample preparation with harmine as the matrix, six anionic species (all in ammonium salt form), i.e., ammonium acetate, fluoride, chloride, bromide, iodide and nitrate, were tested for their abilities to form anionic adducts with a series of neutral and acidic oligosaccharides having different sizes (Table 2.1) (**11**, **22**, **25**, **28-32**) in MALDI-TOF MS. From small monosaccharides such as α-D-glucose (**28**) to larger oligosaccharides such as γ-cyclodextrin (eight sugar units) (**31**), all of the tested saccharides can form anionic adducts with nitrate, chloride, bromide and iodide. In contrast, anionic adducts of oligosaccharides were not observed for fluoride and acetate in this study. When serving as the attaching anions to smaller saccharides (monosaccharides, disaccharides and trisaccharides) in negative ion MALDI, nitrate, chloride, bromide and iodide appear to have the advantage over bisulfate which only forms adducts with tetrasaccharides or larger oligosaccharides[36].

It appears that the gas-phase basicity (GB) plays an important role for the successful observation of anionic adducts in MALDI MS. The gas-phase basicities of fluoride (1529 kJ/mol) and acetate (1427 kJ/mol) are all higher than the gas-phase basicity of $[harmine - H]^-$ (between 1373 and 1407 kJ/mol)[37]. While the gas-phase basicities of all the other anions, i.e., nitrate (GB 1329.7 kJ/mol), chloride (GB 1372.8 kJ/mol), bromide (GB 1331.8 kJ/mol) and iodide (GB 1293.7 ± 0.84 kJ/mol), are all lower than the gas-phase basicity of $[harmine - H]^-$. This is in agreement with our previous finding that the gas-phase basicity of an anion must be lower than that of $[matrix - H]^-$ in order to form the anion adduct with a neutral analyte[37]. Also, it appears that Cl^- gives the strongest adduct signal among all the anions investigated since the gas-phase basicities of harmine, saccharides and chloride are closest.

Table 2.1. Lists of saccharides analyzed by PSD of anion adducts.

No.	Formula	Name
1	Glcβ1-6Glc	gentiobiose
2	Glcα1-6Glc	isomaltose
3	Glcβ1-4Glc	cellobiose
4	Glcα1-4Glc	maltose
5	Glcβ1-3Glc	laminaribiose
6	Glcα1-3Glc	nigerose
7	Glcβ1-2Glc	sophorose
8	Glcα1-2Glc	kojibiose
9	Glcα1-1βGlc	α,β-trehalose
10	Galβ1-6Gal	
11	Galα1-6Glc	melibiose
12	Galβ1-4Glc	lactose
13	Galβ1-4Man	epilactose
14	Galβ1-4Gal	
15	Galα1-4Gal	
16	Glcα1-6Fru	palatinose
17	Glcβ1-4Fru	lactulose
18	Glcα1-3Fru	turanose
19	Glcα1-2Fru	sucrose
20	Galβ1-3Ara	
21	Galα1-6Glcα1-2Fru	raffinose
22	Galα1-6 Galα1-6Glcα1-2Fru	stachyose
23	Glcα1-6Glcα1-6Glc	isomaltotrisoe
24	Glcβ1-4Glcβ1-4Glc	cellotriose
25	Glcα1-4Glcα1-4Glc	maltotriose
26	Glcα1-6Glcα1-4Glc	panose
27	Galα1-3Galβ1-4Galα1-3Gal	3α, 4β, 3α-galactotetraose
28		glucose
29		α-cyclodextrin
30		β-cyclodextrin
31		γ-cyclodextrin
32		glucuronic acid

D-glucuronic acid, an acidic saccharide containing one carboxylic acid moiety, can also form adducts with nitrate (m/z 256), chloride (m/z 229, 231), bromide (m/z 273, 275), and iodide (m/z 321) in MALDI. In all cases, a strong peak corresponding to $[M - H]^-$ (m/z 193) is observed in addition to the respective adduct peaks. Figure 2.1a is a representative negative MALDI reflectron mass spectrum of glucuronic acid and iodide. The acidic oligosaccharides generally produce stronger signals, and deprotonation appears to occur more readily than anion attachment. Nitrate, chloride, bromide and iodide can serve as good candidates for simultaneous detection of intact neutral and acidic oligosaccharides in the negative ion mode since neutral and acidic oligosaccharides often coexist as mixtures for carbohydrates from biological sources.

Of the four anions (i.e., chloride, bromide, iodide and nitrate) that form observable adducts with melibiose (**11**), PSD of $[melibiose + anion]^-$ was performed to see whether structurally-informative fragments could be obtained. PSD of $[melibiose + Br]^-$ (Figure 2.1b), $[melibiose + I]^-$ (Figure 2.1c) and $[melibiose + NO_3]^-$ (Figure 2.1d) produce Br^-, I^- and NO_3^- as the sole major product ions, respectively; hence, structural information of saccharides is not obtained. In contrast, structurally-informative sugar fragments are observed upon PSD of $[melibiose + Cl]^-$. The PSD decomposition patterns might be explained by considering that $[M - H]^-$ ions of disaccharides often have gas-phase basicities close to that of chloride, but substantially higher than those of nitrate, bromide and iodide. Unlike chloride, the weak attractions of nitrate, bromide and iodide for protons cannot compete with the disaccharide upon PSD, leading to loss of anions and neutral disaccharide, without structurally-informative disaccharide fragments. Chloride thus remains a preferred anion for structural determination employing anion attachment followed by PSD using MALDI-TOF[37] and is used for the PSD experiments hereafter.

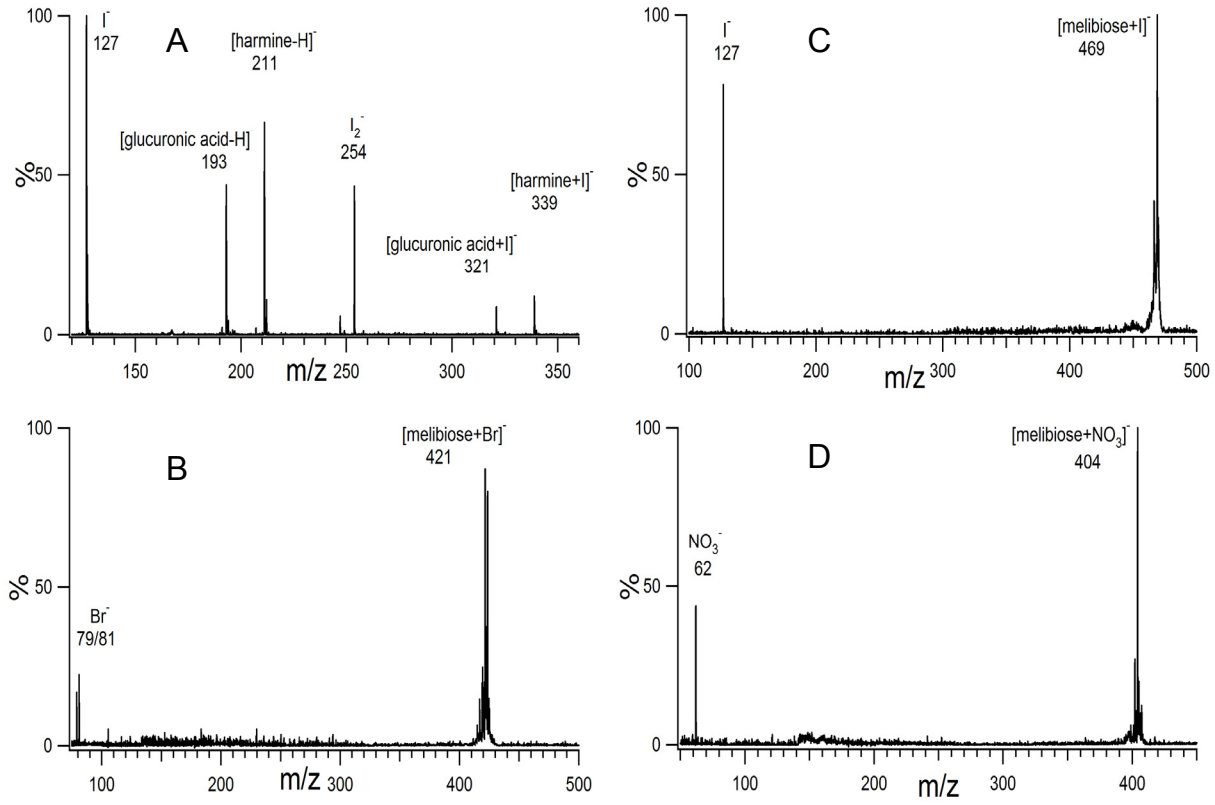

Figure 2.1. (a) MALDI-TOF mass spectrum of iodide adducts of glucuronic acid. Both [glucuronic acid - H]$^-$ at m/z 193 and [glucuronic acid + I]$^-$ at m/z 321 are formed.; PSD of: (b) bromide; (c) iodide; and (d) nitrate adducts of melibiose yield Br^-, I^- and NO_3^-, respectively, without structurally-informative disaccharide fragments.

2.3.2 PSD of Chloride Adducts of Disaccharides for Linkage Differentiation

To further exploit the chloride attachment approach for carbohydrate analysis, four groups of disaccharides (Table 2.1) are investigated by PSD of mass-selected chloride adducts of: (1) nine glucopyranosyl glucoses (**1**-**9**): Glcβ1-6Glc (gentiobiose), Glcα1-6Glc (isomaltose), Glcβ1-4Glc (cellobiose), Glcα1-4Glc (maltose), Glcβ1-3Glc (laminaribiose), Glcα1-3Glc (nigerose), Glcβ1-2Glc (sophorose), Glcα1-2Glc (kojibiose), Glcα1-1βGlc (α,β-trehalose); (2) six different hexose-hexose disaccharides with at least one hexose other than glucose (**10**-**15**): Galβ1-6Gal, Galα1-6Glc (melibiose), Galβ1-4Glc (lactose), Galβ1-4Man (epilactose), Galβ1-4Gal, Galα1-4Gal; (3) three glucopyranosyl fructoses plus one galactopyranosyl fructose (**16**-**19**): Glcα1–6Fru (palatinose), Galβ1–4Fru (lactulose), Glcα1–3Fru (turanose), Glc1–2Fru (sucrose); and (4) one hexose-pentose disaccharide (**20**): Galβ1–3Ara. The negative ion MALDI mass spectra of the disaccharides (Table 2.1, **1**-**19**) all show peaks at m/z 377 ($[M + Cl]^-$) except for Galβ1–3Ara (**20**) ($[M + Cl]^-$ peak appears at m/z 347).

It was shown that the neutral losses observed in PSD spectra of the chloride adducts of 1-6, 1-4 and 1-3 linked glucopyranosyl glucoses disaccharides (1-6 linkage, Figure 2.2a, 2.2b; 1-4 linkage, Figure 2.3a, 2.3b; 1-3 linkage, Figure 2.4a, 2.4b) were diagnostic of the glycosidic linkage positions between adjacent glucose moieties[54]. To widen the applicability of findings to other disaccharides, the PSD spectra of chloride adducts of 1-2 and 1-1 linked glucopyranosyl glucoses disaccharides (1-2 linkage, Figure 2.4c, 2.4d; 1-1 linkage, Figure 2.4e), and a variety of 1-6 and 1-4 linked hexose-hexose disaccharides with at least one hexose other than glucose (Figure 2.2c, 2.2d, 2.3c, 2.3d, 2.3e and 2.3f) are also investigated. From the analysis of these five series of PSD spectra, generalizations can be made about hexose-hexose disaccharides with respect to the relationship between PSD fragmentation patterns and linkage positions (Table 2.2).

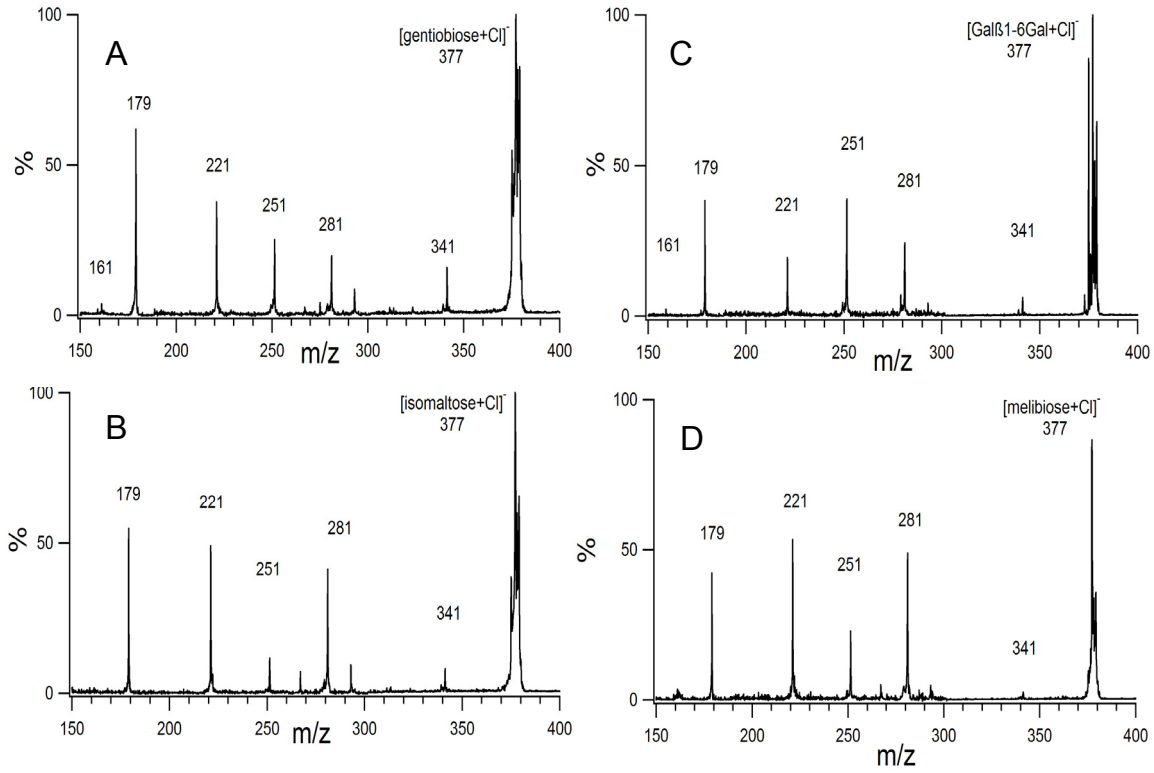

Figure 2.2. Negative ion PSD of chloride adducts of 1-6 linked disaccharides. (a) gentiobiose (Glcβ1-6Glc); (b) isomaltose (Glcα1-6Glc); (c) Galβ1-6Gal; and (d) melibiose (Galα1-6Glc). The α- (isomaltose) and β-configuration (gentiobiose) in 1-6 linked glucopyranosyl disaccharides can be readily differentiated by examining whether the relative abundance ratio of m/z 251:281 is larger than unity (β isomer) (Figure 2.2a) or smaller than unity (α isomer) (Figure 2.2b). This peak intensity difference is also applicable to other 1-6 linked disaccharides.

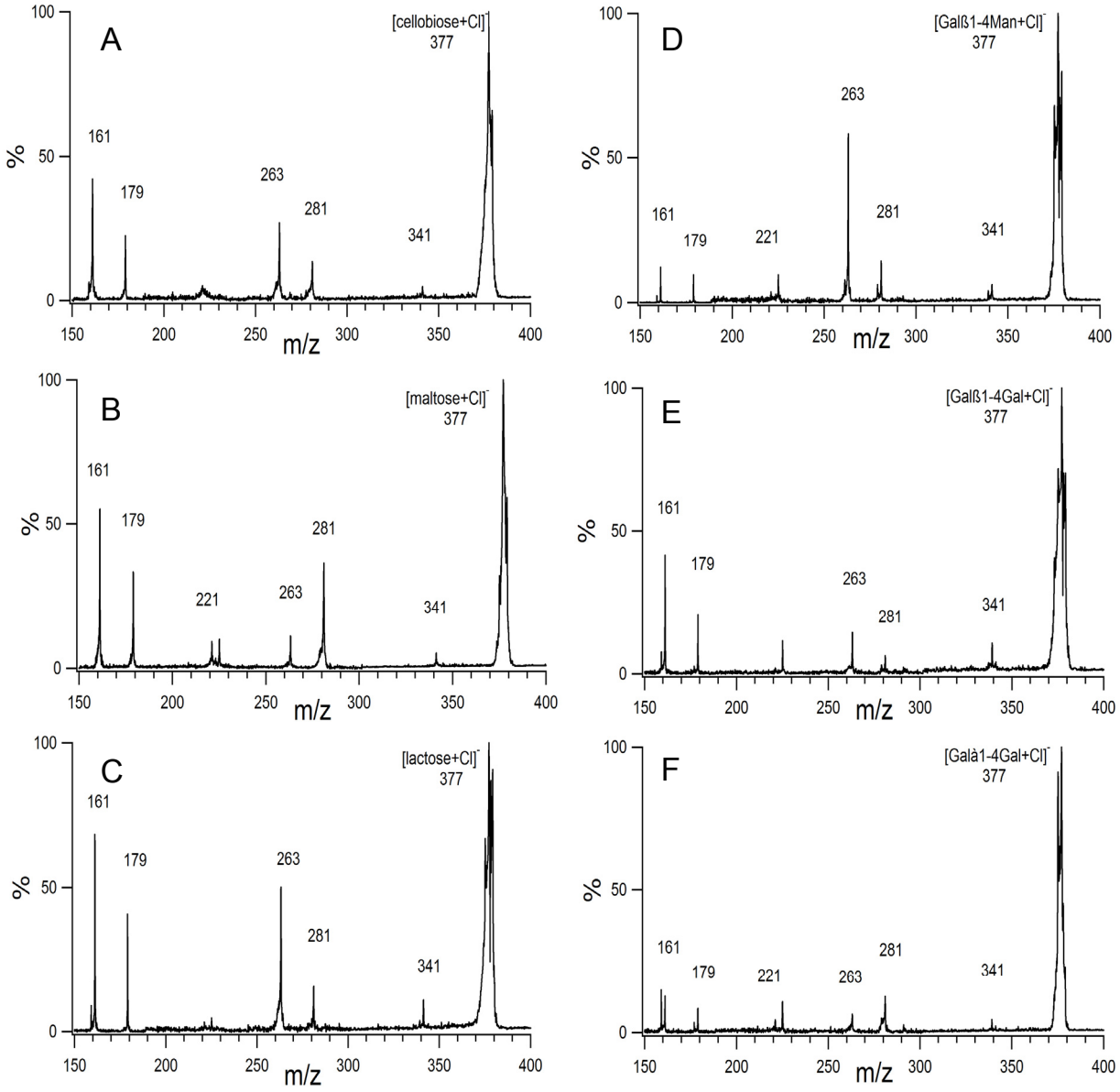

Figure 2.3. Negative ion PSD of chloride adducts of 1-4 linked disaccharides. (a) cellobiose (Glcβ1-4Glc); (b) maltose (Glcα1-4Glc); (c) lactose (Galβ1-4Glc); (d) Galβ1-4Man; (e) Galβ1-4Gal; and (f) Galα1-4Gal. A clear-cut differentiation between the α- (maltose) and β-configuration (cellobiose) in 1-4 linked glucopyranosyl disaccharides can be made by simply checking whether the relative abundance ratio of m/z 263:281 is larger than unity (β isomer) (Figure 2.3a) or smaller than unity (α isomer) (Figure 2.3b). This peak intensity difference also holds true for other 1-4 linked disaccharides.

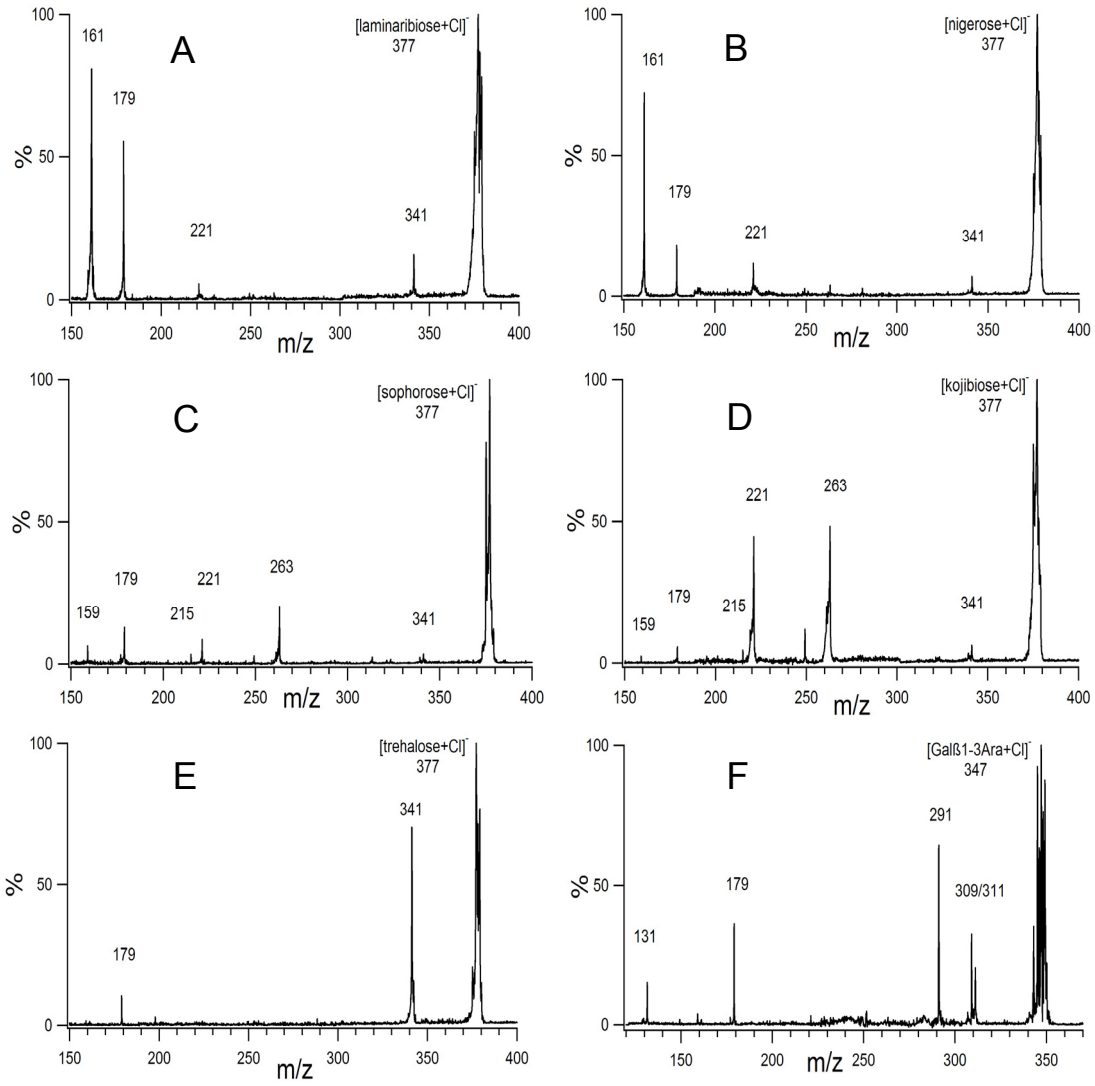

Figure 2.4. Negative ion PSD of chloride adducts of: (a) laminaribiose (Glcβ1-3Glc); (b) nigerose (Glcα1-3Glc); (c) sophorose (Glcβ1-2Glc); (d) kojibiose (Glcα1-2Glc); (e) trehalose (Glcα1-1βGlc); (f) . For 1-3 glycosyl linkages, the relative abundance ratio of m/z 161:179 is consistently lower for the α isomer (nigerose) (Figure 2.4b) than for the β isomer (laminaribiose) (Figure 2.4a). Even though the m/z 161:179 ratio is larger than unity for both 1,3-linked anomers, nevertheless, the difference in relative ratios is sufficiently large to permit distinction between the α- and β-configurations.

For 1-2 glycosyl linkages, the relative abundance ratio of m/z 215:221 is consistently lower for the α isomer (kojibiose) (Figure 2.4d) than for the β isomer (sophorose) (Figure 2.4c) which allows for clear differentiation. Peaks at m/z 215 in Figures 2.4c and 2.4d are chlorine-containing fragment ions.

For 1-1 linked trehalose (Glcα1-1βGlc) (Figure 2.4e), a non-reducing disaccharide, usually high peak intensity at m/z 341 is observed because of the lack of reducing end hydroxyl group.

For Galβ1–3Ara (Figure 2.4f), a hexose-pentose, prominent product ion peaks at m/z 179 with charge retention on the non-reducing ring and at m/z 131 with charge retention on the reducing ring are produced upon unambiguous cleavage of the glycosidic bond on the reducing end side.

Table 2.2. Diagnostic PSD neutral losses and fragment peaks (in parenthesis) of chloride adducts of disaccharides. Mass differences resulting from neutral losses are calculated from deprotonated saccharides.

Link	Presence							Absence			Relative Ion Abundance
1-6		-162 (179)		-120 (221)	-90 (251)		-60 (281)		263		$\alpha_{251/281} < 1 < \beta_{251/281}$
1-4	-180 (161)	-162 (179)				-78 (263)	-60 (281)	251			$\alpha_{263/281} < 1 < \beta_{263/281}$
1-3	-180 (161)	-162 (179)		-120 (221)							$\alpha_{161/179} > 3 > \beta_{161/179}$
1-2		-162 (179)	(215)	-120 (221)		-78 (263)				281	$1 < \alpha_{215/221} < \beta_{215/221}$
1-1		-162 (179)									

The major neutral losses observed in the PSD spectra of chloride adducts of four 1-6 linked disaccharides (Figure 2.2a-d) are the same, and the major neutral losses observed in the PSD spectra of chloride adducts of six 1-4 linked disaccharides (Figure 2.3a-f) also show uniformity. Because the diagnostic losses for these 1-6 and 1-4 linked disaccharides remain virtually unchanged no matter how the reducing end or the non-reducing end vary for these disaccharides, it is fairly safe to conclude that these diagnostic losses are characteristic of the glycosidic linkage positions between adjacent monosaccharide units, independent of the constituent hexose of the disaccharides. It thus appears that negative ion PSD fragmentation patterns of chloride adducts of disaccharides are mainly influenced by the linkage position between the monosaccharide rings independent of the hexose structures and the anomeric configurations.

The characteristic PSD fragmentation patterns for each linkage position can be summarized by stating that observation of the PSD fragments $[M - H - 162]^-$, $[M - H - 120]^-$, $[M - H - 90]^-$, and $[M - H - 60]^-$ with the absence of $[M - H - 78]^-$ are characteristic of the 1-6 linked disaccharides (Figure 2.2a-d, Table 2.2). Appearance of the PSD fragment peaks of $[M - H - 180]^-$, $[M - H - 162]^-$, $[M - H - 78]^-$ and $[M - H - 60]^-$ with the absence of $[M - H - 90]^-$ are indicative of the 1-4 linked disaccharides (Figure 2.3a-f, Table 2.2). Observation of the PSD fragmentation pathways producing $[M - H - 180]^-$ and $[M - H - 162]^-$, as well as the weak $[M - H - 120]^-$, appears to be the pattern for the 1-3 linked disaccharides (Figure 2.4a, 2.4b, Table 2.2). Lastly, the 1-2 linked disaccharides (Figure 2.4c, 2.4d, Table 2.2) are characterized by the appearance of PSD fragment peaks for $[M - H - 162]^-$, $[M - H - 120]^-$, $[M - H - 90]^-$ and $[M - H - 78]^-$.

Observation of the PSD fragment peak of $[M - H - 162]^-$ with a remarkably strong $[M - H]^-$, appears to be characteristic of the 1-1 linked disaccharides (Figure 2.4e). Although only one 1-1 isomer (Glcα1-1βGlc) out of three possibilities (Glcα1-1βGlc, Glcα1-1αGlc and Glcβ1-1βGlc) has been studied here, we have tentatively included in Table 2.2 the fragmentation peaks diagnostic for the 1-1 linked disaccharides since its fragmentation pattern is highly characteristic (Figure 2.4e, Table 2.2). From decompositions of chloride adducts of Glcα1-1βGlc, a high intensity peak at m/z 341 corresponding to the deprotonated molecule $[M -H]^-$ is observed. Unlike other glucopyranosyl glucoses disaccharides where one of the glucoses is considered as the reducing ring, all three forms of trehalose are non-reducing disaccharides wherein the linkage has been formed between two reducing hydroxyl groups on the two glucose units. It appears that upon PSD, chloride adducts of trehalose require more energy to undergo initial HCl loss because they lack the acidic reducing end hydroxyl group. Thus, more of the available energy is consumed in the first step of decomposition (HCl loss) and the remaining $[M - H]^-$ product ions are less susceptible to consecutive decompositions[25]. This rationalizes the unusually high abundance of the $[M - H]^-$ peak for trehalose that does not readily undergo further fragmentations.

Deprotonated molecules $[M - H]^-$ at m/z 341 and the peak at m/z 179, corresponding to the loss of a hexose from $[M - H]^-$, are consistently observed in PSD studies of $[disaccharide + Cl]^-$ adducts for all hexose-hexose disaccharides, although the intensity varies substantially. Observation of peaks at m/z 179 in PSD studies of $[disaccharide + Cl]^-$ for all hexose-hexose disaccharides shows great similarity to the decomposition pattern of $[disaccharide - H]^-$ reported in LSIMS[20], FAB-MS/MS[19] and an ESI MS/MS study of $[disaccharide + Cl]^-$ [25], but differs somewhat from a previous FAB-MS/MS study of $[disaccharide - H]^-$ [18]. Similarities in the

decomposition spectra of [disaccharide + Cl]$^-$ and [disaccharide - H]$^-$ precursors strongly suggest that the fragmentation pathway of the former requires neutral loss of HCl from the chloride adducts prior to consecutive decompositions.

The neutral losses for differentiating linkage positions observed in our MALDI-PSD of [saccharides + Cl]$^-$ investigation are similar but not identical to those from other studies[15, 18-20, 25, 38]. These similarities are observed even under largely variable conditions (positive mode, negative mode; lithiated cations, deprotonated ion, chloride adduct of saccharides; sector high energy CAD, low energy CAD, PSD; LSI, FAB, ES, MALDI) suggest a correlation between the linkage positions and fragmentation mechanisms and/or steric requirements for cross-ring fragmentations. The minor differences between our results and those obtained by Yamagaki et al.[38] are possibly due to the different experimental conditions employed: PSD with linear-field reflectron vs. PSD with curved-field reflectron. It appears that more fragment ions are observed in our PSD with linear-field reflectron perhaps because of the smaller sizes of oligosaccharides employed in our study. Another contributing factor might be that the laser intensity in our PSD experiments using the linear-field reflectron can be changed greatly from segment to segment to improve fragment ion abundances without saturating the detector. It is a real advantage compared to PSD with a curved-field reflectron where the chosen laser intensity may create a dynamic range problem whereby lower fragment ion signals are barely visible next to high intensity peaks.

2.3.3 Determination of the Reducing End

So far, all the disaccharides studied are hexose-hexose and the constituent monosaccharide units are stereoisomers which cannot be discriminated by single-stage MS. Sequence information can be obtained by MS when the constituent monosaccharide units have

different masses. For example, the hexose-pentose disaccharide: Galβ1–3Ara (**20**), has two monosaccharide units with different masses. The PSD mass spectrum of the chloride adduct of Galβ1–3Ara at m/z 347 is shown in Figure 2.4f. Along with the deprotonated molecule $[M - H]^-$, prominent product ion peaks at m/z 179 (with charge retention on the non-reducing ring) and at m/z 131 (with charge retention on the reducing ring) are produced upon unambiguous cleavage of the glycosidic bond on the reducing end side. Cleavages on the non-reducing side forming product ions at m/z 161 or m/z 149 are disfavored[20] and are detected in much lower abundances. A very weak peak at m/z 221 is also observed. This fragmentation pattern is very similar to the 1-3 linked hexose-hexose disaccharides (Table 2.2).

2.3.4 PSD of Chloride Adducts of Fructose-Containing Saccharides

Figure 2.5 shows the PSD mass spectra of $[M + Cl]^-$ of fructose-containing saccharides. Three glucopyranosyl fructoses plus one galactopyranosyl fructose (**16-19**) characterized by different linkages are studied. It is obvious that these fructose-containing isomers with differing linkage position give quite different PSD product ion spectra. For the fructose-containing disaccharide series (Figure 2.5a-d), observation of PSD peaks at m/z 179, 221, 251, 281 and 341 is characteristic of the 1–6 linkage; appearance of PSD peaks at m/z 161, 179 and 251 is indicative of the 1–3 linkage; and PSD peaks appearing at m/z 179, 197, 215 and 341 is characteristic of the 1–2 linkage. Cross-ring cleavages are not prominent for the 1–4 linked Gal-Fru and observation of PSD peaks at m/z 161, 179 with small cross-ring cleavage peaks at m/z 263 and 281 are characteristic of the 1-4 linkage. The PSD spectra presented here are qualitatively similar to those obtained by ES-CID of chloride adducts of these fructose-containing disaccharides[25], except for Galβ1–4Fru whereas the cross-ring cleavages of fructose were not observed under ES-CID[25]. On the other hand, our PSD spectrum of chloride adducts of

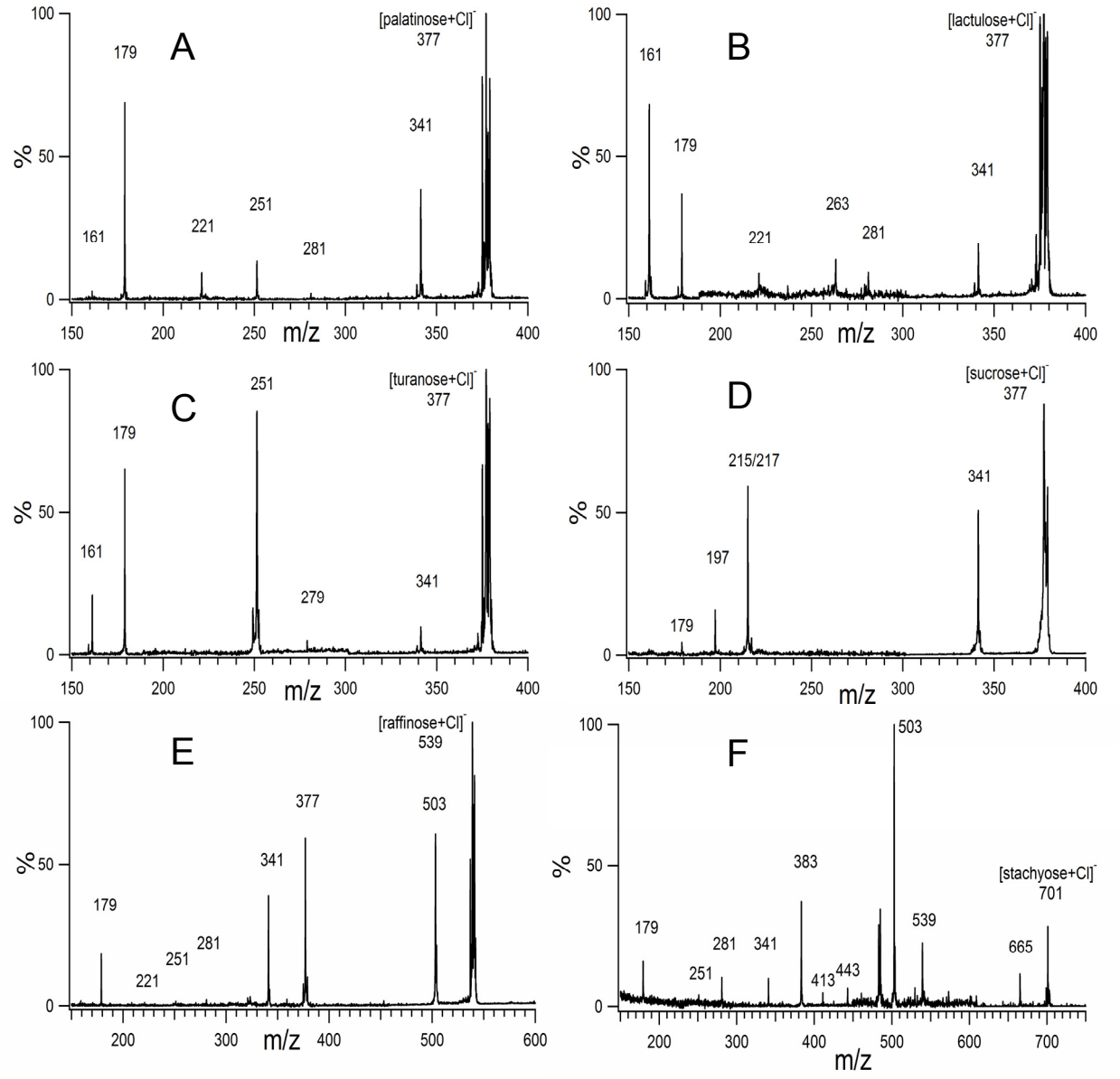

Figure 2.5. Negative ion PSD of chloride adducts of fructose-containing saccharides. (a) palatinose (Glcα1–6Fru); (b) lactulose (Galβ1–4Fru); (c) turanose (Glcα1–3Fru); (d) sucrose (Glc1–2Fru); (e) raffinose (Galα1-6Glcα1-2Fru); and (f) stachyose (Galα1-6Galα1-6Glcα1-2Fru). PSD of the chloride adduct of non-reducing sucrose yields chlorine-containing fragment ions (m/z 215 and m/z 197). Chlorine-containing product ions are also observed at m/z 377 for raffinose (Figure 2.5e) and at m/z 539 for stachyose (Figure 2.5f) due to the neutral loss of the fructose residue (162 Da neutral) from the corresponding $[M + Cl]^-$ precursors.

Galβ1–4Fru is very similar to that of $[M - H]^-$ obtained under FAB-CID [19]. Also, the PSD fragmentation patterns of 1-6 and 1-4 linked fructose-containing disaccharides were similar to their counterparts obtained from non fructose-containing disaccharides.

Sucrose (Glcα1–2Fru) (Figure 2.5d) is unique among all the disaccharides studied here. First, it is a fructose-containing disaccharide. Second, it is a non-reducing disaccharide wherein the linkage is formed between two reducing hydroxyl groups on the glucose and the fructose units. Figure 2.5d shows the PSD spectra of chloride adduct of 1-2 linked sucrose. The deprotonated molecule $[M - H]^-$ at m/z 341 is substantially higher in abundance than those with 1-3, 1-4 and 1-6 linkages. An interesting phenomenon is that the PSD spectrum of chloride adducts of sucrose also shows chloride-containing product ions at m/z 197 and 215 as shown in Figure 2.5d. The observation of chlorine-containing fragments from chloride adduct precursors has not yet been reported in MALDI-PSD MS. The unusually high abundance of $[M - H]^-$ peaks at m/z 341 may be attributed to the lower acidity of the non-reducing end sugar, causing more energy to be consumed during the neutral loss of HCl from $[M + Cl]^-$, leaving the formed $[M - H]^-$ ion with less internal energy for further decomposition[25].

2.3.5 PSD of Chloride Adducts for Differentiation of Anomeric Configurations

In our previous study[54], with the linkage position assigned, anomeric configurations of 1-6, 1-4 and 1-3 linked glucopyranosyl-glucose disaccharides were successfully differentiated by comparing the relative abundances of diagnostic peaks that were intentionally acquired within the same PSD segment from the chloride adducts of these disaccharides.

As shown in Table 2.2, the disaccharides with different anomeric configuration, but the same linkage, have significant differences in the PSD mass spectra of their chloride adducts, independent of the hexose rings. For example, the α- (melibiose: Galα1-6Glc) (Figure 2.2d) and

β-configuration (Galβ1-6Gal) (Figure 2.2c) with 1-6 linkage can be readily differentiated by examining whether the relative abundance ratio of m/z 251:281 is larger than unity (β isomer) (Figure 2.2c) or smaller than unity (α isomer) (Figure 2.2d). This finding agrees well with the peak intensity difference between the α anomer (isomaltose) (Figure 2.2b) and β anomer (gentiobiose) (Figure 2.2a) in 1-6 linked glucopyranosyl glucose[54].

Similarly, a clear-cut differentiation between the α- (Galα1-4Gal) (Figure 2.3f) and β-configuration, i.e., lactose (Galβ1-4Glc) (Figure 2.3c), Galβ1-4Man (epilactose) (Figure 2.3d) and Galβ1-4Gal (Figure 2.3e), with 1-4 linkage can be made by simply checking whether the relative abundance ratio of m/z 263:281 is larger than unity (β isomer) or smaller than unity (α isomer). This finding agrees well with the peak intensity difference between the α anomer (maltose) (Figure 2.3b) and β anomer (cellobiose) (Figure 2.3a) in 1-6 linked glucopyranosyl glucose[54].

For 1-3 glycosyl linkages, the relative abundance ratio of m/z 161:179 is consistently lower for the α isomer (nigerose) (Figure 2.4a) than for the β isomer (laminaribiose) (Figure 2.4b). Even though the m/z 161:179 ratio is larger than unity for both 1,3-linked anomers, nevertheless, the difference in relative ratios is sufficiently large to permit distinction between the α- and β-configurations[54].

For 1-2 linked glucopyranosyl glucose disaccharides, the relative abundance of m/z 215 vs m/z 221 ($[M - H - 120]^-$) of the β isomer (sophorose) (Figure 2.4c) is much higher than that of the corresponding α isomer (kojibiose) (Figure 2.4d).

Notably, the relative abundance of m/z 161 vs m/z 179 in the negative ion PSD mass spectra of $[disaccharide + Cl]^-$ vary largely for the different linkages. The 1-6, 1-2 and 1-1 linked disaccharides show higher abundances of m/z 179 vs m/z 161, while the reverse is observed for

1-4 and 1-3 linked disaccharides, which is similar to previous studies in LSIMS/FTMS [20] and ES MS/MS [25]. Similar tendencies are also observed in disaccharides other than glucopyranosyl glucose disaccharides and larger oligosaccharides. This distinction appears to be a potential indicator to differentiate the 1-6, 1-2, and 1-1 linkages (higher m/z 179) from the 1-4 and 1-3 linkages (higher m/z 161). For the PSD of chloride adducts of fructose-containing disaccharides, Glcα1–2Fru, Glcα1–3Fru and Glcα1–6Fru display higher m/z 179 peaks than m/z 161, while Galβ1–4Fru gives the reverse tendency. This difference is likely a reflection of the varying steric requirements for glycosidic bond cleavage.

Noteworthy is the fact that the PSD spectra of disaccharides with the same anomeric configuration and same linkage position show comparable relative ion abundances for our proposed diagnostic peaks, regardless of the constituent monosaccharide structures.

2.3.6 Influence of Laser Intensity on Relative Peak Intensities of Diagnostic PSD fragment pairs

Relative peak intensities (RPI) are not generally reliably reproducible in PSD when these spectra are composites of several different "stitched" spectral segments acquired under somewhat varying ionization conditions[29]. However, employing a novel approach, we demonstrated that even without a curved-field reflectron[38-40, 55-62] that allows acquisition of an entire PSD spectrum under the same conditions for each laser shot, and even if the target crystals may vary substantially in shape and quality, rather reproducible relative PSD peak intensities acquired within the same PSD segment of a limited m/z range (approximately 40 m/z units) with our MALDI linear-field reflectron TOF mass spectrometer can be obtained under the same laser intensity[54].

It is impossible to acquire all PSD spectra using the same laser intensity all the time, even for anomeric disaccharides. So a study was further undertaken to see whether the relative peak intensities of our proposed diagnostic fragment pairs vary greatly with laser intensity. The 1-6 and 1-4 linked glucopyranosyl glucose disaccharides were selected for this study. The stability of the relative ion abundances was checked in four measurements with the laser intensity value set at increasing increments up to about 1.5 times the threshold value (Figure 2.6). The relative intensity of each diagnostic peak pair was calculated with the peak intensity of m/z 281 normalized to 100%. As can be seen from figure 2.6, the relative peak intensities are fairly stable regardless of the laser intensity used. Considering the uncontrollable variations of crystallization on the MALDI target, the reproducibility was satisfactorily high and the anomeric configurations can be unambiguously distinguished.

2.3.7 PSD of Chloride Adducts of Oligosaccharides

It is desirable to extend the results obtained from disaccharides to oligosaccharides and see how the PSD of chloride adduct precursors can be used to establish the linkage position and anomeric configuration in saccharides of larger size.

Both raffinose (Galα1-6Glcα1-2Fru) (**21**) and stachyose (Galα1-6Galα1-6Glcα1-2Fru) (**22**) are non-reducing saccharides, containing the identical Glcα1-2Fru linkage at what is normally the reducing end. The formation of chlorine-containing product ions is also observed at m/z 377 for raffinose (Figure 2.5e) and at m/z 539 for stachyose (Figure 2.5f) due to the neutral loss of the fructose residue (162 Da neutral) from the corresponding $[M + Cl]^-$ precursors in PSD mass spectra. But no PSD peaks at m/z 197 are observed in either case, which contrasts with the previous ES-CID study. As concluded previously for decomposition of ES-generated chloride adducts[25], the observation of chlorine-containing product ions corresponding to loss of fructose

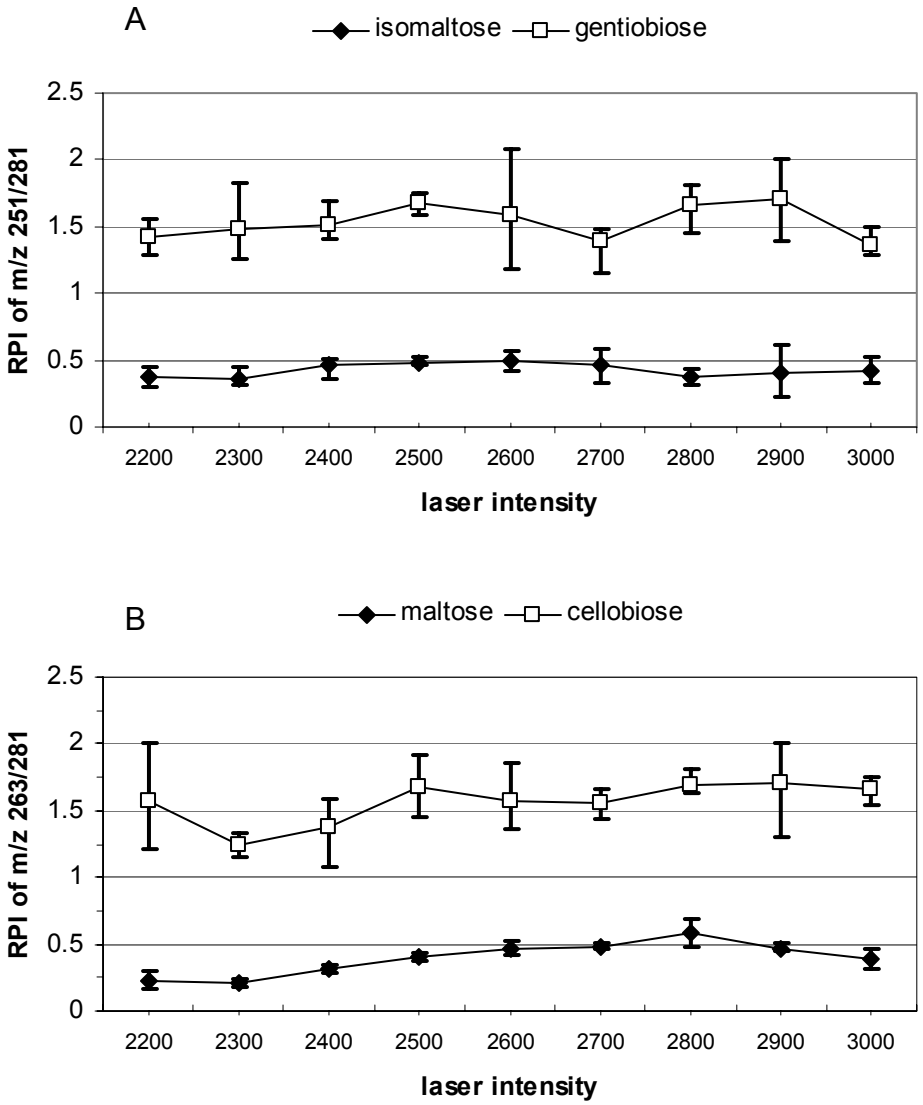

Figure 2.6. Relative peak intensities as a function of laser intensity: (a) RPI of m/z 251 vs. m/z 281 in 1-6 linked disaccharides; (b) RPI of m/z 263 vs. m/z 281 in 1-4 linked disaccharides. RPI in each pair is calculated with peak intensity of m/z 281 normalized to 100%. Subtle variations in the PSD experiments are inevitable, but the RPI is fairly stable regardless of laser intensity.

as a result of cleavage on the fructose side of the glycosidic bond upon PSD of $[M + Cl]^-$, e.g., m/z 215 from sucrose (Figure 2.5d), m/z 377 from raffinose (Figure 2.5e), and m/z 539 from stachyose (Figure 2.5f) is diagnostic for the Glcα1-2Fru linkage at the downstream end. In sharp contrast, chlorine-containing fragments are not observed in PSD of the 1-1 linked pyranose on the reducing end (Figure 2.4f). PSD of chloride adducts clearly serves as a means to differentiate a fructose on the reducing end from a 1-1 linked pyranose on the same position which is virtually indistinguishable previously[21].

As shown in Figure 2.5e, the 1-6 linkage between two glucose rings in raffinose can be clearly obtained by the major losses of 60 Da (m/z 281), 90 Da (m/z 251), 120 Da (m/z 221) and 162 Da (m/z 179) from the negatively charged disaccharide moiety at m/z 341 resulting from the fructose unit loss in raffinose, together with the absence of a peak corresponding to loss of 78 Da. The α anomeric configuration of this 1-6 linkage in raffinose can be safely assigned since the relative abundance of m/z 251:281 is smaller than unity, which is characteristic of the α anomeric configuration with 1-6 linkage (Table 2.2). The 1-2 linkage between rings 2 and 3 in raffinose can be readily identified by the chlorine-containing product ions observed at m/z 377.

The linkages and anomeric configurations in stachyose (Galα1-6Galα1-6Glcα1-2Fru) can be identified by the negative ion MALDI-PSD mass spectrum of $[stachyose+Cl]^-$ (Figure 2.5f) via a similar process. The major losses of 60 Da (m/z 281), 90 Da (m/z 251), 120 Da (m/z 221) and 162 Da (m/z 179) from the negatively charged disaccharide moiety at m/z 341 resulting from the glucose-fructose unit loss in stachyose, together with the absence of peaks corresponding to loss of 78 Da, indicate the 1-6 linkage between the first and second glucose ring. The major losses of 60 Da (m/z 443), 90 Da (m/z 413), 120 Da (m/z 383) and 162 Da (m/z 341) from the negatively charged trisaccharide moiety at m/z 503 resulting from the fructose unit

loss in stachyose, indicate another 1-6 linkage between rings 2 and 3. The α anomeric configuration of these two 1-6 linkages in stachyose can be safely assigned since the relative abundances of both m/z 251:281 and m/z 413:443 are smaller than unity, which is characteristic of the α anomeric configuration with 1-6 linkage (Table 2.2). The 1-2 linkage between the third and fourth ring can be easily identified by chlorine-containing product ions observed at m/z 539.

The negative ion MALDI-PSD mass spectrum of the chloride adduct ions of isomaltotriose (Glcα1-6Glcα1-6Glc) (**23**) is shown in Figure 2.7a, which is essentially the same as that of the truncated stachyose (Figure 2.5f). Both the two 1-6 linkages and two α anomeric configurations of these two 1-6 linkages can be deduced by a similar process.

The negative ion MALDI-PSD mass spectrum of $[cellotriose+Cl]^-$ (Glcβ1-4Glcβ1-4Glc) (**24**) is reported in Figure 2.7b. The major losses from the $[M - H]^-$ ion at m/z 503 of 60 Da (m/z 443), 78 Da (m/z 425) and 162 Da (m/z 341), together with the absence of peaks corresponding to loss of 90 Da clearly reveal the 1-4 linkage of the reducing end in cellotriose (Table 2.2). The 1-4 linkage between the first and second ring (non-reducing end) can also be clearly obtained by the major consecutive losses from the negatively charged disaccharide moiety at m/z 341 resulting from the glucose unit loss from the reducing end in cellotriose. These consecutive losses are: 60 Da (peak at m/z 281), 78 Da (peak at m/z 263) and 162 Da (peak at m/z 179), together with the absence of a peak corresponding to loss of 90 Da. The β anomeric configuration of these two 1-4 linkages in cellotriose can be safely assigned since the relative abundances of both m/z 263:281 and m/z 425:443 are larger than unity, which is characteristic of the β anomeric configuration with 1-4 linkage (Table 2.2).

The negative ion MALDI-PSD mass spectrum of the chloride adduct of maltotriose (Glcα1-4Glcα1-4Glc) (**25**) (Figure 2.7c) is similar to that of cellotriose (Figure 2.7b). The two 1-

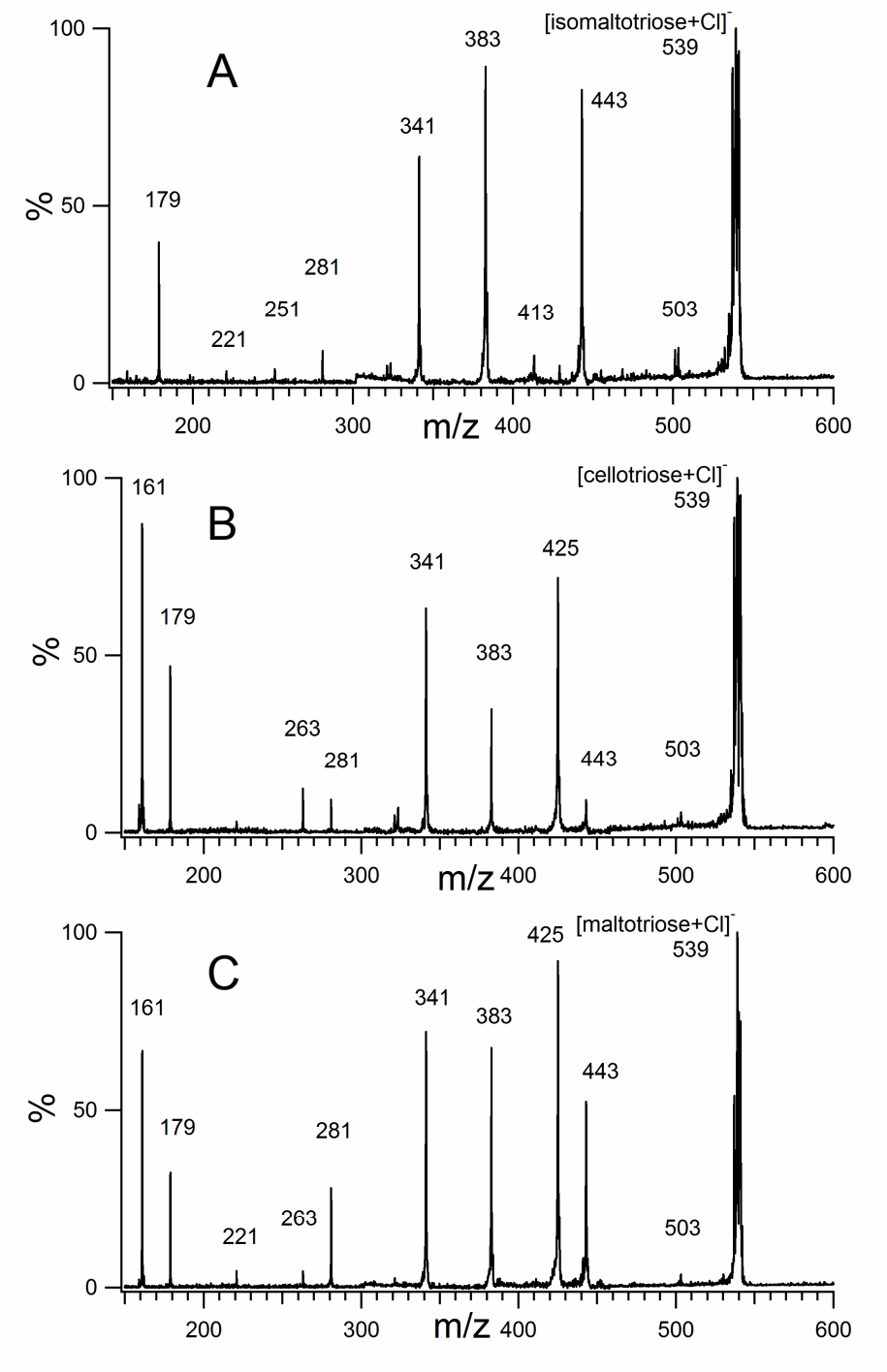

Figure 2.7. Negative ion PSD of chloride adducts of oligosaccharides. (a) isomaltotriose (Glcα1-6Glcα1-6Glc); (b) cellotriose (Glcβ1-4Glcβ1-4Glc); (c) maltotriose (Glcα1-4Glcα1-4Glc).

4 linkages can be determined as was done above. The α anomeric configuration between the first and second ring (non-reducing end) in maltotriose can be safely assigned since the relative abundance of m/z 263:281 is smaller than unity, which is characteristic of the β anomeric configuration with 1-4 linkage (Table 2.2). However, the relative ion abundance of m/z 425 vs m/z 443 is larger than unity, which implies β anomeric configuration with 1-4 linkage and fails to show the correct α configuration of the reducing end 1-4 linkage in maltotriose. Careful review of the spectra reveals that the relative abundance of m/z 425 vs m/z 443 is much closer to unity in maltotriose (Figure 2.7c) than that in cellotriose (Figure 2.7b).

The negative ion MALDI-PSD mass spectrum of the chloride adduct of panose (Glcα1-6Glcα1-4Glc) (**26**) is reported in Figure 2.8a. The major losses from the $[M - H]^-$ ion at m/z 503: 60 Da (m/z 443), 78 Da (m/z 425) and 162 Da (m/z 341), together with the absence of peaks corresponding to loss of 90 Da clearly reveal the 1-4 linkage of the reducing end in panose (Table 2.2). The 1-6 linkage type between the first and second ring (non-reducing end) in panose can also be clearly obtained by the major consecutive losses from the disaccharide moiety at m/z 341 resulting from the glucose unit loss from the reducing end. These consecutive losses are: 60 Da (m/z 281), 90 Da (m/z 251), 120 Da (m/z 221) and 162 Da (m/z 179) together with the absence of a peak corresponding to loss of 78 Da. The α anomeric configuration of the 1-6 linkage can be safely assigned since the relative abundance of m/z 251:281 is smaller than unity, which is characteristic of the α anomeric configuration with 1-6 linkage (Table 2.2). Similar to what happens in cellotriose, the relative abundance of m/z 425 vs m/z 443 in panose also fails to show characteristics of the α anomeric configuration with a 1-4 linkage of the reducing end. In this case, the relative abundance of m/z 425:443 deviates far from unity in panose (Figure 2.8a).

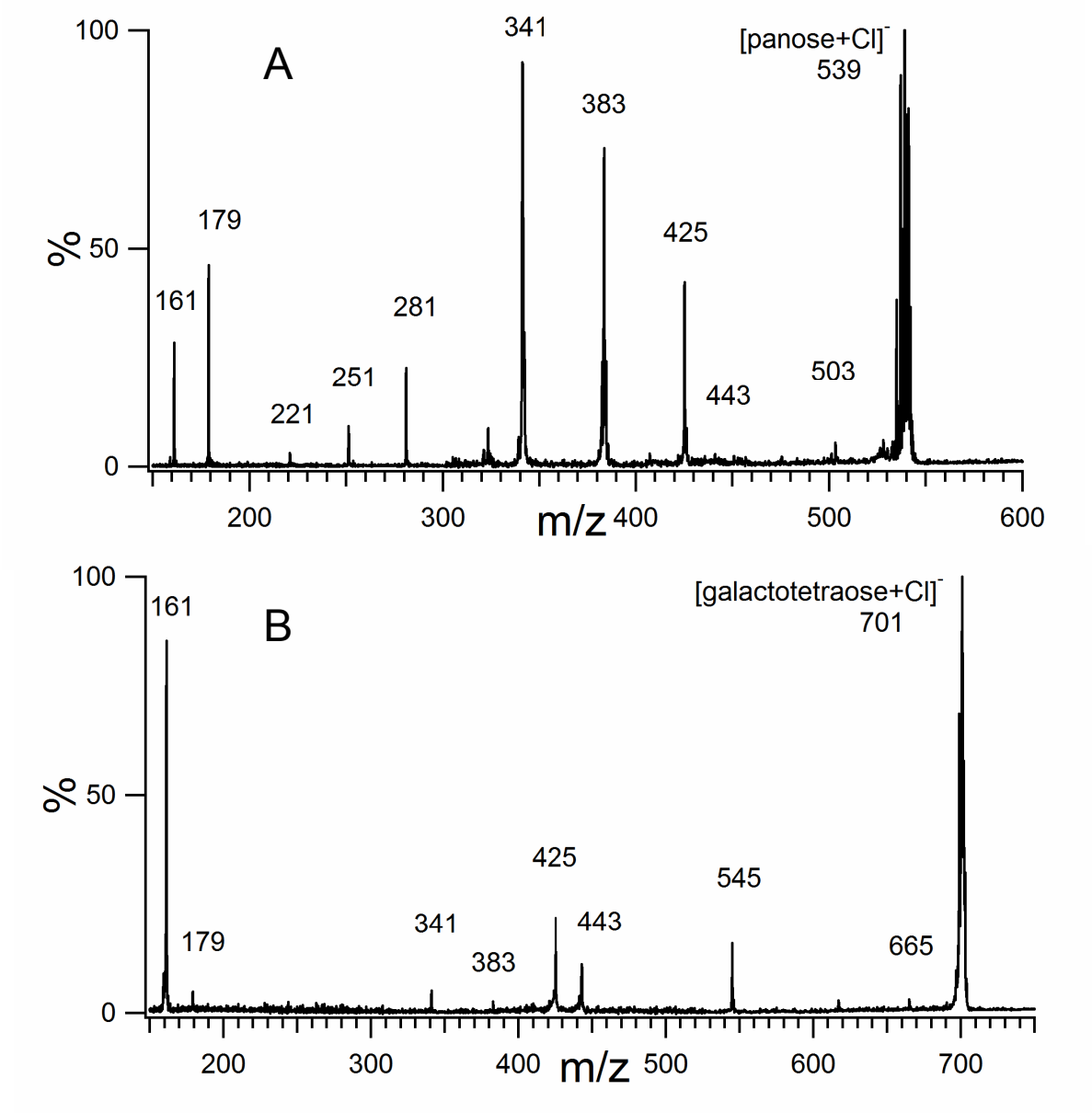

Figure 2.8. Negative ion PSD of chloride adducts of oligosaccharides. (a) panose (Glcα1-6Glcα1-4Glc); (b) 3α, 4β, 3α-galactotetraose (Galα1-3Galβ1-4Galα1-3Gal).

The negative ion MALDI-PSD mass spectrum of the chloride adducts of 3α, 4β, 3α-galactotetraose (Galα1-3Galβ1-4Galα1-3Gal) (**27**) appears in Figure 2.8b. The identity of the 1-3 linkage of the reducing end in galactotetraose is only supported by one major loss of 120 Da (m/z 545) from the $[M - H]^-$ ion at m/z 665. In PSD of chloride adducts of 1-3 linked disaccharides (laminaribiose and nigerose), only one cross-ring fragment via loss of 120 is observed (Figures 2.4a and 2.4b). The major losses from the negatively charged trisaccharide moiety at m/z 503 resulting from one galactose unit loss from the reducing end in galactotetraose, of 60 Da (m/z 443), 78 Da (m/z 425) and 162 Da (m/z 341), together with the absence of a peak corresponding to loss of 90 Da clearly reveal the 1-4 linkage between the second and third ring in galactotetraose (Table 2.2). The 1-3 linkage type between the first and second ring (non-reducing end) in this galactotetraose can also be obtained by the major losses of 162 Da (peak at m/z 179) and 180 Da (peak at m/z 161) from the negatively charged disaccharide moiety at m/z 341 resulting from two galactose units loss from the reducing end in galactotetraose. In this case, the cross-ring fragment at m/z 221 is not observable. The α anomeric configuration between the first and second ring (non-reducing end) in this galactotetraose can be determined by the relative abundance of m/z 161 vs m/z 179 which is much closer to that of nigerose (Figure 2.4b). The larger than unity relative abundance of m/z 425:443 is consistent with the β anomeric configuration with a 1-4 linkage (Table 2.2), clearly reveals the β anomeric configuration between rings 2 and 3 in galactotetraose. The anomeric configuration of the 1-3 linkage of the reducing end in galactotetraose cannot be determined because of the lack of pertinent fragmentations.

It appears that for the α anomeric configuration with 1-6 linkage and the β anomeric configuration with 1-4 linkage other than at the non-reducing end, the relative peak abundances of diagnostic fragments still hold and the differences exaggerate in both cases. For the α anomeric configuration with 1-4 linkage not in the non-reducing end, the relative peak abundances of diagnostic fragments flip and vary significantly, in ways that are quite different from that of β anomeric configuration with 1-4 linkage: relative ion abundances of m/z 443:425 are too low in panose (almost zero) (Figure 2.8a) and much higher in maltotriose (Figure 2.7c) than that of cellotriose (Figure 2.7b).

2.4 Conclusions

Various anions can form anionic adducts with oligosaccharides in negative ion MALDI-MS. Employing negative ion MALDI in the presence of various anions, weakly acidic and neutral oligosaccharides can form $[M + anion]^-$ adducts in varying degrees of preference to $[M - H]^-$. The anion attachment approach provides a simple means to simultaneously analyze neutral and acidic carbohydrates without switching the instrument polarity.

Contrary to common opinion that relative peak intensities are not generally reliable in linear reflectron PSD, we demonstrate that the relative peak intensities of the oligosaccharide fragment peaks intentionally acquired within the same PSD segment are rather stable, even if the laser intensities vary greatly and the target crystals may vary substantially in shape and quality. Our proposed characteristic neutral losses in MALDI-PSD mass spectra of the chloride adducts of neutral oligosaccharides and the relative ion abundances of selected diagnostic fragment pairs allow simultaneous determination of both linkage information and anomeric configurations of the oligosaccharides.

Competitive fragmentation pathways are revealed and rationalized in PSD processes of chloride adducts of oligosaccharides. For specific glycosidic linkage types, PSD spectra of oligosaccharides with the same anomeric configuration show the same trend of relative ion abundance for the diagnostic fragment peaks, independent of monosaccharide structure. It strongly indicates that the fragmentation pathways observed in negative ion PSD spectra are largely affected by the anomeric configuration between the monosaccharide rings for the particular linkage positions. It becomes clear that differentiating anomeric configuration of glycosidic bonds is viable by comparing relative peak intensities of diagnostic peaks in negative ion PSD via anion attachment. The fragmentation profiles and relative peak abundance in PSD spectra are expected to present important hints in determining the glycosidic linkage types and anomeric configuration of more complex glycoconjugates. The potential usage of MALDI linear reflectron TOF MS in stereoisomeric chemistry thus has been greatly expanded. Considering the popularity of normal MALDI-TOF MS world-wide and the fact it will remain a major workhorse in the near future, our results will hopefully inspire more interest in PSD analysis of glycoconjugates.

2.5 References

1. Bertozzi, C. R.; Kiessling, L. L., Chemical glycobiology. *Science* **2001,** 291, (5512), 2357-2364.
2. Hellerqvist, C. G., *Methods in Enzymology*. Academic Press: San Diego, 1990; Vol. 1993, p 554-573.
3. Aspinall, G. O., *The Polysaccharides*. Academic Press: New York, 1982; Vol. 1.
4. Dwek, R. A.; Edge, C. J.; Harvey, D. J.; Wormald, M. R.; Parekh, R. B., Analysis of Glycoprotein-Associated Oligosaccharides. *Annual Review of Biochemistry* **1993,** 62, 65-100.
5. Schulten, H. R., Biochemical, Medical, and Environmental Applications of Field-Ionization and Field-Desorption Mass-Spectrometry. *International Journal of Mass Spectrometry and Ion Processes* **1979,** 32, (2-3), 97-283.

6. Cerny, R. L.; Tomer, K. B.; Gross, M. L., Desorption Ionization Combined with Tandem Mass-Spectrometry - Advantages for Investigating Complex Lipids, Disaccharides and Organometallic Complexes. *Organic Mass Spectrometry* **1986,** 21, (10), 655-660.
7. Coates, M. L.; Wilkins, C. L., Laser Desorption Fourier-Transform Mass-Spectra of Malto-Oligosaccharides. *Biomedical Mass Spectrometry* **1985,** 12, (8), 424-428.
8. Lam, Z.; Comisarow, M. B.; Dutton, G. G. S., Structural and Reaction Assignments for Some Common Polysaccharides Using Laser Desorption Ionization Fourier-Transform Ion-Cyclotron Resonance Spectroscopy. *Analytical Chemistry* **1988,** 60, (20), 2304-2306.
9. Domon, B.; Costello, C. E., Structure Elucidation of Glycosphingolipids and Gangliosides Using High-Performance Tandem Mass-Spectrometry. *Biochemistry* **1988,** 27, (5), 1534-1543.
10. Dell, A.; Taylor, G. W., High-Field-Magnet Mass-Spectrometry of Biological Molecules. *Mass Spectrometry Reviews* **1984,** 3, (3), 357-394.
11. Dell, A., Preparation and Desorption Mass-Spectrometry of Permethyl and Peracetyl Derivatives of Oligosaccharides. *Methods in Enzymology* **1990,** 193, 647-660.
12. Dallinga, J. W.; Heerma, W., Positive-Ion Fast-Atom-Bombardment Mass-Spectrometry of Some Small Oligosaccharides. *Biological Mass Spectrometry* **1991,** 20, (3), 99-108.
13. Teesch, L. M.; Adams, J., Metal-Ions as Special Reagents in Analytical Mass-Spectrometry. *Organic Mass Spectrometry* **1992,** 27, (9), 931-943.
14. Zhou, Z. R.; Ogden, S.; Leary, J. A., Linkage Position Determination in Oligosaccharides - Ms/Ms Study of Lithium-Cationized Carbohydrates. *Journal of Organic Chemistry* **1990,** 55, (20), 5444-5446.
15. Hofmeister, G. E.; Zhou, Z.; Leary, J. A., Linkage Position Determination in Lithium-Cationized Disaccharides - Tandem Mass-Spectrometry and Semiempirical Calculations. *Journal of the American Chemical Society* **1991,** 113, (16), 5964-5970.
16. Staempfli, A.; Zhou, Z. R.; Leary, J. A., Gas-Phase Dissociation Mechanisms of Dilithiated Disaccharides - Tandem Mass-Spectrometry and Semiempirical Calculations. *Journal of Organic Chemistry* **1992,** 57, (13), 3590-3594.
17. Smith, G.; Leary, J. A., Differentiation of stereochemistry of glycosidic bond configuration: Tandem mass spectrometry of diastereomeric cobalt-glucosyl-glucose disaccharide complexes. *Journal of the American Society for Mass Spectrometry* **1996,** 7, (9), 953-957.
18. Garozzo, D.; Giuffrida, M.; Impallomeni, G.; Ballistreri, A.; Montaudo, G., Determination of Linkage Position and Identification of the Reducing End in Linear Oligosaccharides by Negative-Ion Fast Atom Bombardment Mass-Spectrometry. *Analytical Chemistry* **1990,** 62, (3), 279-286.
19. Dallinga, J. W.; Heerma, W., Reaction-Mechanism and Fragment Ion Structure Determination of Deprotonated Small Oligosaccharides, Studied by Negative-Ion Fast-Atom-Bombardment (Tandem) Mass-Spectrometry. *Biological Mass Spectrometry* **1991,** 20, (4), 215-231.
20. Carroll, J. A.; Ngoka, L.; Beggs, C. G.; Lebrilla, C. B., Liquid Secondary-Ion Mass-Spectrometry Fourier-Transform Mass-Spectrometry of Oligosaccharide Anions. *Analytical Chemistry* **1993,** 65, (11), 1582-1587.
21. Carroll, J. A.; Willard, D.; Lebrilla, C. B., Energetics of Cross-Ring Cleavages and Their Relevance to the Linkage Determination of Oligosaccharides. *Analytica Chimica Acta* **1995,** 307, (2-3), 431-447.

22. Fura, A.; Leary, J. A., Differentiation of Ca2+-Coordinated and Mg2+-Coordinated Branched Trisaccharide Isomers - an Electrospray-Ionization and Tandem Mass-Spectrometry Study. *Analytical Chemistry* **1993,** 65, (20), 2805-2811.
23. Garozzo, D.; Impallomeni, G.; Spina, E.; Green, B. N.; Hutton, T., Linkage Analysis in Disaccharides by Electrospray Mass-Spectrometry. *Carbohydrate Research* **1991,** 221, 253-257.
24. Mulroney, B.; Traeger, J. C.; Stone, B. A., Determination of Both Linkage Position and Anomeric Configuration in Underivatized Glucopyranosyl Disaccharides by Electrospray Mass-Spectrometry. *Journal of Mass Spectrometry* **1995,** 30, (9), 1277-1283.
25. Zhu, J. H.; Cole, R. B., Ranking of gas-phase acidities and chloride affinities of monosaccharides and linkage specificity in collision-induced decompositions of negative ion electrospray-generated chloride adducts of oligosaccharides. *Journal of the American Society for Mass Spectrometry* **2001,** 12, (11), 1193-1204.
26. Jiang, Y. J.; Cole, R. B., Oligosaccharide analysis using anion attachment in negative mode electrospray mass spectrometry. *Journal of the American Society for Mass Spectrometry* **2005,** 16, (1), 60-70.
27. Mulroney, B.; Peel, J. B.; Traeger, J. C., Theoretical study of deprotonated glucopyranosyl disaccharide fragmentation. *Journal of Mass Spectrometry* **1999,** 34, (8), 856-871.
28. Zaia, J., Mass spectrometry of oligosaccharides. *Mass Spectrometry Reviews* **2004,** 23, (3), 161-227.
29. Harvey, D. J., Matrix-assisted laser desorption/ionization mass spectrometry of carbohydrates. *Mass Spectrometry Reviews* **1999,** 18, (6), 349-450.
30. Dell, A.; Morris, H. R., Glycoprotein structure determination mass spectrometry. *Science* **2001,** 291, (5512), 2351-2356.
31. Penn, S. G.; Cancilla, M. T.; Lebrilla, C. B., Collision-induced dissociation of branched oligosaccharide ions with analysis and calculation of relative dissociation thresholds. *Analytical Chemistry* **1996,** 68, (14), 2331-2339.
32. Powell, A. K.; Harvey, D. J., Stabilization of sialic acids in N-linked oligosaccharides and gangliosides for analysis by positive ion matrix-assisted laser desorption ionization mass spectrometry. *Rapid Communications in Mass Spectrometry* **1996,** 10, (9), 1027-1032.
33. Nonami, H.; Fukui, S.; ErraBalsells, R., beta-carboline alkaloids as matrices for matrix-assisted ultraviolet laser desorption time-of-flight mass spectrometry of proteins and sulfated oligosaccharides: A comparative study using phenylcarbonyl compounds, carbazoles and classical matrices. *Journal of Mass Spectrometry* **1997,** 32, (3), 287-296.
34. Nonami, H.; Tanaka, K.; Fukuyama, Y.; Erra-Balsells, R., beta-carboline alkaloids as matrices for UV-matrix-assisted laser desorption/ionization time-of-flight mass spectrometry in positive and negative ion modes. Analysis of proteins of high molecular mass, and of cyclic and acyclic oligosaccharides. *Rapid Communications in Mass Spectrometry* **1998,** 12, (6), 285-296.
35. Nonami, H.; Wu, F. Y.; Thummel, R. P.; Fukuyama, Y.; Yamaoka, H.; Erra-Balsells, R., Evaluation of pyridoindoles, pyridylindoles and pyridylpyridoindoles as matrices for ultraviolet matrix- assisted laser desorption/ionization time-of-flight mass spectrometry. *Rapid Communications in Mass Spectrometry* **2001,** 15, (23), 2354-2373.

36. Wong, A. W.; Cancilla, M. T.; Voss, L. R.; Lebrilla, C. B., Anion dopant for oligosaccharides in matrix-assisted laser desorption/ionization mass spectrometry. *Analytical Chemistry* **1999,** 71, (1), 205-211.
37. Cai, Y.; Jiang, Y. J.; Cole, R. B., Anionic adducts of oligosaccharides by matrix-assisted laser desorption/ionization time-of-flight mass spectrometry. *Analytical Chemistry* **2003,** 75, (7), 1638-1644.
38. Yamagaki, T.; Suzuki, H.; Tachibana, K., In-source and postsource decay in negative-ion matrix-assisted laser desorption/ionization time-of-flight mass spectrometry of neutral oligosaccharides. *Analytical Chemistry* **2005,** 77, (6), 1701-1707.
39. Yamagaki, T.; Suzuki, H.; Tachibana, K., Semiquantitative analysis of isomeric oligosaccharides by negative-ion mode UV-MALDI TOF postsource decay mass spectrometry and their fragmentation mechanism study at N-acetylhexosamine. *Journal of Mass Spectrometry* **2006,** 41, (4), 454-462.
40. Yamagaki, T.; Suzuki, H.; Tachibana, K., A comparative study of the fragmentation of neutral lactooligosaccharides in negative-ion mode by UV-MALDI-TOF and UV-MALDI ion-trap/TOF mass spectrometry. *Journal of the American Society for Mass Spectrometry* **2006,** 17, (1), 67-74.
41. Spengler, B.; Kirsch, D.; Kaufmann, R., Metastable Decay of Peptides and Proteins in Matrix-Assisted Laser-Desorption Mass-Spectrometry. *Rapid Communications in Mass Spectrometry* **1991,** 5, (4), 198-202.
42. Spengler, B.; Kirsch, D.; Kaufmann, R.; Jaeger, E., Peptide Sequencing by Matrix-Assisted Laser-Desorption Mass-Spectrometry. *Rapid Communications in Mass Spectrometry* **1992,** 6, (2), 105-108.
43. Spengler, B.; Kirsch, D.; Kaufmann, R.; Lemoine, J., Structure-Analysis of Branched Oligosaccharides Using Post-Source Decay in Matrix-Assisted Laser-Desorption Ionization Mass-Spectrometry. *Organic Mass Spectrometry* **1994,** 29, (12), 782-787.
44. Harvey, D. J.; Naven, T. J. P.; Kuster, B.; Bateman, R. H.; Green, M. R.; Critchley, G., Comparison of fragmentation modes for the structural determination of complex oligosaccharides ionized by matrix-assisted laser desorption/ionization mass spectrometry. *Rapid Communications in Mass Spectrometry* **1995,** 9, (15), 1556-1561.
45. Gibson, B. W.; Engstrom, J. J.; John, C. M.; Hines, W.; Falick, A. M., Characterization of bacterial lipooligosaccharides by delayed extraction matrix-assisted laser desorption ionization time-of-flight mass spectrometry. *Journal of the American Society for Mass Spectrometry* **1997,** 8, (6), 645-658.
46. Fukuyama, Y.; Ciancia, M.; Nonami, H.; Cerezo, A. S.; Erra-Balsells, R.; Matulewicz, M. C., Matrix-assisted ultraviolet laser-desorption ionization and electrospray-ionization time-of-flight mass spectrometry of sulfated neocarrabiose oligosaccharides. *Carbohydrate Research* **2002,** 337, (17), 1553-1562.
47. Talbo, G.; Mann, M., Aspects of the sequencing of carbohydrates and oligonucleotides by matrix-assisted laser desorption/ionization post-source decay. *Rapid Communications in Mass Spectrometry* **1996,** 10, (1), 100-103.
48. Zhu, J. H.; Cole, R. B., Formation and decompositions of chloride adduct ions, [M+Cl](-), in negative ion electrospray ionization mass spectrometry. *Journal of the American Society for Mass Spectrometry* **2000,** 11, (11), 932-941.
49. Cai, Y.; Cole, R. B., Stabilization of anionic adducts in negative ion electrospray mass spectrometry. *Analytical Chemistry* **2002,** 74, (5), 985-991.

50. Cai, Y.; Concha, M. C.; Murray, J. S.; Cole, R. B., Evaluation of the role of multiple hydrogen bonding in offering stability to negative ion adducts in electrospray mass spectrometry. *Journal of the American Society for Mass Spectrometry* **2002,** 13, (12), 1360-1369.
51. Harvey, D. J., Fragmentation of negative ions from carbohydrates: Part 1. Use of nitrate and other anionic adducts for the production of negative ion electrospray spectra from N-linked carbohydrates. *Journal of the American Society for Mass Spectrometry* **2005,** 16, (5), 622-630.
52. Harvey, D. J., Fragmentation of negative ions from carbohydrates: Part 2. Fragmentation of high-mannose N-linked glycans. *Journal of the American Society for Mass Spectrometry* **2005,** 16, (5), 631-646.
53. Harvey, D. J., Fragmentation of negative ions from carbohydrates: Part 3. Fragmentation of hybrid and complex N-linked glycans. *Journal of the American Society for Mass Spectrometry* **2005,** 16, (5), 647-659.
54. Guan, B.; Cole, R. B., Differentiation of Both Linkage Position and Anomeric Configuration in Underivatized Glucopyranosyl Disaccharides by Anion Attachment with Post-Source Decay in MALDI Linear-Field Reflectron TOFMS. *Rapid Communications in Mass Spectrometry*, In Press.
55. Yamagaki, T.; Nakanishi, H., Distinguishing of linkage isomers of lactotetra oligosaccharides by using the relative ion intensity analysis of post-source decay fragment ions in curved-field reflectron matrix-assisted laser desorption/ionization time-of-flight mass spectrometry. *Analytical Sciences* **2001,** 17, (1), 83-87.
56. Yamagaki, T.; Nakanishi, H., Ion intensity analysis of post-source decay fragmentation in curved-field reflectron matrix-assisted laser desorption/ionization time-of-flight mass spectrometry of carbohydrates: For structural characterization of glycosylation in proteome analysis. *Proteomics* **2001,** 1, (2), 329-339.
57. Yamagaki, T.; Nakanishi, H., Post-source decay fragmentation analyses of linkage isomers of Lewis-type oligosaccharides in curved-field reflectron matrix-assisted laser desorption/ionization time-of-flight mass spectrometry: combined in-source decay/post-source decay experiments and relative ion abundance analysis. *Journal of Mass Spectrometry* **2000,** 35, (11), 1300-1307.
58. Yamagaki, T.; Nakanishi, H., Influence of acceleration voltages on relative ion intensities in the post-source decay fragmentation of isomeric cyclic oligosaccharides by matrix-assisted laser desorption/ionization time-of-flight mass spectrometry. *Rapid Communications in Mass Spectrometry* **1999,** 13, (21), 2199-2203.
59. Yamagaki, T.; Nakanishi, H., Influence of stereoisomeric glucose, galactose and mannose residues on fragmentation at their glycosidic linkages in post-source decay fragment analyses for oligosaccharides using matrix-assisted laser desorption/ionization time-of-flight mass spectrometry. *Rapid Communications in Mass Spectrometry* **1998,** 12, (16), 1069-1074.
60. Yamagaki, T.; Mitsuishi, Y.; Nakanishi, H., Influence of different glycosidic linkages on relative ion intensities in post-source decay fragmentation of a xyloglucan heptaoligosaccharide using matrix-assisted laser desorption/ionization time-of-flight mass spectrometry. *Rapid Communications in Mass Spectrometry* **1998,** 12, (6), 307-311.
61. Yamagaki, T.; Ishizuka, Y.; Kawabata, S.; Nakanishi, H., Analysis of glycosidic linkages in saccharide compounds by post-source decay fragment methods in matrix-assisted laser

desorption/ionization time-of-flight mass spectroscopy. *Rapid Communications in Mass Spectrometry* **1997,** 11, (5), 527-531.
62. Yamagaki, T.; Ishizuka, Y.; Kawabata, S.; Nakanishi, H., Post-source decay fragment spectra of cyclomalto-octaose and branched cyclomalto-hexaose by matrix-assisted laser desorption/ionization time-of-flight mass spectrometry. *Rapid Communications in Mass Spectrometry* **1996,** 10, (15), 1887-1890.

Chapter 3: Characterization of Synthesized Titanium Oxide Nanoclusters by MALDI-TOF Mass Spectrometry

3.1 Introduction

Titania (i. e. species composed of titanium and oxygen) represents an important material which is used widely in photocatalysis[1-3], sensor technology[4], optical coatings[5], and pigments[6]. It has been used for the destruction of toxic organic compounds and microorganisms such as bacteria and viruses, in addition to its applications in purification of polluted air and wastewaters[2, 3]. Titania's advantages over other materials are that it is relatively inexpensive, non-toxic, and it exhibits a high photo-stability in adverse environments, among other desirable surface properties. It is also being used in low-cost, highly efficient dye-sensitized solar cells[7, 8]. Titania itself has a relatively large band gap and is unable to absorb a significant part of the visible light spectrum. But when coupled with suitable charge transfer dyes, it can quantitatively convert visible light photons into electric current[7, 8]. It has been widely used as a model transition metal oxide due to its rather simple electronic structure which is characterized by a filled valence band and an empty conduction band[9].

Cluster models have been frequently used in theoretical calculations of titanium dioxide bulk or surface properties[10-12]. However, for experimental study of titania clusters produced by evaporation and sputtering, it is difficult to achieve control over particle size, size distribution, and shape because the reactions of molecular precursors require rather high temperatures. There are many reports on isolated titanium (IV) nanoclusters produced by wet chemical methods[13, 14], but, to our knowledge, there are no reports on isolated stable nanoclusters with diameters less than 1 nm.

High-temperature organic solution phase synthesis is a very promising method to develop many nanocrystals with controlled shapes and sizes. In this method, one can control the growth of the nanoparticles by choosing the proper capping ligand. We seek to produce titania clusters by reaction of titanium alkoxide in a non-polar solvent, along with an air- and water-free environment, because hydrolysis of titanium alkoxide is difficult to control if there are even trace amounts of water.

Both transmission electron microscopy (TEM) and powder X-ray Diffraction (XRD) analyses are typically employed to measure the shapes, sizes, and size distributions of nanocrystal samples. However, standard TEM instrumentation is not so readily adapted to the analysis of nanoparticles that are less than 1 nm in size. First, it is statistically insignificant to infer average size and a size distribution for the ensemble by examining only a tiny region in a TEM image because the chosen areas of the grid may not be representative of the ensemble[15]. Second, it is not easy to definitively determine the boundary between the cluster and grid on a TEM image when cluster sizes are smaller than about 2-3 nm[15]. Moreover, changes in the size of clusters may occur during the drying process, possibly caused by, but not limited to, aggregation and chemical changes (e.g., oxidation or hydration). Fitting XRD data to the Scherer equation to calculate cluster size is of limited accuracy, because the Scherer equation strictly applies only to uniformly shaped, noninteracting nanoparticles with an assigned distribution of sizes[15, 16].

Mass spectrometry (MS) represents an alternative means to determine sizes and size distributions of nanoparticles by obtaining accurate mass information. The mass spectra of nanoparticles will provide size information through calculation from the known particle density values. Also, valuable structural information may be obtained concerning nanoparticle composition through knowledge of fragmentation pathways, and the relative abundances of

nanoparticle components. Beyond its widely acknowledged applications in biological, molecular and polymeric systems, MS has been successfully used to characterize various nanoparticles such as fullerences[17, 18], silica clusters[19], metal chalcogenide clusters[20-24], gold nanocrystals[25-28] and several other nanomaterials[29-33].

Electrospray (ES) ionization[34, 35] coupled with tandem MS (MS/MS) has become a powerful tool for analyses of nanoparticle composition[22-24, 30, 36-38] provided that the nanoparticle can be suspended in a solvent of moderate polarity without decomposition or other reactions. Laser desorption/ionization (LDI) TOF-MS has also been used to record mass spectra and determine specific atomic compositions of large gold nanocrystals with masses of tens of kilo-Daltons without the use of matrixes[25-28]. In sharp contrast, in the absence of suitable matrixes, biological polymers like proteins, DNAs and carbohydrates, as well as large (e.g., 10,000 Da) synthetic polymers tend to fragment under laser irradiation, thus making it very problematic to observe intact molecular ions. However, matrix-assisted laser desorption/ionization (MALDI) can be used for fast analyses of sizes and size distributions of nanoparticles when suitable matrixes are found. Although not truly tandem MS, post-source decay (PSD)[39, 40] can provide additional valuable information about the structure of analytes observed by MALDI-TOF. Because TiO_2 has been used as a photo-catalyst for killing bacteria, but bactericidal efficiency has been shown to be dependent on the size of the nanoparticles present, the current study seeks to determine sizes and size distributions of ultra small TiO_2 nanoparticles using MALDI-TOF and LDI-TOF mass spectrometry with PSD analysis. This report presents results of our synthesis and characterization of ultra small TiO_2 nanoparticles (i.e., < 1 nm).

3.2 Experimental

3.2.1 Materials

All chemicals were purchased and used as received without further purification. Distilled, de-ionized water (Milli-Q Systems, Millipore Corporation, Billerica, MA) was used throughout. Matrixes used in this experiment: dithranol, α-cyano-4-hydroxycinnamic acid (α-CHCA), 2,5-dihydroxybenzoic acid (DHB), or sinapinic acid were purchased from Aldrich Chemical (Milwaukee, WI, USA). Titanium tetrabutoxide ($Ti(OC_4H_9)_4$), trioctylamine ($[CH_3(CH_2)_7]_3N$), benzyl ether, toluene, methanol, and chloroform were also purchased from Aldrich Chemical (Milwaukee, WI, USA).

3.2.2 Nanoparticle Preparation

Titania clusters were prepared using titanium tetrabutoxide ($Ti(OC_4H_9)_4$) as the precursor and trioctylamine as the capping agent in a benzyl ether solvent with heating. Trioctylamine was chosen as the capping ligand because its 3-dimensional structure may prevent smaller clusters from aggregating to form larger particles. The synthesis experiment was carried out in a three-necked flask equipped with a condenser and an argon stream. Typically, 1 ml $Ti(OC_4H_9)_4$ and 1 ml trioctylamine were added into 10 ml hot benzyl ether at 563 K with stirring for 24 hours; the color of the solution changed gradually from yellow to dark red as the reaction continued. The size-selection process involved centrifugation using a pair of solvents (i.e., toluene and methanol) to get different sized TiO_2 clusters; the final products were re-dissolved in toluene. The term “raw nanoparticles” refers to precipitation without size-selection throughout this paper. After size selection, the cluster sample suspensions appeared red, except for the raw nanoparticles suspensions which were slightly gray. Although one could anticipate the formation of stoichiometric Ti_xO_{2x}, when clusters are formed, there is usually a slight deviation from this strict 1:2 stoichiometry.

3.2.3 XRD and TEM

XRD patterns were recorded using an x-ray diffractometer (CuKα, Philips X'pert systems, Natick, MA). The TiO_2 cluster suspensions were deposited onto a single Si substrate, and each diffraction pattern (2θ = 20 - 80 degrees) was scanned for 12 hours due to the relatively low signal-to-noise ratio of TiO_2 clusters. A JEOL-2010 (JEOL, Peabody, MA) transmission electron microscope (TEM) operating at an accelerating voltage of 200 kV was used to investigate the morphology of the raw clusters.

3.2.4 Mass Spectrometry

Mass spectra were acquired on an Applied Biosystems Voyager Elite MALDI-TOF mass spectrometer with delayed extraction (Applied Biosystems, Framingham, MA) equipped with a pulsed N_2 laser (λ = 337 nm). Either dithranol was used as the matrix, or no matrix at all was used, which implies Laser Desorption/Ionization (LDI) in the latter case. An extraction voltage of 20 kV was typically employed. Laser intensity was adjusted to just above the threshold energy for appearance of titanium-containing ions except in PSD experiments where the energy was 20-30% higher. All mass spectra were acquired in the positive reflectron mode employing delayed extraction. Each nanoparticle mass spectrum consists of an average of 50-100 traces. In preparation for MALDI, 3 μL of nanoparticle suspension was mixed with 3 μL of dithranol matrix in chloroform; then, 1 μL of the mixture was deposited onto the MALDI plate and allowed to air-dry. The diameters of the investigated particles were always smaller than the surface area illuminated by the laser beam, thus, data in mass spectra originate from many individual nanoparticles. The instrument was externally calibrated using monoisotopic peaks from the dithranol matrix (MH^+ at m/z 227.071) and from oxidized insulin chain B (MH^+ at m/z 3494.651); Angiotensin I was used for PSD calibration. Data processing was performed using IGOR Pro 4.07 (Wave Metrics Inc., Lake Oswego, OR).

3.3 Results and Discussions

When Ti_xO_{2x} clusters are formed, there is usually a small deviation from this exact stoichiometry, but for the purpose of this text, we will use the term "TiO_2" to represent the clusters. TiO_2 nanoparticles are usually produced by hydrolysis of organometallic compounds. During the hydrolysis process, it is very easy to incur aggregation to form larger particles. In our case, TiO_2 nanoclusters were produced by reaction of $Ti(OC_4H_9)_4$ in a thermal solvent system. Trioctylamine was chosen as the capping ligand because its bulky 3-dimensional structure may prevent smaller clusters from aggregating to form larger particles. Like most organometallic compounds, $Ti(OC_4H_9)_4$ is highly moisture-sensitive. The reaction was therefore carried out under an argon atmosphere. After reaction, post-treatment size-selection would allow tuning of the particle size and size distribution.

In the suspension of nanoparticles, the energetic barrier to aggregation caused by steric hindrance from capping ligands (such as trioctylamine used here) is strongly dependent on the energy of mixing between the tethered capping groups and the solvent. Introduction of a nonsolvent (methanol in this case), miscible with the original dispersing solvent (toluene), destabilizes the nanoparticle dispersions. The nanoparticles then "aggregate" and precipitate, leaving many of the synthetic by-products in solution. The resulting powders may be redispersed in a variety of solvents, e.g. alkanes and aromatics, if the capping ligands are well bound to the surface of the nanoparticles. By employing this treatment, fine tuning of the particle size and size-distribution can be achieved. After such size-selection, the resulting TiO_2 clusters (with capping ligands) were maintained in toluene where they exhibit good stability.

TEM images of the raw nanoparticles are shown in Fig 3.1(a); from these, we can estimate that the mean nanoparticles size is about 2.5 nm and that there are some elongated

nanocrystals produced as well. The length of these less predominant elongated nanocrystals is approximately 5 nm with widths of ~ 1-2 nm. Because of the projective nature of the TEM image, it is not straight-forward to deduce the exact percentage of elongated particles vs spherical ones. The high resolution micrograph (Fig 3.1(b)) clearly shows that the lattice plane along the growth direction of the nanocrystals is (001). After size selection, the cluster dimensions could not be determined by TEM because the employed TEM is not capable of adequate resolution. For particles with even smaller size (estimated to be less than 1 nm in our case), owing to the low contrast across the boundary between a cluster and the grid, high quality TEM images are challenging to obtain. The organic layer on cluster surfaces also affects the quality of TEM images. The organic groups at the cluster surface cannot be observed with electron beams, nor can the size of this organic group "shell" be determined[15].

TiO_2 has seven different polymorphic forms, four of which are found in nature. The three common natural crystalline forms are: anatase, rutile and brookite. All consist of octahedrally coordinated Ti cations arranged in edge sharing chains, but they differ in the number of shared edges and corners. The octahedra in anatase share four edges and four corners, whereas the rutile Ti octahedral shares two edges and six corners, while brookite Ti octahedral shares three edges and five corners[6, 41, 42]. Figure 3.2 shows the XRD patterns of TiO_2 raw nanoparticles (Curve A) and size-selected TiO_2 clusters (Curves B-D). According to the XRD data, all the peaks in curve A (raw nanoparticles) can be indexed as anatase TiO_2[43]. We estimated the raw anatase particle size using the Scherer equation[16]. On the basis of the (100) peak, the average particle size is 2.3 nm, whereas on the basis of the (200) peak, it is 2.5 nm. These estimations are in good agreement with the results from TEM observations except that there are some elongated nanocrystals observed in the TEM images. After size-selection, there are large differences between XRD

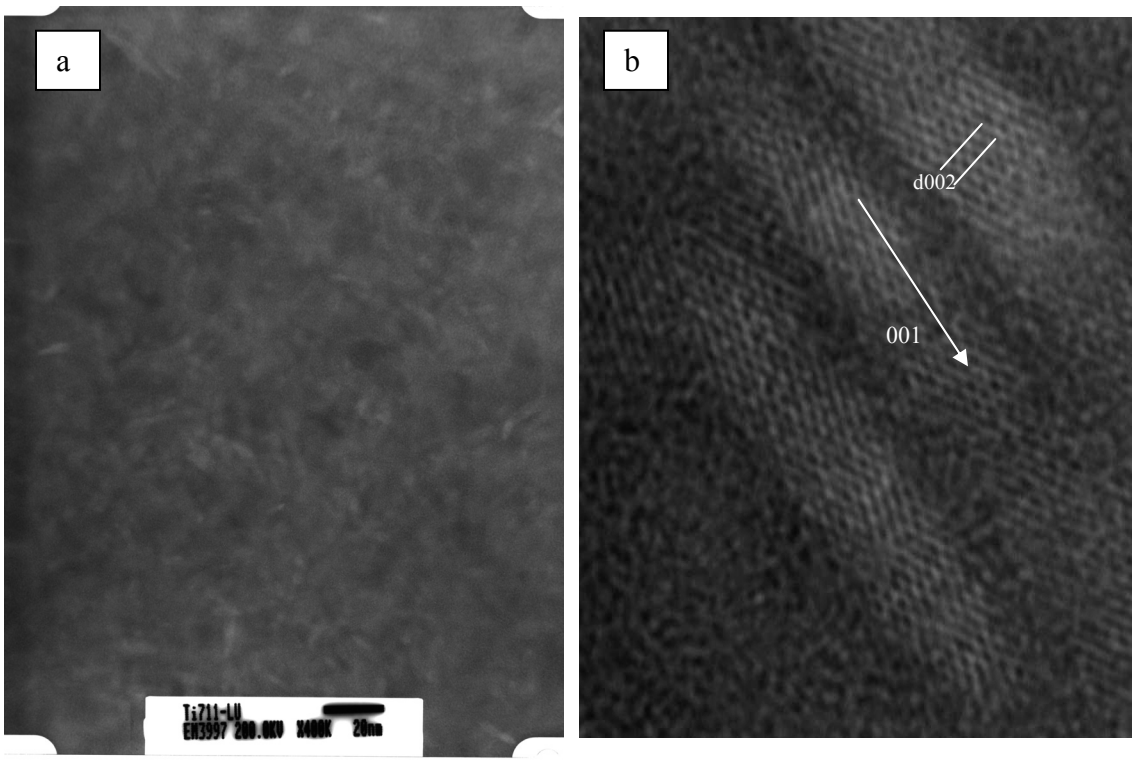

Figure 3.1. TEM images of anatase raw nanoparticles: (a) Low resolution TEM shows some elongated nanoparticles by ~5×1.5nm in size; (b)High resolution micrograph demonstrate the elongated nanoparticles growth along [001] direction.

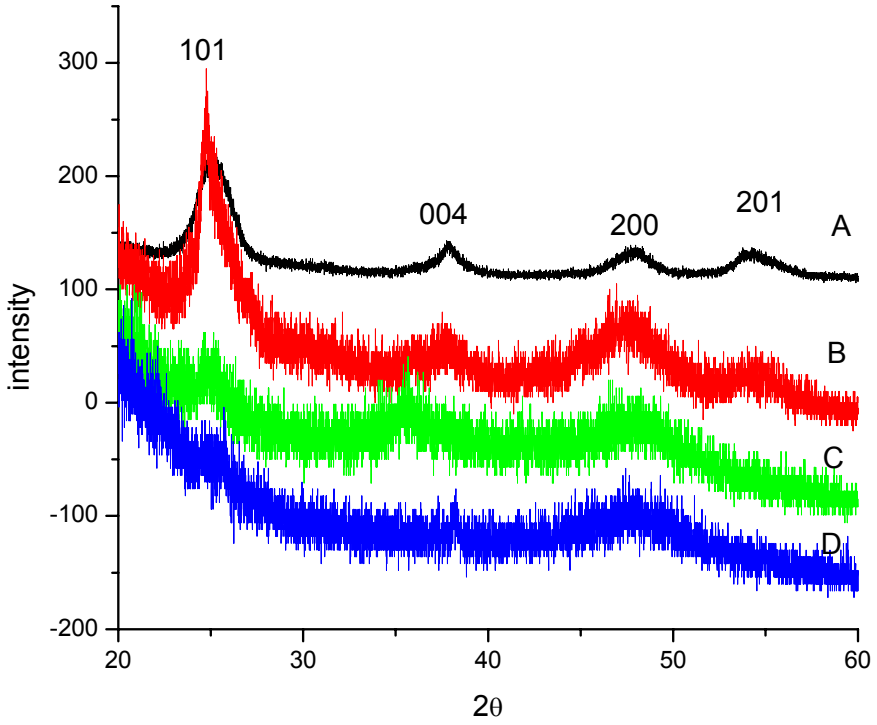

Figure 3.2. XRD patterns of Raw TiO_2 nanoparticles and Size-selected TiO_2 clusters: Curve A is the pattern of nanoparticles, which can be indexed as anatase, the size of the clusters decreases from curve B to curve D.

patterns. For curve B, the (200) peak becomes much broader compared with other peaks in this curve. However, the XRD pattern of curve B can still be confidently indexed as the anatase phase of TiO_2. The XRD patterns presented in curve C and curve D are extremely weak, peaks are broad, and the data are noisy. They are quite different from the XRD patterns of anatase and rutile, although the positions of the broad (200) peak maxima seem to coincide more with those of anatase. This suggests that long range ordering structures in the size-selected clusters do not exist, and that the solids are essentially X-ray amorphous[6]. This may be caused by the extremely high surface area-to-volume ratio. Experimental X-ray absorption fine structure (XAFS) data show that Ti-O bond lengths in nanocrystalline titanium dioxide are shorter than the bulk phase value of 1.94 Å and can be as low as 1.79 Å for surface atoms, resulting from Ti-OH bonding[44, 45]. It was also reported that the curvature of the surface causes a decrease in the coordination number of the titanium ion from the normal octahedral environment (six) to where it has a coordination number of four or five[44-46]. According to the simulation of Naicker et al.[47] for small nanoparticles, the bulk phase structural features of TiO_2 will exhibit decreased importance as the surface atoms make up a larger fraction of the total.

Initially, a limited effort was made to find appropriate matrixes that would allow us to obtain MALDI-TOF mass spectra of the size-selected clusters. However, the use of several commonly employed matrixes (i.e., α-cyano-4-hydroxycinnamic acid (α-CHCA), 2,5-dihydroxybenzoic acid (DHB), and sinapinic acid) failed to result in detection of titanium oxide ions; only matrix peaks were observed. In the presence of these organic acid matrixes, the titanium oxide nanoparticles appeared to clump together, which makes the usual functions of the MALDI matrix (i.e. isolation of analyte molecules and transfer of absorbed photon energy to analyte species) inefficient. Moreover, the use of methanol as solvent for these matrixes was

found to accelerate precipitation and aggregation (clumping) of the titanium oxides, further obscuring the ability to observe titanium oxide species in mass spectra.

The use of dithranol as the matrix, however, did yield signals representative of positively charged titanium oxide species. Unlike the above three organic acid matrixes, dithranol lacks a strongly acidic group. Matrix solutions were prepared by dissolving 10 mg of dithranol in 1 mL of dry chloroform without the use of methanol. Naturally occurring titanium is composed of five stable isotopes: ^{46}Ti (10.8%), ^{47}Ti (9.9%), ^{49}Ti (7.5%), ^{50}Ti (7.3%), with ^{48}Ti (73.8%) being the most abundant; this unique isotopic pattern facilitates the assignment of titanium-containing species. Using Laser Desorption/Ionization (LDI) without any matrix also gave signals corresponding to titanium oxide cations. This is in accordance with the fact that TiO_2 is a fairly strong UV absorber, and TiO_2 itself has been used as a matrix for MALDI experiments[48-50]. The observation of similar results by MALDI and LDI without the presence of a matrix has some precedent; similar behavior was observed when studying ferrite nanoparticles[29] and rhenium halide nanoparticles[51].

Numerous detected peaks in the spectra showed isotopic clusters characteristic of titanium-containing ions. Careful review of the isotopic patterns revealed that these titanium oxide species were uniformly singly charged. Above m/z 250, titanium isotopic peak patterns exhibited considerable overlap, thus making the spectra rather complicated to interpret. Figure 3.3 shows the isotopic distribution comparison of the m/z range from 440 to 455 centered at m/z 448. The top spectrum is the positive ion reflectron MS experimental result, the middle spectrum is the theoretical isotopic distribution of $Ti_6O_{10}^+$, and the bottom one is the theoretical isotopic distribution of Ti_6^+. The singly charged ions can be directly assigned from the experimental data due to the high resolution of the instrument in the reflectron mode used in this experiment. The

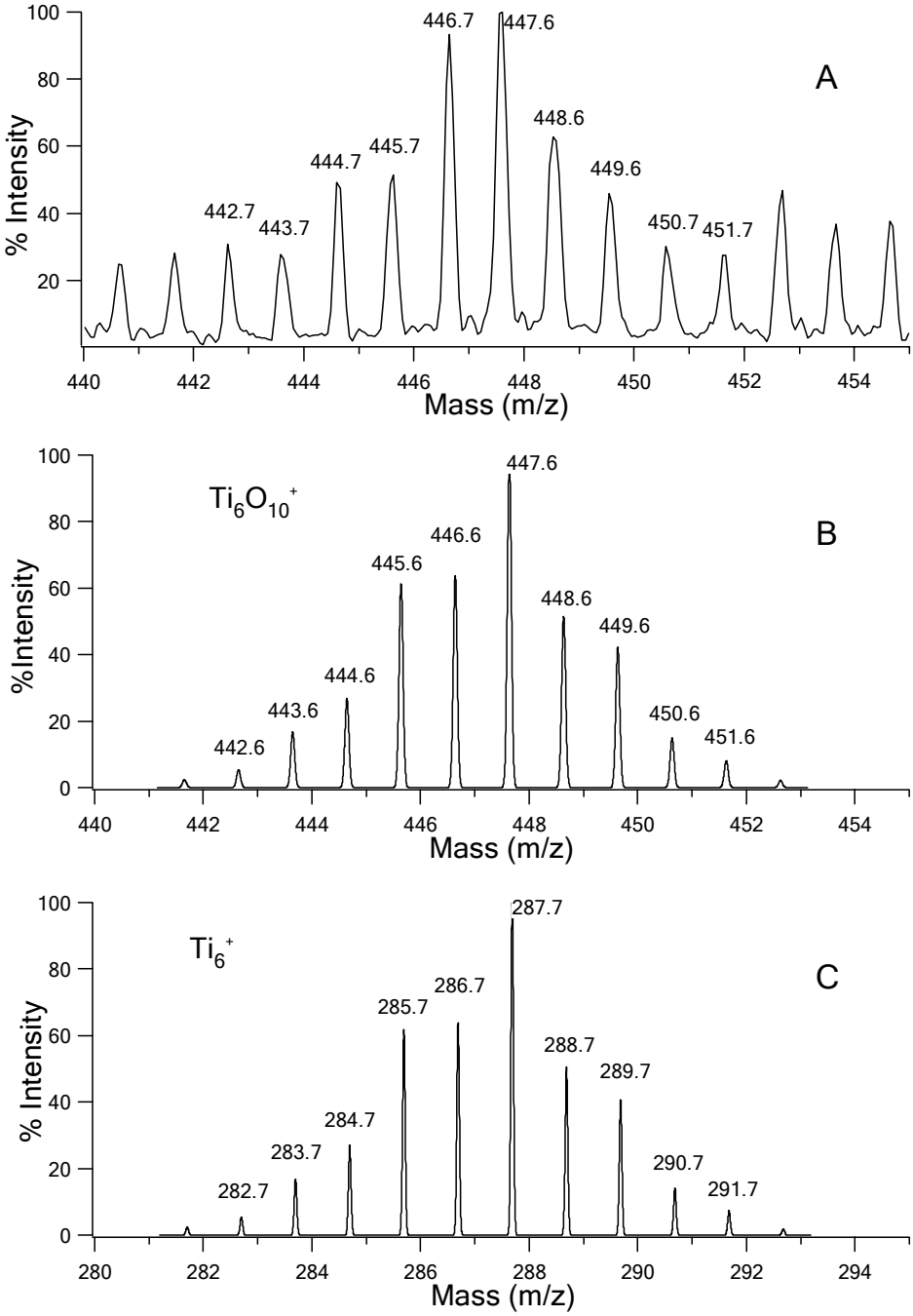

Figure 3.3. Isotopic distribution comparison for TiO_2 nanoparticle sample that has undergone size selective precipitation. (A) Positive reflectron MS experimental results centered at m/z 448; (B) theoretical isotopic distribution of $Ti_6O_{10}^+$; (C) theoretical isotopic distribution of Ti_6^+.

experimental data deviate slightly from the theoretical isotopic distribution and some overlap with other desorbed ions at both ends of the isotopic pattern can be clearly seen.

Figure 3.4 shows the MALDI mass spectra from m/z 250-5000 acquired for three TiO_2 nanoparticle preparations, each being characterized by a different size distribution. Upon MALDI irradiation, each monodispersed sample presented a broad normal-shaped distribution of ions with a single maximum that were analyzed and subjected to mathematical treatment. The smoothed peak maxima were determined to be around m/z 1130 (A), 1030 (B) and 520 (C) for samples of progressively decreasing cluster size, as determined by fractional crystallization. Possibly owing to the fact that each spectrum represents data obtained from irradiation of multiple particles, the obtained maxima exhibited only minor variations (4.7 ± 1.7 %) in replicate samples. Coupled to the peak shift, a narrowing of the peak shape is also observed as size becomes smaller. It should be noted that the major dithranol matrix peaks (i.e., m/z 225, 226, 227 and 211) are well below the range of the smoothed peak maxima. Higher mass matrix peaks appear in only minor abundances, hence, they have a negligible influence on nanoparticle size calculations.

Varying the laser power changes the individual titanium oxide peak intensities without a significant change in the position and shape of the high-intensity broad normal-shaped MS peak maximum. No m/z shift suggests that titanium oxide nanomaterials are ionized without the ligand shell. Even at lower laser powers, the capping material is most likely lost in the laser plume, as was previously observed for other nanocrystal measurements by LDI-TOF MS[21, 27].

Employing certain assumptions, LDI- and MALDI-TOF MS have found use for the determination of nanoparticle sizes[21, 26-28]. If the nanocrystals are presumed to be spherically

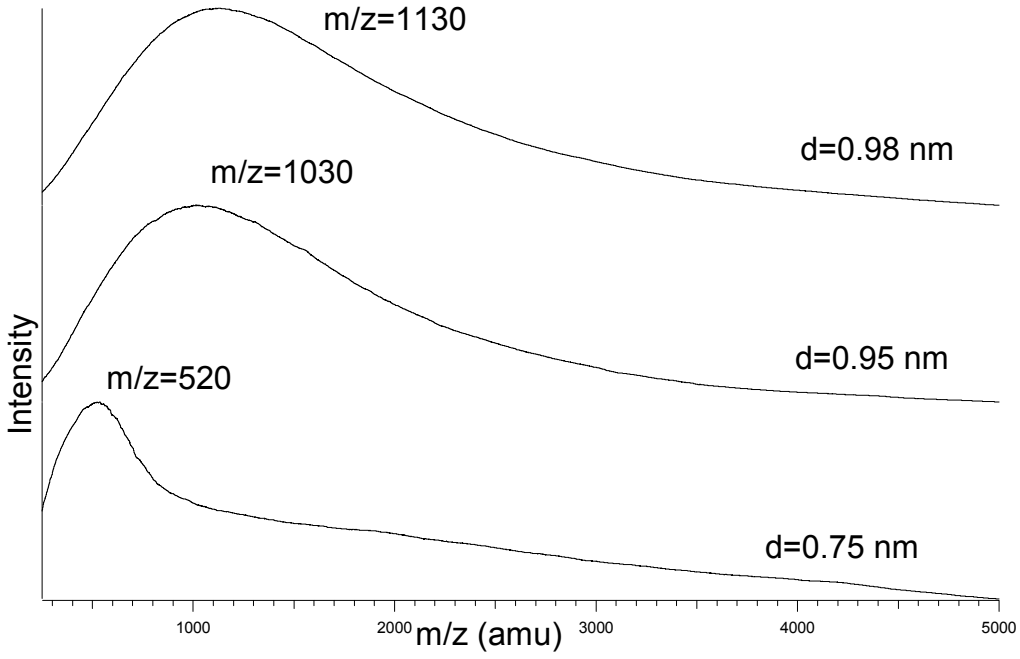

Figure 3.4. Positive ion reflectron mode MALDI-MS spectra of TiO_2 nanoparticles with progressively decreasing size as the result of size-selective precipitation. Dithranol was used as the matrix. Using the density value of anatase crystalline form, the diameters of the three samples were calculated to be 0.98nm (A), 0.95 nm (B) and 0.75 nm (C), respectively. Data processing was performed using IGOR Pro 4.07 (Wave Metrics Inc., Lake Oswego, OR). LDI-TOF mass spectra yielded similar results.

shaped and the mass of attached protons or cations can be ignored, the diameter (d) of nanomaterials can be calculated employing eq. 1.

$$(m/z)_{exp} = (\pi/6)\, N_A (d^3)\, \rho\, /z \qquad (1)$$

where $(m/z)_{exp}$ is the smoothed peak maximum obtained from MALDI or LDI mass spectra, N_A is Avogadro's number, ρ and z are the density of, and charge carried by, the nanoparticles, respectively.

Assuming TiO_2 nanoparticles have the same density as the bulk TiO_2, the densities (ρ) of the two most important TiO_2 crystalline forms, anatase and rutile, are 3.84×10^{-21} g/nm^3 and 4.26×10^{-21} g/nm^3, respectively. Using the density value of the anatase crystalline form, the diameters of the three samples (Fig. 3.4A-C) were calculated to be 0.98 nm, 0.95 nm and 0.75 nm, respectively. Thus, low resolution MALDI-TOF peak maxima are shown to correlate with anatase cluster size, and the possibility to use MALDI-TOF-MS to estimate clusters size is affirmed. The size distributions of TiO_2 nanoparticles obtained from MALDI-TOF-MS and equation (1) are in good agreement with our TEM observations.

Upon increasing the laser power, peaks below m/z 200 progressively emerge, and these were subjected to PSD. Figure 3.5A is the LDI-TOF mass spectrum of TiO_2 nanoparticles showing the mass range centered at m/z 167. Figure 3.5B is the theoretical isotopic distribution of $Ti_2O_3Na^+$, while figure 3.5C is the PSD spectrum of the precursor ion $[Ti_2O_3+Na]^+$ at m/z 167. Neutral loss of Ti_2O_3 yields Na^+ at m/z 23. This demonstrates that MALDI-TOF and LDI-TOF peaks originating from titanium oxide nanoparticles can contain sodium (a ubiquitous contaminant).

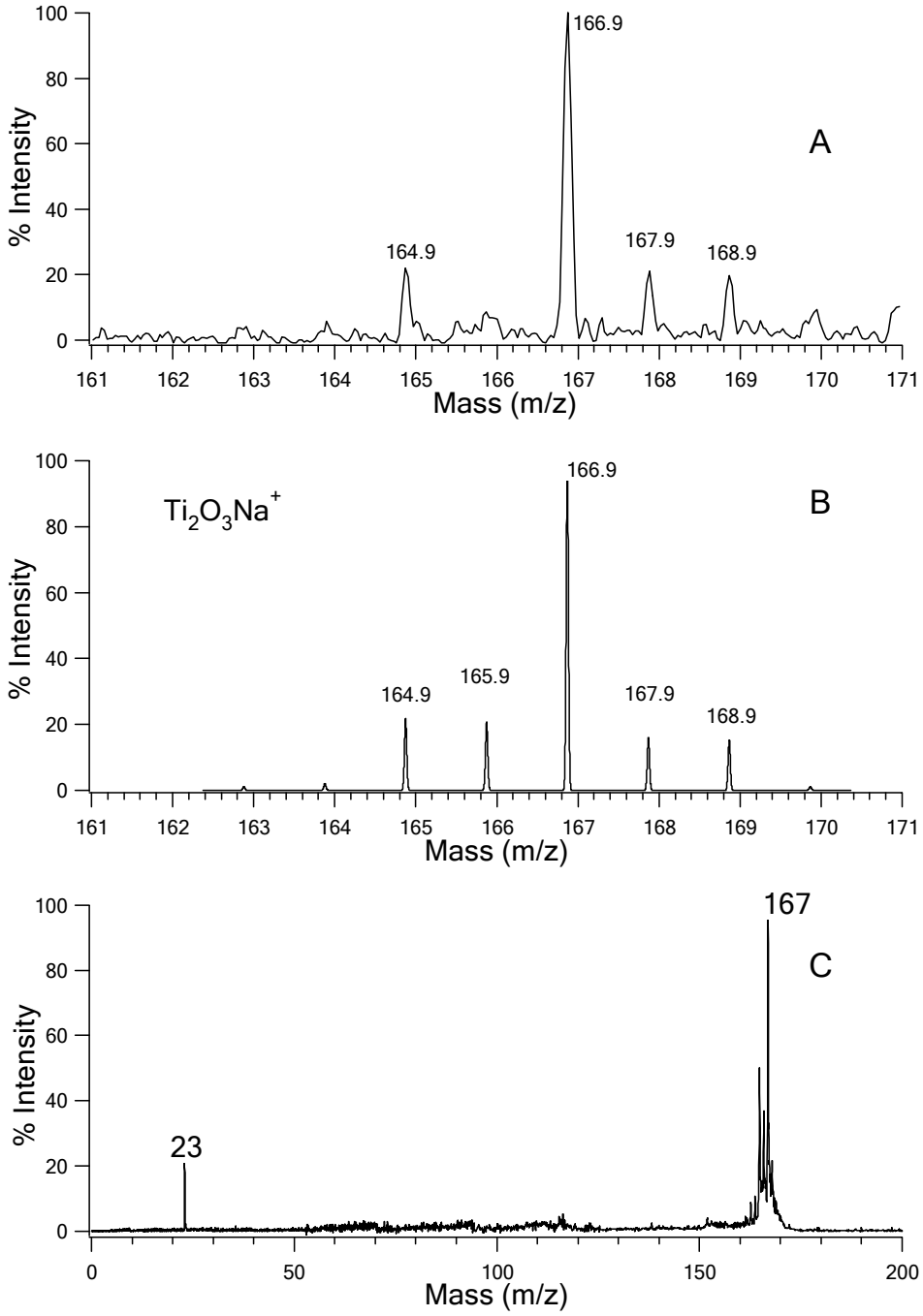

Figure 3.5. (A) LDI-TOF mass spectrum of TiO_2 nanoparticles showing mass range centered at m/z 167. (B) theoretical isotopic distribution of $Ti_2O_3Na^+$. (C) PSD spectrum of precursor ion $[Ti_2O_3+Na]^+$ at m/z 167. Neutral loss of Ti_2O_3 yields Na^+ at m/z 23. This demonstrates that MALDI-TOF and LDI-TOF peaks originating from titanium oxide nanoparticles may contain sodium.

Characterization of an isolated titanium oxide molecular cluster prepared by controlled hydrolysis of titanium tetraethoxide in the presence of methacrylic acid was previously performed by electrospray TOF-MS[30]. The cluster fragmentation patterns were carefully studied and the experimental results suggest that the core structures of the fragmentation products are analogous to those found in bulk titanium oxide materials. The polycondensation of $Ti(OC_4H_9)_4$ has been studied by electrospray, LDI and MALDI[52-54]. Several possible structures of the oligomers of $Ti(OC_4H_9)_4$ detected by ESI using direct infusion of alcoholic solutions were given[53, 54]. The LDI and MALDI mass spectra resulting from alcoholic preparations of $Ti(OC_4H_9)_4$ also showed three series of peaks corresponding to ions containing at least three titanium atoms[52]. Our mass spectra are more complex than those of previous reports[52-54], with titanium isotopic peak patterns spread from m/z 200 to around 3000. One major difference between those experiments and ours is that the previous studies focused on the hydrolysis-polycondensation behavior of alcoholic solutions containing $Ti(OC_4H_9)_4$, whereas we are interested in the TiO_2 nanoparticles synthesized by the thermal solvent process.

It should be noted that the expected molecular ions of $Ti(OC_4H_9)_4$ (e.g. protonated at m/z 340) did not stand out in mass spectra because of their low abundances and because of the significant number of other species appearing in this region of the spectrum. Potentially, incomplete hydrolysis[6] of all butoxide ligands may be responsible for some of the background peaks. It is very likely that some proportion of the alkoxy groups will remain in the hydrolysates. Similarly, complete condensation of the alkoxide to TiO_2 was very unlikely, and some proportion of the hydroxide groups formed during hydrolysis is likely to remain in the hydrolysates. Sample impurities and the complexity of resulting cluster compounds complicate interpretation, especially without separation of synthetic products[55].

3.4 Conclusions

We have shown that a stable TiO_2 cluster suspension is produced by the thermal solvent process, and clusters with different sizes are obtained by size-selection. XRD patterns of clusters with sizes less than 1 nm are very different from the principal peaks of the larger particles stemming from the extreme surface area-to-volume ratio. We successfully used MALDI-TOF and LDI-TOF MS to characterize ultra small (< 1 nm) nanoparticles. Peak maxima observed in MALDI-TOF and LDI-TOF mass spectra were shown to correlate with nanoparticle size. The obtained size distributions of TiO_2 nanoparticles are in good agreement with TEM measurements made on the identical samples. PSD analysis of inorganic nanomaterials has also been performed. PSD data demonstrate that MALDI-TOF and LDI-TOF peaks originating from titanium oxide nanoparticles may appear as sodium adducts. The ability to obtain detailed information concerning subnanometer titania nanoparticles has important implications for the continuing development of nanoparticle-based bactericidal agents.

3.5 References

1. Fujishima, A.; Rao, T. N.; Tryk, D. A., TiO2 photocatalysts and diamond electrodes. *Electrochimica Acta* **2000,** 45, (28), 4683-4690.
2. Hoffmann, M. R.; Martin, S. T.; Choi, W. Y.; Bahnemann, D. W., Environmental Applications of Semiconductor Photocatalysis. *Chemical Reviews* **1995,** 95, (1), 69-96.
3. Linsebigler, A. L.; Lu, G. Q.; Yates, J. T., Photocatalysis on Tio2 Surfaces - Principles, Mechanisms, and Selected Results. *Chemical Reviews* **1995,** 95, (3), 735-758.
4. Garzella, C.; Comini, E.; Tempesti, E.; Frigeri, C.; Sberveglieri, G., TiO2 thin films by a novel sol-gel processing for gas sensor applications. *Sensors and Actuators B-Chemical* **2000,** 68, (1-3), 189-196.
5. Rao, K. N.; Murthy, M. A.; Mohan, S., Optical-Properties of Electron-Beam-Evaporated Tio2 Films. *Thin Solid Films* **1989,** 176, (2), 181-186.

6. Venz, P. A.; Kloprogge, J. T.; Frost, R. L., Chemically modified titania hydrolysates: Physical properties. *Langmuir* **2000,** 16, (11), 4962-4968.
7. Oregan, B.; Gratzel, M., A Low-Cost, High-Efficiency Solar-Cell Based on Dye-Sensitized Colloidal Tio2 Films. *Nature* **1991,** 353, (6346), 737-740.
8. Hagfeldt, A.; Gratzel, M., Light-Induced Redox Reactions in Nanocrystalline Systems. *Chemical Reviews* **1995,** 95, (1), 49-68.
9. Henrich, V. E.; Cox, P. A., *The Surface Science of Metal Oxides*. Cambridge University Press: New York, 1994.
10. Pacchioni, G.; Ferrari, A. M.; Bagus, P. S., Cluster and band structure ab initio calculations on the adsorption of CO on acid sites of the TiO2(110) surface. *Surface Science* **1996,** 350, (1-3), 159-175.
11. Sousa, C.; Illas, F., Ionic-Covalent Transition in Titanium-Oxides. *Physical Review B* **1994,** 50, (19), 13974-13980.
12. Hagfeldt, A.; Siegbahn, H.; Lindquist, S. E.; Lunell, S., Semiempirical Calculations of Tio2 (Rutile) Clusters. *International Journal of Quantum Chemistry* **1992,** 44, (4), 477-495.
13. Doeuff, S.; Dromzee, Y.; Taulelle, F.; Sanchez, C., Synthesis and Solid-State and Liquid-State Characterization of a Hexameric Cluster of Titanium(Iv) - Ti6(Mu-2-O)2(Mu-3-O)2(Mu-2-Oc4h9)2(Oc4h9)6(Ococh3)8. *Inorganic Chemistry* **1989,** 28, (25), 4439-4445.
14. Schubert, U.; Arpac, E.; Glaubitt, W.; Helmerich, A.; Chau, C., Primary Hydrolysis Products of Methacrylate-Modified Titanium and Zirconium Alkoxides. *Chemistry of Materials* **1992,** 4, (2), 291-295.
15. Wilcoxon, J. P.; Martin, J. E.; Provencio, P., Size distributions of gold nanoclusters studied by liquid chromatography. *Langmuir* **2000,** 16, (25), 9912-9920.
16. Cullity, B. D., *Elements of X-ray Diffraction*. Addison-Wesley: Reading, MA,, 1978.
17. Kubler, B.; Millon, E.; Gaumet, J. J.; Muller, J. F., Formation of high mass C-n clusters (n>100) by laser ablation/desorption coupled with mass spectrometry. *Fullerene Science and Technology* **1996,** 4, (6), 1247-1261.
18. Hummelen, J. C.; Knight, B.; Pavlovich, J.; Gonzalez, R.; Wudl, F., Isolation of the Heterofullerene C59n as Its Dimer (C59n)(2). *Science* **1995,** 269, (5230), 1554-1556.
19. Lafargue, P. E.; Gaumet, J. J.; Muller, J. F.; Labrosse, A., Laser ablation of silica: Study of induced clusters by Fourier transform ion cyclotron resonance mass spectrometry. *Journal of Mass Spectrometry* **1996,** 31, (6), 623-632.
20. Kasuya, A.; Sivamohan, R.; Barnakov, Y. A.; Dmitruk, I. M.; Nirasawa, T.; Romanyuk, V. R.; Kumar, V.; Mamykin, S. V.; Tohji, K.; Jeyadevan, B.; Shinoda, K.; Kudo, T.; Terasaki, O.; Liu, Z.; Belosludov, R. V.; Sundararajan, V.; Kawazoe, Y., Ultra-stable nanoparticles of CdSe revealed from mass spectrometry. *Nature Materials* **2004,** 3, (2), 99-102.
21. Khitrov, G. A.; Strouse, G. F., ZnS nanomaterial characterization by MALDI-TOF mass spectrometry. *Journal of the American Chemical Society* **2003,** 125, (34), 10465-10469.
22. Gaumet, J. J.; Strouse, G. F., Nanospray Mass Spectrometry Technique for Analyzing Nanomaterials from Molecular Precursors up to 1.5 nm in Diameter Clusters. *Materials Sceince and Engineering C* **2002,** 19, 299-304
23. Gaumet, J. J.; Khitrov, G. A.; Strouse, G. F., Mass spectrometry analysis of the 1.5 nm sphalerite-CdS core of [Cd32S14(SC6H5)(36)center dot DMF4]. *Nano Letters* **2002,** 2, (4), 375-379.

24. Gaumet, J. J.; Strouse, G. F., Electrospray mass spectrometry of semiconductor nanoclusters: Comparative analysis of positive and negative ion mode. *Journal of the American Society for Mass Spectrometry* **2000,** 11, (4), 338-344.
25. Schaaff, T. G.; Shafigullin, M. N.; Khoury, J. T.; Vezmar, I.; Whetten, R. L., Properties of a ubiquitous 29 kDa Au : SR cluster compound. *Journal of Physical Chemistry B* **2001,** 105, (37), 8785-8796.
26. Whetten, R. L.; Khoury, J. T.; Alvarez, M. M.; Murthy, S.; Vezmar, I.; Wang, Z. L.; Stephens, P. W.; Cleveland, C. L.; Luedtke, W. D.; Landman, U., Nanocrystal gold molecules. *Advanced Materials* **1996,** 8, (5), 428-&.
27. Arnold, R. J.; Reilly, J. P., High-resolution time-of-flight mass spectra of alkanethiolate-coated gold nanocrystals. *Journal of the American Chemical Society* **1998,** 120, (7), 1528-1532.
28. Vezmar, I.; Alvarez, M. M.; Khoury, J. T.; Salisbury, B. E.; Shafigullin, M. N.; Whetten, R. L., Cluster beams from passivated nanocrystals. *Zeitschrift Fur Physik D-Atoms Molecules and Clusters* **1997,** 40, (1-4), 147-151.
29. d'Avray, A. T. D.; Carpenter, E. E.; O'Connor, C. J.; Cole, R. B., Characterization of ferrite nanoparticles by laser desorption/ionization mass spectrometry. *European Mass Spectrometry* **1998,** 4, (6), 441-449.
30. Khitrov, G. A.; Strouse, G. F.; Gaumet, J. J., Characterization of Ti6O4(O2C4H5)(8)(OCH2CH3)(8) by electrospray time of flight mass spectrometry. *Journal of the American Society for Mass Spectrometry* **2004,** 15, (2), 260-267.
31. Mori, H.; Lanzendorfer, M. G.; Muller, A. H. E.; Klee, J. E., Silsesquioxane-based nanoparticles formed via hydrolytic condensation of organotriethoxysilane containing hydroxy groups. *Macromolecules* **2004,** 37, (14), 5228-5238.
32. Alves, S.; Kalberer, M.; Zenobi, R., Direct detection of particles formed by laser ablation of matrices during matrix-assisted laser desorption/ionization. *Rapid Communications in Mass Spectrometry* **2003,** 17, (18), 2034-2038.
33. Bauer, F.; Sauerland, V.; Ernst, H.; Glasel, H. A.; Naumov, S.; Mehnert, R., Preparation of scratch- and abrasion-resistant polymeric nanocomposites by monomer grafting onto nanoparticles, 4 - Application of MALDI-TOF mass spectrometry to the characterization of surface modified nanoparticles. *Macromolecular Chemistry and Physics* **2003,** 204, (3), 375-383.
34. Colton, R.; Dagostino, A.; Traeger, J. C., Electrospray mass spectrometry applied inorganic and organometallic chemistry. *Mass Spectrometry Reviews* **1995,** 14, (2), 79-106.
35. Gatlin, C. L.; Turecek, F., In *Electrospray Ionization Mass spectrometry: Fundamentals, Instrumentation, and Applications*, Cole, R. B., Ed. Wiley-Interscience: NY, 1997; p 527.
36. Traeger, J. C., Electrospray mass spectrometry of organometallic compounds. *International Journal of Mass Spectrometry* **2000,** 200, (1-3), 387-401.
37. Lover, T.; Henderson, W.; Bowmaker, G. A.; Seakins, J. M.; Cooney, R. P., Functionalization and capping of a CdS nanocluster: A study of ligand exchange by electrospray mass spectrometry. *Chemistry of Materials* **1997,** 9, (8), 1878-1886.
38. Lover, T.; Henderson, W.; Bowmaker, G. A.; Seakins, J. M.; Cooney, R. P., Electrospray mass spectrometry of thiophenolate-capped clusters of CdS, CdSe, and ZnS and of cadmium and zinc thiophenolate complexes: Observation of fragmentation and metal,

chalcogenide, and ligand exchange processes. *Inorganic Chemistry* **1997,** 36, (17), 3711-3723.
39. Spengler, B.; Kirsch, D.; Kaufmann, R., Metastable Decay of Peptides and Proteins in Matrix-Assisted Laser-Desorption Mass-Spectrometry. *Rapid Communications in Mass Spectrometry* **1991,** 5, (4), 198-202.
40. Spengler, B.; Kirsch, D.; Kaufmann, R.; Jaeger, E., Peptide Sequencing by Matrix-Assisted Laser-Desorption Mass-Spectrometry. *Rapid Communications in Mass Spectrometry* **1992,** 6, (2), 105-108.
41. Mitsuhashi, T.; Kleppa, O. J., Transformation Enthalpies of the Tio2 Polymorphs. *Journal of the American Ceramic Society* **1979,** 62, (7-8), 356-357.
42. Cheng, H. M.; Ma, J. M.; Zhao, Z. G.; Qi, L. M., Hydrothermal Preparation of Uniform Nanosize Rutile and Anatase Particles. *Chemistry of Materials* **1995,** 7, (4), 663-671.
43. JCPDS, file no. 21-1272.
44. Chen, L. X.; Rajh, T.; Wang, Z. Y.; Thurnauer, M. C., XAFS studies of surface structures of TiO2 nanoparticles and photocatalytic reduction of metal ions. *Journal of Physical Chemistry B* **1997,** 101, (50), 10688-10697.
45. Chen, L. X.; Rajh, T.; Jager, W.; Nedeljkovic, J.; Thurnauer, M. C., X-ray absorption reveals surface structure of titanium dioxide nanoparticles. *Journal of Synchrotron Radiation* **1999,** 6, 445-447.
46. Rajh, T.; Poluektov, O.; Dubinski, A. A.; Wiederrecht, G.; Thurnauer, M. C.; Trifunac, A. D., Spin polarization mechanisms in early stages of photoinduced charge separation in surface-modified TiO2 nanoparticles. *Chemical Physics Letters* **2001,** 344, (1-2), 31-39.
47. Naicker, P. K.; Cummings, P. T.; Zhang, H. Z.; Banfield, J. F., Characterization of titanium dioxide nanoparticles using molecular dynamics simulations. *Journal of Physical Chemistry B* **2005,** 109, (32), 15243-15249.
48. Chen, C. T.; Chen, Y. C., Desorption/ionization mass spectrometry on nanocrystalline titania sol-gel-deposited films. *Rapid Communications in Mass Spectrometry* **2004,** 18, (17), 1956-1964.
49. Chen, C. T.; Chen, Y. C., Molecularly imprinted TiO2-matrix-assisted laser desorption/ionization mass spectrometry for selectively detecting alpha-cyclodextrin. *Analytical Chemistry* **2004,** 76, (5), 1453-1457.
50. Kinumi, T.; Saisu, T.; Takayama, M.; Niwa, H., Matrix-assisted laser desorption/ionization time-of-flight mass spectrometry using an inorganic particle matrix for small molecule analysis. *Journal of Mass Spectrometry* **2000,** 35, (3), 417-422.
51. Dopke, N. C.; Treichel, P. M.; Vestling, M. M., Matrix-assisted laser desorption/ionization time-of-flight mass spectrometry (MALDI-TOF MS) of rhenium(III) halides: A characterization tool for metal atom clusters. *Inorganic Chemistry* **1998,** 37, (6), 1272-1277.
52. Seraglia, R.; Armelao, L.; Cristoni, S.; Gross, S.; Tondello, E.; Traldi, P., Matrix-assisted laser desorption/ionisation mass spectrometry in the study of polycondensation of Ti(OBun)(4) in the presence of Si(OEt)(4). *Rapid Communications in Mass Spectrometry* **2003,** 17, (23), 2649-2654.
53. Cristoni, S.; Armelao, L.; Gross, S.; Tondello, E.; Traldi, P., Electrospray ionization in the study of the polycondensation of Ti(O-i-C3H7)(4) and Ti(O-n-C4H9)(4). *Rapid Communications in Mass Spectrometry* **2000,** 14, (8), 662-668.

54. Cristoni, S.; Armelao, L.; Gross, S.; Tondello, E.; Traldi, P., Electrospray ionization in the study of sol-gel processes: the polycondensation of Ti(O-n-Bu)(4) in the presence of Si(OEt)(4). *Rapid Communications in Mass Spectrometry* **2001,** 15, (6), 386-392.
55. Schaaff, T. G., Laser desorption and matrix-assisted laser desorption/ionization mass spectrometry of 29-kDa Au : SR cluster compounds. *Analytical Chemistry* **2004,** 76, (21), 6187-6196.

Chapter 4: Characterization of Inorganic Nitrate and Perchlorate Compounds by Negative MALDI-TOF Mass Spectrometry and Post-Source Decay

4.1 Introduction

Inorganic nitrate and perchlorate salts are widely used as oxidizing reagents in a variety of industrial applications, including use as blasting agents in mining explosives, and composite propellants in solid rocket fuel[1, 2]. They are also the major ingredients of home-made improvised explosive devices utilized by terrorists[3]. In construction and development, dynamite, i.e., nitroglycerin, has almost been replaced totally with ammonium nitrate fuel oil (ANFO) and slurry explosives in which inorganic nitrates and perchlorates are the main components. Nitrate salts are also widely used as the oxidizers in black powder in addition to their wide utilization as fertilizers. Furthermore, inorganic nitrate salts exist as pollutants and have been found in sidestream cigarette smoke (SSS) and mainstream cigarette smoke (MSS)[4]. Even higher abundances of nitrates exist in ashes of the cigarette after combustion. The carcinogenicity of cigarette smoke caused by nitrosamines and nitrate compounds in MSS has been linked to the nitrates in fertilizers[5]. Nitrates, nitric acid and closely related nitrogen oxides are also important atmospheric[6] and stratospheric species[7].

Perchlorate, an iodide uptake inhibitor, has increasingly been detected in new places and in new matrices, such as milk[8], vegetables[9, 10] and fruits[10]. There is great concern that perchlorate contamination may be far more widespread and serious than currently known. The use of perchlorate-containing Chilean nitrate as a major source of fertilizer until 1930s and the use of ammonium perchlorate as oxidizers in solid fuel rockets are cited as the major sources[11]. Perchlorate can form naturally by atmospheric processes[11]. Widespread perchlorate

contamination in the environment likely increases the risk of human exposure[12, 13] which might impair thyroid function.

Because of the potential illegal use of the commercially available inorganic oxidizers as well as concerns over human exposure, it is of major significance to unambiguously identify these inorganic salts.

Ion chromatography (IC) has been recognized as a powerful technique for the analysis of both cations and anions in water-soluble inorganic explosives[14, 15]. But the separate detection of positive or negative ions constituting each oxidizer instead of identifying the oxidizer as one entity may leave compositional ambiguity in some cases. It is often found that IC does not provide definitive identification. It has been observed that in many real samples, high concentrations of species that elute in the same region as perchlorate often contain no perchlorate at all[16]. The same problem also existed in the application of capillary electrophoresis (CE) for the determination of inorganic ions in explosive residues[17], as positive and negative ions were detected separately.

Electrospray mass spectrometry (ES-MS) has already been used for the analysis of inorganic and organometallic compounds[18] when the chosen solvent can dissolve the analytes without causing decomposition and/or reactions. A number of inorganic cations have been studied[19, 20] and often metal-solvent clusters are formed[20, 21]. Negative ion mode studies have also been carried out recently by ES-MS[22-24] and collision-induced dissociation (CID) of these anionic clusters has also been attempted[22, 24].

Laser desorption/ionization (LDI) and matrix-assisted laser desorption/ionization mass spectrometry (MALDI MS) have not routinely been used for the analyses of inorganic compounds and most of the existing studies focus on the characterization of organometallic and

inorganic coordination complexes[25-29]. MALDI or LDI has also been successfully used to characterize various nanoclusters[30-41]. MALDI is a soft ionization technique and favors observation of intact molecular ions whereas LDI is more likely to fragment ions since the analytes have to directly absorb energy during the laser event. In many cases, both LDI and MALDI yielded similar ion peaks with different relative peak abundances[25, 32, 40, 41]. The applications of inorganic compounds as matrixes has also attracted attention[42, 43] ever since the success of Tanaka et al. who used cobalt powder as a matrix in experiments leading up to MALDI[44].

Inorganic nitrates and their clusters[22, 24, 45] have been studied in detail by ES-MS and MS/MS. Perchlorates and their clusters have also been investigated by ES-MS[24, 46]. In contrast, MALDI MS has not yet been used to characterize these inorganic nitrate and perchlorates species. Although not truly tandem MS, post-source decay (PSD)[47, 48] can provide additional valuable information about the structure of analytes observed by MALDI-TOF MS. The properties of these inorganic metal cluster ions are relevant in a number of areas. Studying the properties of cluster species provides valuable clues to the transitions between the gaseous and condensed phases because cluster ions serve as the essential bridges linking together discrete atoms or molecules and bulk materials[49, 50]. In this study, we explore the use of MALDI-TOF MS for the positive identification of inorganic oxidizers. The identities and properties of the ions are further investigated by PSD.

4.2 Experimental

4.2.1 Chemicals

The following inorganic salts were used for mass spectrometric determinations: magnesium nitrate $Mg(NO_3)_2$, calcium nitrate $Mg(NO_3)_2$, strontium nitrate $Sr(NO_3)_2$, barium nitrate $Ba(NO_3)_2$, mangnanese nitrate $Mn(NO_3)_2$, cobalt nitrate $Co(NO_3)_2$, nickel nitrate $Ni(NO_3)_2$, copper nitrate $Cu(NO_3)_2$, zinc nitrate $Zn(NO_3)_2$, cadmium nitrate $Cd(NO_3)_2$, silver nitrate $AgNO_3$, sodium perchlorate $NaClO_4$, potassium perchlorate KClO4, magnesium perchlorate $Mg(ClO_4)_2$ and calcium perchlorate $Ca(ClO_4)_2$, and they were all purchased from Aldrich (Milwaukee, WI). Methanol, nitrate acid, harmine and harmane were also purchased from Aldrich (Milwaukee, WI) and Milli-Q purified water was used throughout the experimental procedures. All chemicals were used as received without further purification.

4.2.2 Mass Spectrometry

Mass spectra were acquired on an Applied Biosystems Voyager Elite MALDI-TOF mass spectrometer (Applied Biosystems, Framingham, MA) equipped with a pulsed N_2 laser ($\lambda = 337$ nm). An extraction voltage of 20 kV was typically employed. All mass spectra were acquired in the negative reflectron mode employing delayed extraction. Laser intensity was adjusted to just above the threshold energy for appearance of metal cluster ions. When acquiring PSD spectra, laser intensity was adjusted to a value 10-30% above the threshold energy for appearance of metal cluster ions and the mirror ratios in the PSD segment list were manually calculated and specified such that all possible fragments would be collected. All mass spectra and PSD spectra consist of an average of 50-100 laser shots. Reported m/z values show nominal masses only (i.e., values after the decimal places have been truncated). The instrument was externally calibrated by monoisotopic peaks of nitrate, harmine or harmane matrix and oliogsaccharides. Data processing was performed using IGOR Pro 4.07 (Wave Metrics Inc., Lake Oswego, OR).

MALDI samples were prepared using the "dried-droplet" method[51]. For inorganic nitrates, 5 μL of 3 mM inorganic nitrate solution, 5 μL of 3 mM HNO_3 and 5 μL of 10 mg/mL harmine or harmine matrix solution (all in 4:1 methanol/water) were mixed; for inorganic perchlorates, 5 μL of 2 mM inorganic perchlorate solution and 5 μL of 10 mg/mL harmine or harmine matrix solution (both in 4:1 methanol/water) were mixed. Then, a 0.5 μL aliquot of this mixture solution was deposited onto a sample plate and allowed to air dry.

4.3 Results and Discussions

4.3.1 MS and PSD of Nitrate Complexes of Group 2 Metals

A negative ion mode MALDI-TOF mass spectrum of a $Mg(NO_3)_2$ sample with harmine as matrix is shown in Figure 4.1a. Nitrate monomer (NO_3^-, m/z 62) and the proton-bound dimer ($H(NO_3)_2^-$, m/z 125) are the main background ions. Deprotonated harmine (m/z 211) and the nitrate adduct of harmine (m/z 274) are the main matrix ions. Magnesium ions are doubly charged in solution and thus yield primary $Mg(NO_3)_3^-$ ions (m/z 210) and some $Mg_2(NO_3)_5^-$ cluster ions. Because of the overlapping of $Mg(NO_3)_3^-$ ions (m/z 210) and deprotonated harmine ions (m/z 211), LDI without any matrix was attempted and the resulting mass spectrum is shown in Figure 4.1b. The spectrum is quite similar to that observed under MALDI conditions except for the absence of matrix ions. Magnesium cluster ions $Mg(NO_3)_3^-$ and $Mg_2(NO_3)_5^-$ are unambiguously observed in LDI without the interference of matrix ions. Compared to MALDI experiments, much higher laser intensities have to be used in LDI experiments to obtain useful spectra, and concomitantly, in-source fragments are observed in LDI. It has been previously observed that, compared to organic compounds, inorganic compounds often have higher laser desorption thresholds and lower sensitivities[52, 53]. In addition, higher laser energy is generally

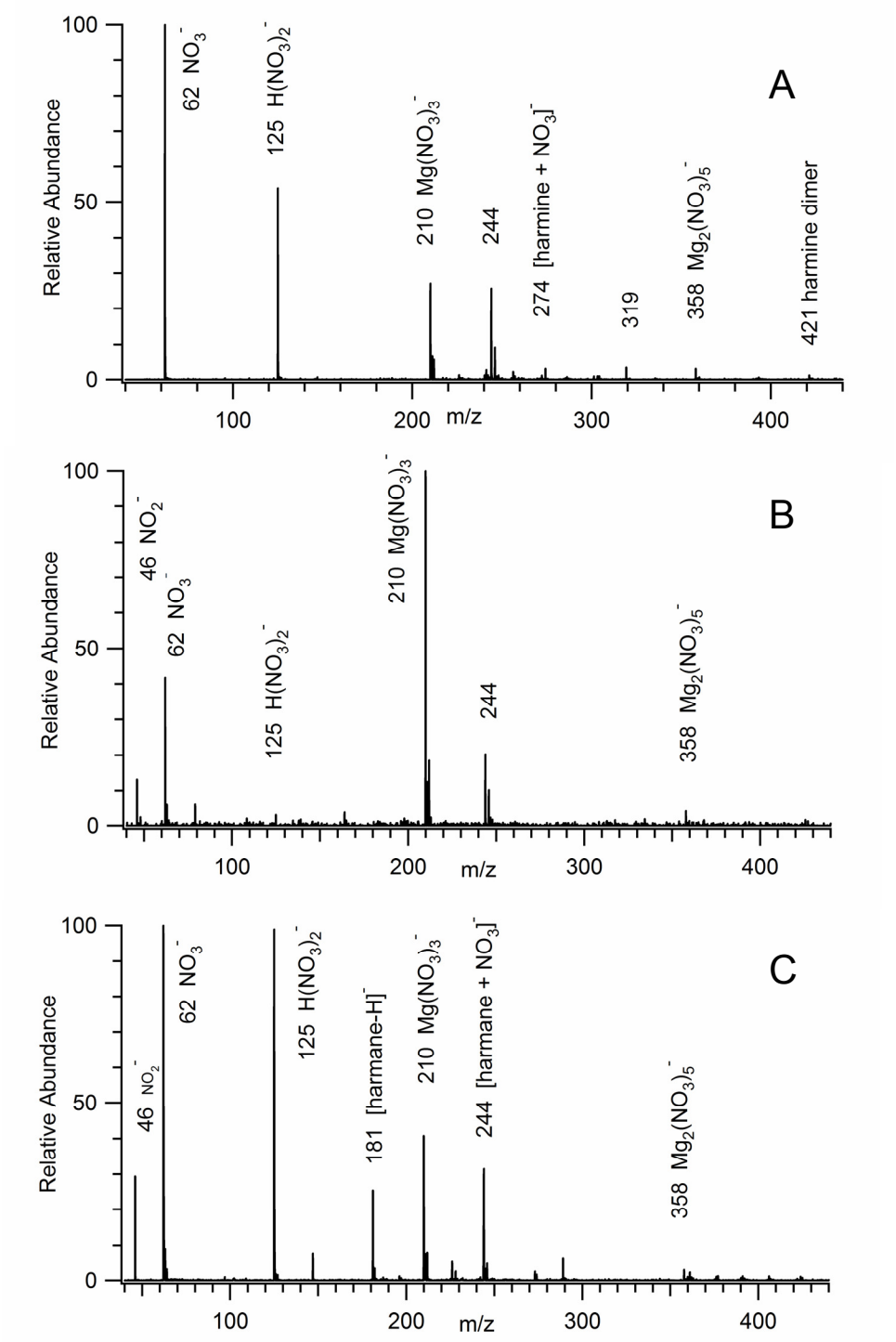

Figure 4.1. (a) MALDI mass spectrum of $Mg(NO_3)_2$ with harmine as matrix. (b) LD mass spectrum of $Mg(NO_3)_2$. (c) MALDI mass spectrum of $Mg(NO_3)_2$ with harmane as matrix.

required to break the stronger interactions between inorganic cations and anions. The peak at m/z 46 is assigned as NO_2^- and the peak at m/z 78 might be ONO_3^-, which are consistent with early observations that losses of NO, O_2 and O atoms are typical in LDI of nitrate or nitrite compounds[54, 55]. Magnesium cluster ions $Mg(NO_3)_3^-$ and $Mg_2(NO_3)_5^-$ are also clearly observed in MALDI spectrum (Figure 4.1c) with harmane as matrix ([harmane-H]$^-$ at m/z 181 and [harmane+NO_3]$^-$ at m/z 244).

A negative ion mode PSD spectrum is shown for $Mg(NO_3)_3^-$ (m/z 210) in Figure 4.2a. Nitrate is the only product ion observed from PSD of $Mg(NO_3)_3^-$; presumably, the remaining products are neutral $Mg(NO_3)_2$ molecules. A mass spectrum from PSD of the cluster $Mg_2(NO_3)_5^-$ (m/z 358) is shown in Figure 4.2b. The only ionic product is the next lower species $Mg(NO_3)_3^-$ and the neutral loss of $Mg(NO_3)_2$ molecules is assumed; nitrate is not observed.

Similarly, all other nitrates of alkaline earth metals (Ca, Sr, Ba) studied yield primarily $M(NO_3)_3^-$ and some $M_2(NO_3)_5^-$ cluster ions with two metal atoms. The PSD of $M(NO_3)_3^-$ yields NO_3^- as the only product ion whereas the PSD of $M_2(NO_3)_5^-$ yields $M(NO_3)_3^-$ as the only product ion with no free NO_3^- formed from metal nitrate clusters with two metal atoms (data not shown). No intra-molecular redox reactions are observed. Table 4.1 summarizes the various ions observed in MALDI MS and their PSD reactions. The general forms of PSD reaction for these two kinds of alkaline earth metal nitrate cluster ions can be written as follows:

$$M(NO_3)_3^- \rightarrow NO_3^- + M(NO_3)_2 \quad (1)$$

$$M_2(NO_3)_5^- \rightarrow M(NO_3)_3^- + M(NO_3)_2 \quad (2)$$

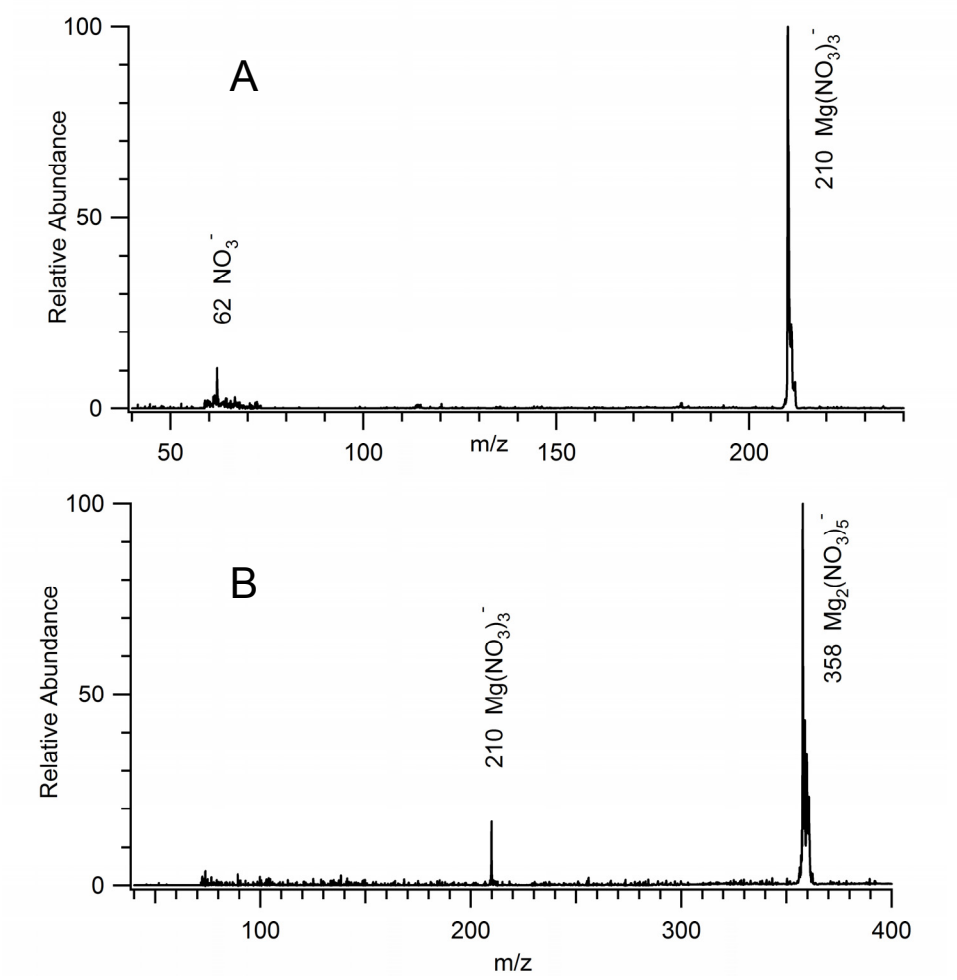

Figure 4.2. (a) PSD mass spectrum of $Mg(NO_3)_3^-$. (b) PSD mass spectrum of $Mg_2(NO_3)_5^-$.

Table 4.1. PSD reactions of metal nitrate and perchlorate complexes

Metal complex Precursor	PSD Reactions
$Mg(NO_3)_3^-$	$Mg(NO_3)_3^- \rightarrow Mg(NO_3)_2 + NO_3^-$
$Mg_2(NO_3)_5^-$	$Mg_2(NO_3)_5^- \rightarrow Mg(NO_3)_2 + Mg(NO_3)_3^-$
$Ca(NO_3)_3^-$	$Ca(NO_3)_3^- \rightarrow Ca(NO_3)_2 + NO_3^-$
$Ca_2(NO_3)_5^-$	$Ca_2(NO_3)_5^- \rightarrow Ca(NO_3)_2 + Ca(NO_3)_3^-$
$Sr(NO_3)_3^-$	$Sr(NO_3)_3^- \rightarrow Sr(NO_3)_2 + NO_3^-$
$Sr_2(NO_3)_5^-$	$Sr_2(NO_3)_5^- \rightarrow Sr(NO_3)_2 + Sr(NO_3)_3^-$
$Ba(NO_3)_3^-$	$Ba(NO_3)_3^- \rightarrow Ba(NO_3)_2 + NO_3^-$
$Ba_2(NO_3)_5^-$	$Ba_2(NO_3)_5^- \rightarrow Ba(NO_3)_2 + Ba(NO_3)_3^-$
$Mn(NO_3)_3^-$	$Mn(NO_3)_3^- \rightarrow MnO(NO_3)_2^- + NO_2$
	$Mn(NO_3)_3^- \rightarrow Mn(NO_3)_2 + NO_3^-$
$Co(NO_3)_3^-$	$Co(NO_3)_3^- \rightarrow CoO(NO_3)_2^- + NO_2$
	$Co(NO_3)_3^- \rightarrow Co(NO_3)_2 + NO_3^-$
$Ni(NO_3)_3^-$	$Ni(NO_3)_3^- \rightarrow NiO(NO_3)_2^- + NO_2$
	$Ni(NO_3)_3^- \rightarrow Ni(NO_3)_2 + NO_3^-$
$Cu^{II}(NO_3)_3^-$	$Cu^{II}(NO_3)_3^- \rightarrow Cu^{I}(NO_3)_2^- + NO_3$
	$Cu^{II}(NO_3)_3^- \rightarrow Cu^{II}(NO_3)_2 + NO_3^-$
$Cu^{I}(NO_3)_2^-$	$Cu^{I}(NO_3)_2^- \rightarrow Cu^{I}ONO_3^- + NO_2$
	$Cu^{I}(NO_3)_2^- \rightarrow Cu^{I}NO_3 + NO_3^-$
$Zn(NO_3)_3^-$	$Zn(NO_3)_3^- \rightarrow ZnO(NO_3)_2^- + NO_2$
	$Zn(NO_3)_3^- \rightarrow Zn(NO_3)_2 + NO_3^-$
$Ag(NO_3)_2^-$	$Ag(NO_3)_2^- \rightarrow AgNO_3 + NO_3^-$
$Cd(NO_3)_3^-$	$Cd(NO_3)_3^- \rightarrow Cd(NO_3)_2 + NO_3^-$
$Na(ClO_4)_2^-$	$Na(ClO_4)_2^- \rightarrow NaClO_4 + ClO_4^-$
$Na_2(ClO_4)_3^-$	$Na_2(ClO_4)_3^- \rightarrow Na(ClO_4)_2^- + NaClO_4$
$Na_3(ClO_4)_4^-$	$Na_3(ClO_4)_4^- \rightarrow Na(ClO_4)_2^- + 2NaClO_4$
$K(ClO_4)_2^-$	$K(ClO_4)_2^- \rightarrow KClO_4 + ClO_4^-$
$Ca(ClO_4)_3^-$	$Ca(ClO_4)_3^- \rightarrow Ca(ClO_4)_2 + ClO_4^-$
$Ca_2(ClO_4)_5^-$	$Ca_2(ClO_4)_5^- \rightarrow Ca(ClO_4)_3^- + Ca(ClO_4)_2$
$Mg(ClO_4)_3^-$	$Mg(ClO_4)_3^- \rightarrow Mg(ClO_4)_2 + ClO_4^-$
$Mg_2(ClO_4)_5^-$	$Mg_2(ClO_4)_5^- \rightarrow Mg(ClO_4)_3^- + Mg(ClO_4)_2$

4.3.2 MS and PSD of Nitrate Complexes of Transition Metals

In this study, MALDI-TOF mass spectra of nitrates of transition metal ions with a stable 2+ oxidation state in solution yield mainly $M(NO_3)_3^-$ ions. There might be some traces of $M(NO_2)(NO_3)_2^-$ ions, but their origins cannot be confirmed by PSD because of their low abundances and the rather large ion selection window (~ 30 Thomsons) of the MALDI-TOF MS employed in this study. For manganese nitrate, cluster ions containing two manganese atoms ($M_2(NO_3)_5^-$) are also observed. The identity of this ion was confirmed by its appearance in the MALDI-TOF PSD spectrum using harmane as matrix.

Unlike group II metal nitrates, more in-source fragmentation is observed for transition metal nitrates, as shown in the spectrum for Cu^{2+} in Figure 4.3a. While abundant $Cu(NO_3)_3^-$ is observed from the Cu^{2+} sample as expected, there is also a substantial amount of $Cu(NO_3)_2^-$. The assignment of $Cu(NO_3)_2^-$ is confirmed by the PSD spectrum in Figure 4.3b, and $Cu(NO_3)_3^-$ is confirmed by the PSD spectrum in Figure 4.3c. It has been previously reported that Cu^{2+} present in MALDI samples can be easily reduced to Cu^+[56, 57].

Three kinds of fragmentation pathways exist in PSD of clusters of copper (I or II) nitrate. The inferred neutral molecules balance the reaction equation. The first pathway is the elimination of neutral metal nitrate complex with the generation of nitrate as shown in equation 3 and 4. The same fragmentation pathway also exists in PSD of nitrate complexes with one Group II metal atom, where NO_3^- is the only product ion as shown in equation 1. Although NO_3^- is a product ion in PSD of all tested nitrate complexes with one transition metal atom, it is not the only product ion, nor is it the major one. The second pathway is the elimination of NO_2 with formation of an oxo-nitrate complex as shown in Equation 5. This reaction is observed for most transition metals studied except Cu^{2+}, Ag^+ and Cd^{2+} (Table 4.1). It is not expected that the metal

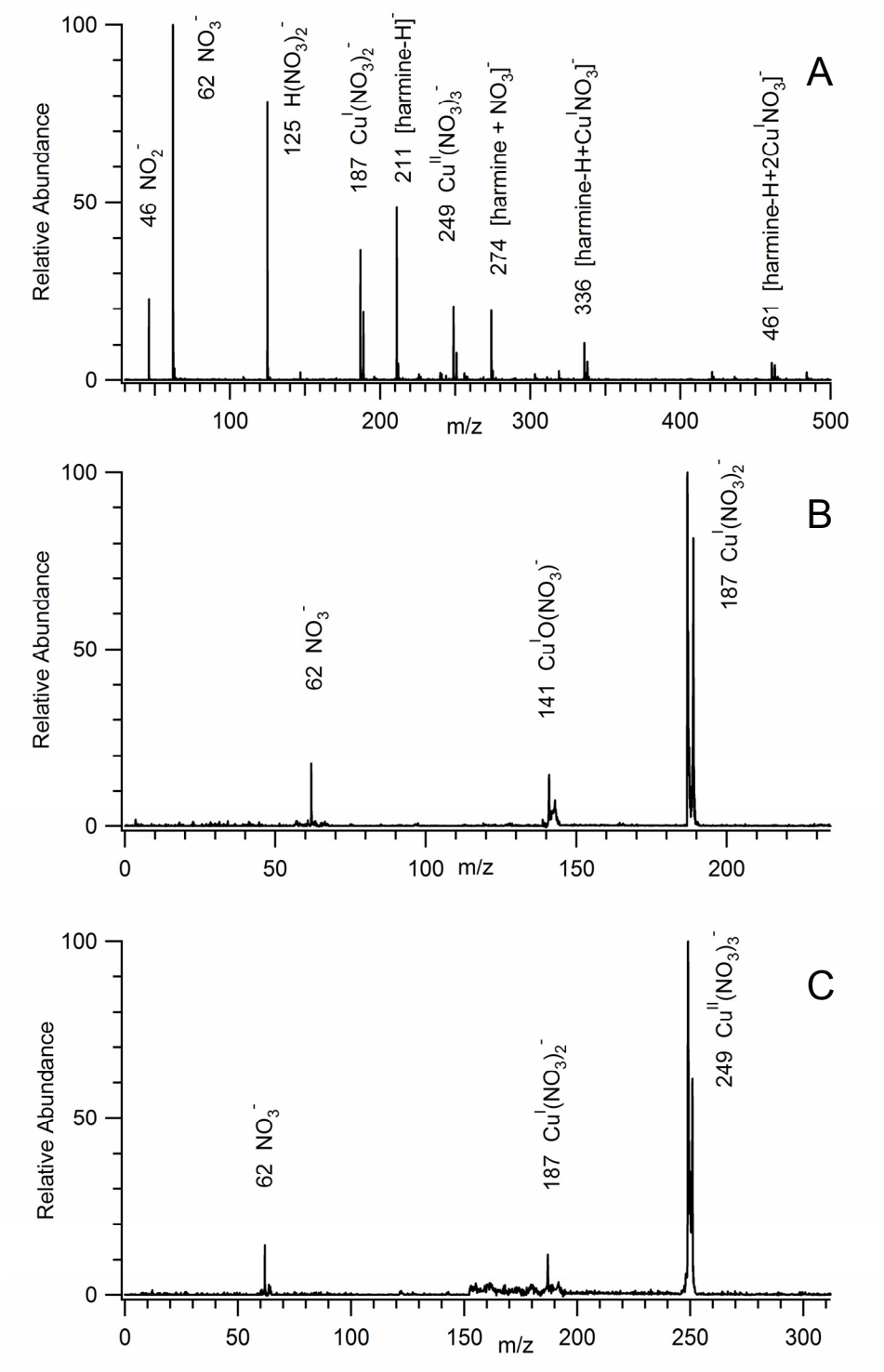

Figure 4.3. (a) MALDI mass spectrum of $Cu(NO_3)_2$ with harmine as matrix. (b) PSD mass spectrum of $Cu(NO_3)_2^-$. (c) PSD mass spectrum of $Cu(NO_3)_3^-$.

atoms are oxidized to higher oxidation states during these reactions, i.e., metal atoms will probably remain in their initial oxidation state upon formation of the oxo-nitrate complex. The third pathway is the reduction of metal atom with oxidation of nitrate to neutral NO_3 in the gas phase via internal redox process during PSD as shown in Equation 6.

$$Cu^{II}(NO_3)_3^- \rightarrow Cu^{II}(NO_3)_2 + NO_3^- \quad (3)$$

$$Cu^{I}(NO_3)_2^- \rightarrow Cu^{I}(NO_3) + NO_3^- \quad (4)$$

$$Cu^{I}(NO_3)_2^- \rightarrow Cu^{I}O(NO_3)^- + NO_2 \quad (5)$$

$$Cu^{II}(NO_3)_3^- \rightarrow Cu^{I}(NO_3)_2^- + NO_3 \quad (6)$$

Figure 4.4a is the negative ion mode MALDI mass spectrum of $Cd(NO_3)_2$. Cluster ions of the type $Cd(NO_3)_3^-$ are observed as expected. Surprisingly, peaks corresponding to $[Cd(NO_3)_2$ + harmane - $H]^-$ are also observed. The PSD of $Cd(NO_3)_3^-$ is shown in Figure 4.4b. In general, the intensity distributions of the Cd isotope peaks in the cluster ions correspond to the expected patterns (^{106}Cd, 1.25%; ^{108}Cd, 0.89%; ^{110}Cd, 12.49%; ^{111}Cd, 12.80%; ^{112}Cd, 24.13%; ^{113}Cd, 12.22%; ^{114}Cd, 28.73%; ^{115}Cd, 7.49%) as shown by the measured and calculated spectra for $Cd(NO_3)_3^-$ in Figures 4.5a and 4.5b, respectively. The measured and calculated spectra for $[Cd(NO_3)_2$ + harmane - $H]^-$ are shown in Figures 6a and 6b, respectively. These provide an additional confirmation of the identity of the recorded cluster ions appearing in Figure 4.4a.

4.3.3 MS and PSD of Perchlorates Complexes of Group I and II Metals

The MALDI-TOF mass spectra of sodium perchlorate and potassium perchlorate recorded with harmane as matrix yielded a series of cluster ions in the negative-ion mode. Figures 4.7a and 4.7b show the respective MALDI mass spectra of sodium perchlorate and potassium perchlorate. As the natural isotopic abundance of ^{35}Cl and ^{37}Cl is 75.77 and 24.23%,

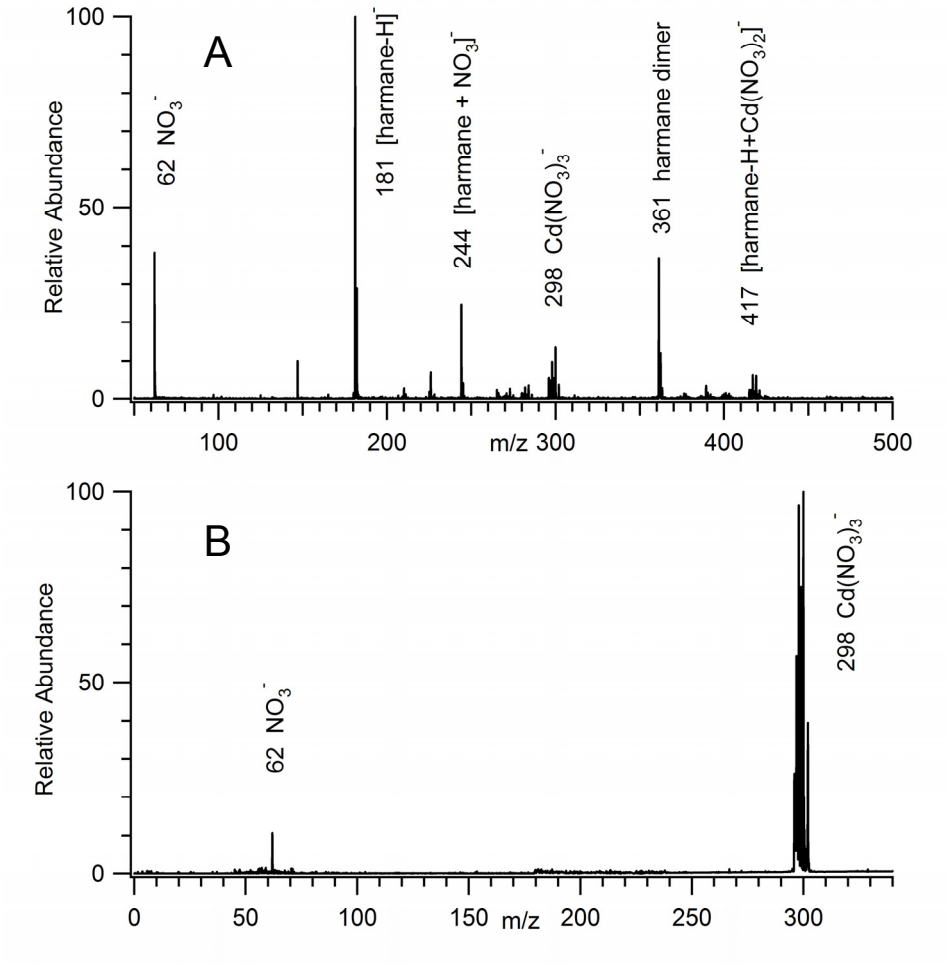

Figure 4.4. (a) MALDI mass spectrum of $Cd(NO_3)_2$ with harmane as matrix. (b) PSD mass spectrum of $Cd(NO_3)_3^-$.

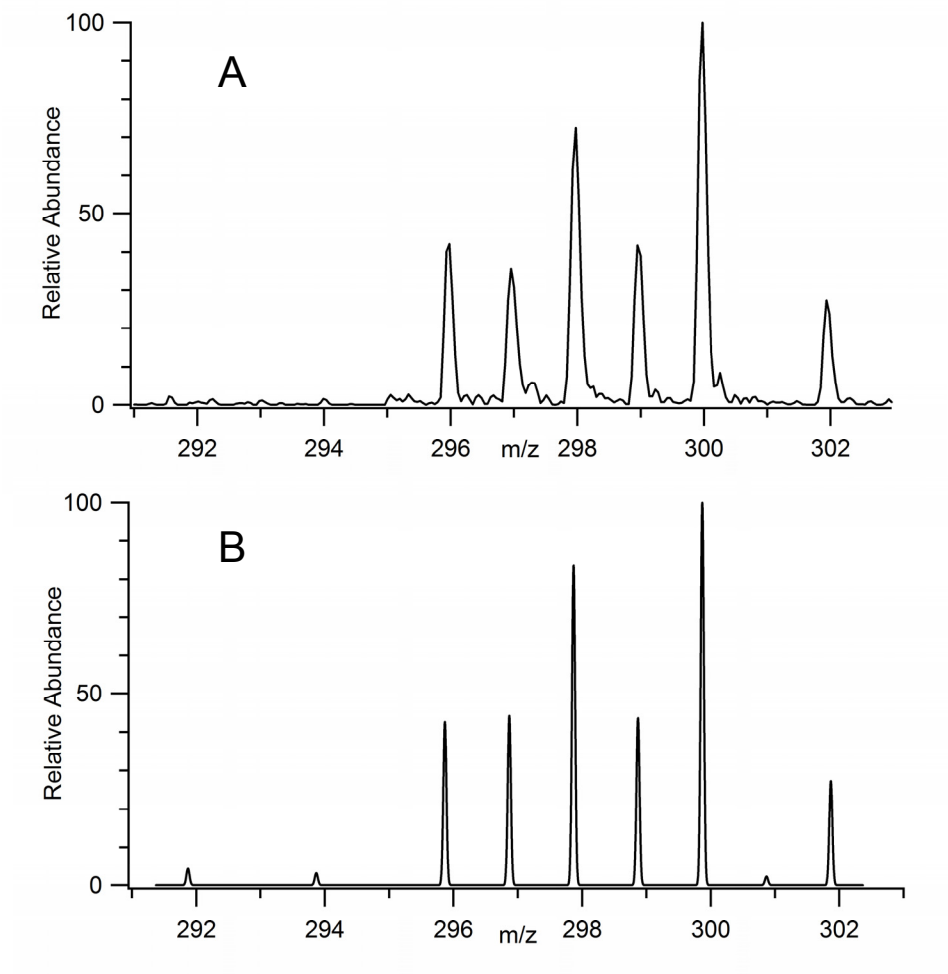

Figure 4.5. Measured (a) and calculated (b) mass spectra for $Cd(NO_3)_3^-$.

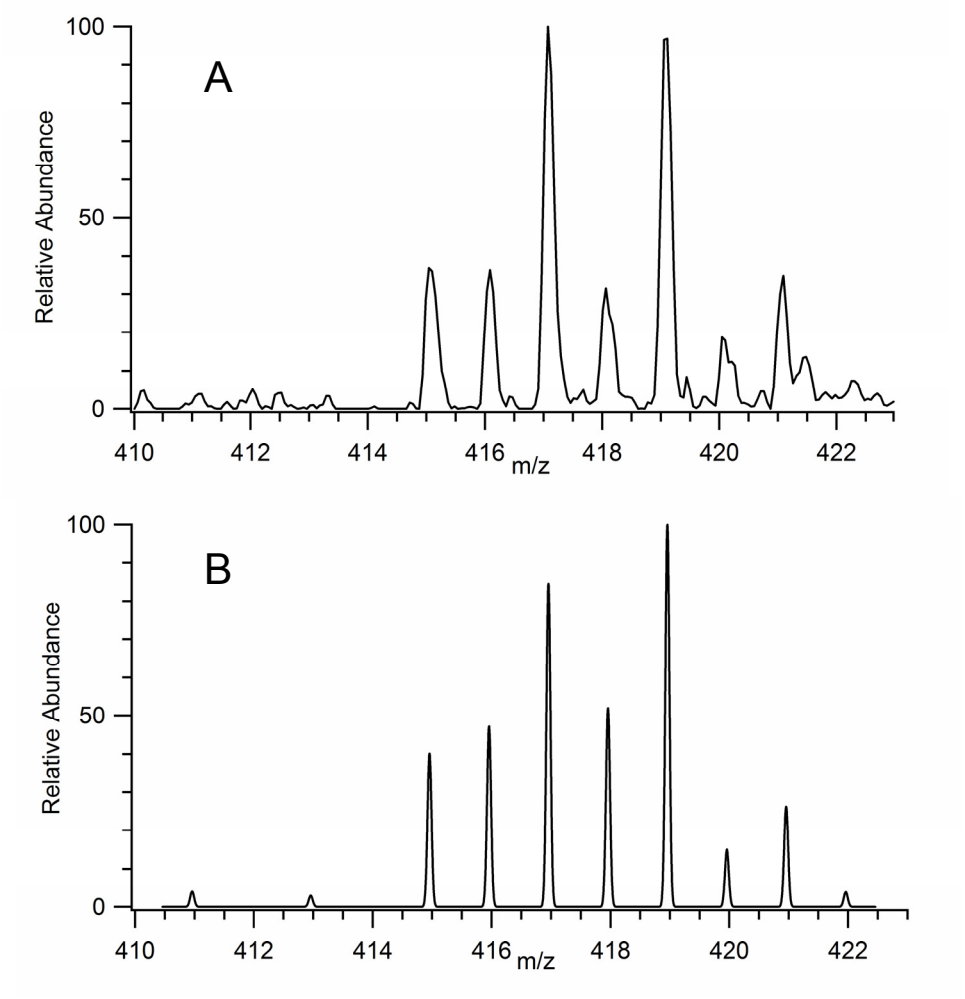

Figure 4.6. Measured (a) and calculated (b) mass spectra for $[Cd(NO_3)_2 + \text{harmane} - H]^-$.

respectively, the relative sizes of the two peaks generated by the presence of two chlorine atoms are approximately at a ratio of 9:6:1. This ratio is evidenced by the ions at m/z 221, 223 and 225 for sodium perchlorate and m/z 237, 239 and 241 for potassium perchlorate (if the contribution of potassium isotopes, i.e., ^{39}K, 93.26%; ^{41}K, 6.73% and ^{40}K, 0.01%, was neglected). In the negative-ion mass spectra of both compounds, the relative peak intensities of m/z 99 and 101 (ClO_4^-) are somewhat smaller than 3:1 while the relative peak intensities of m/z 83 and 85 (ClO_3^-) are much closer to 3:1. For sodium perchlorate, the mass spectrum in the negative-ion mode was characterized by cluster ions of the general formula $Na_n(ClO_4)_{n+1}^-$ (n = 1, 2, 3) that are detected as the predominant cluster ions (Figure 4.7a). As anticipated, the MALDI mass spectrum of potassium perchlorate (Figure 4.7b) recorded in the negative-ion mode is very similar to that of sodium perchlorate, however, only one cluster ion $K(ClO_4)_2^-$ is observed.

These ion compositions were further supported by PSD analysis of selected precursor ions. A typical PSD mass spectrum is shown for $Na(ClO_4)_2^-$ (m/z 221) in Figure 4.8a. Perchlorate is the only product ion observed from PSD of $Na(ClO_4)_2^-$. The mass difference between perchlorate product ion and $Na(ClO_4)_2^-$ precursor ion is 122 Da, indicating that the complementary product is a neutral $NaClO_4$ molecule. A PSD spectrum of the cluster $Na_2(ClO_4)_3^-$ (m/z 343) is shown in Figure 4.8b. The only ionic product is $Na(ClO_4)_2^-$ (m/z 221) (indicating neutral loss of $NaClO_4$ molecules); perchlorate is not formed. Interestingly, in the PSD spectrum (Figure 4.8c) of the cluster $Na_3(ClO_4)_4^-$ (m/z 465), the next lower species $Na_2(ClO_4)_3^-$ (m/z 343) is not observed this time, instead $Na(ClO_4)_2^-$ (m/z 221) is the only ionic product as shown in equation 7. Perchlorate is also not formed. The neutral loss of two $NaClO_4$ molecules is implied.

$$Na_3(ClO_4)_4^- \rightarrow Na(ClO_4)_2^- + 2NaClO_4 \qquad (7)$$

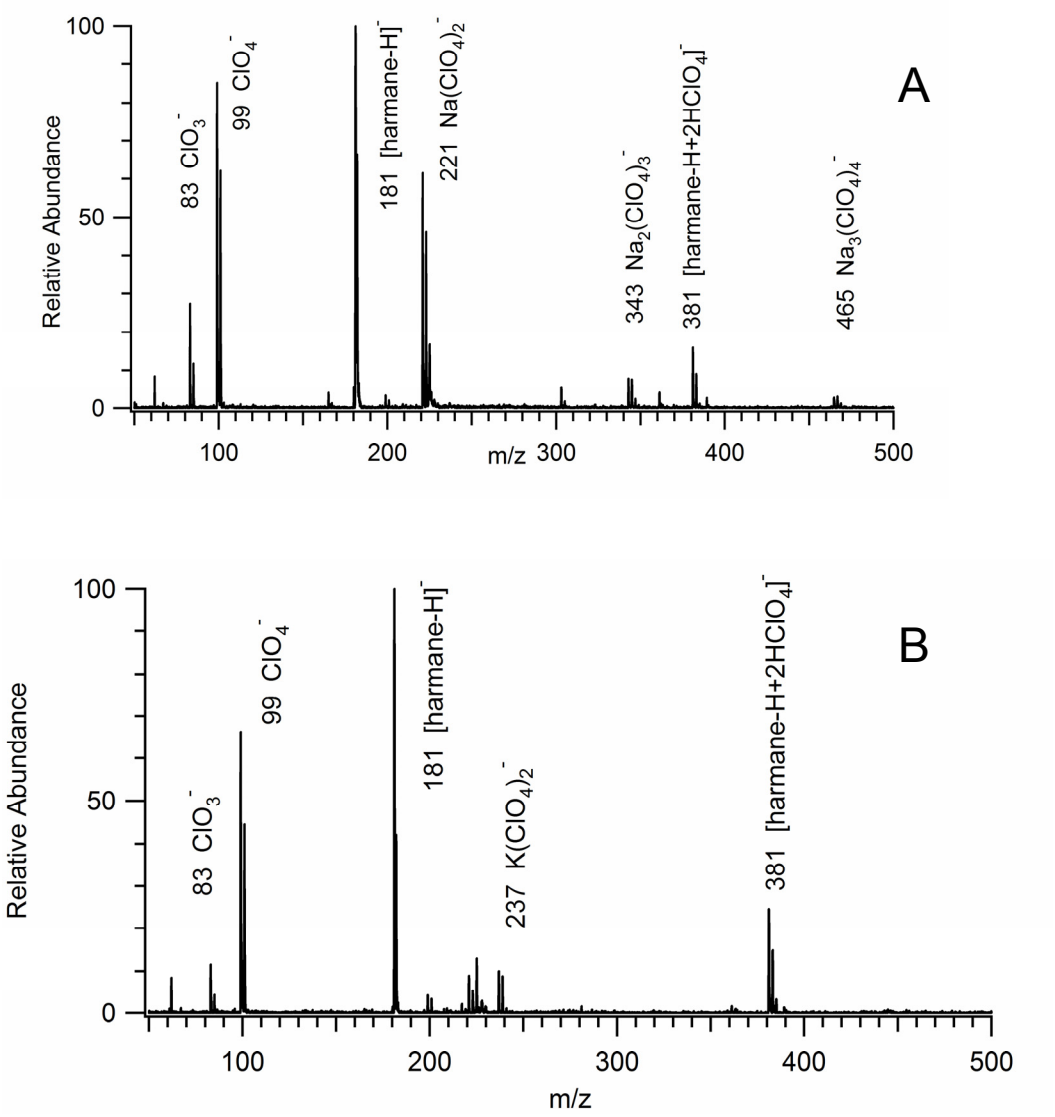

Figure 4.7. MALDI mass spectra of sodium perchlorate (a) and potassium perchlorate (b).

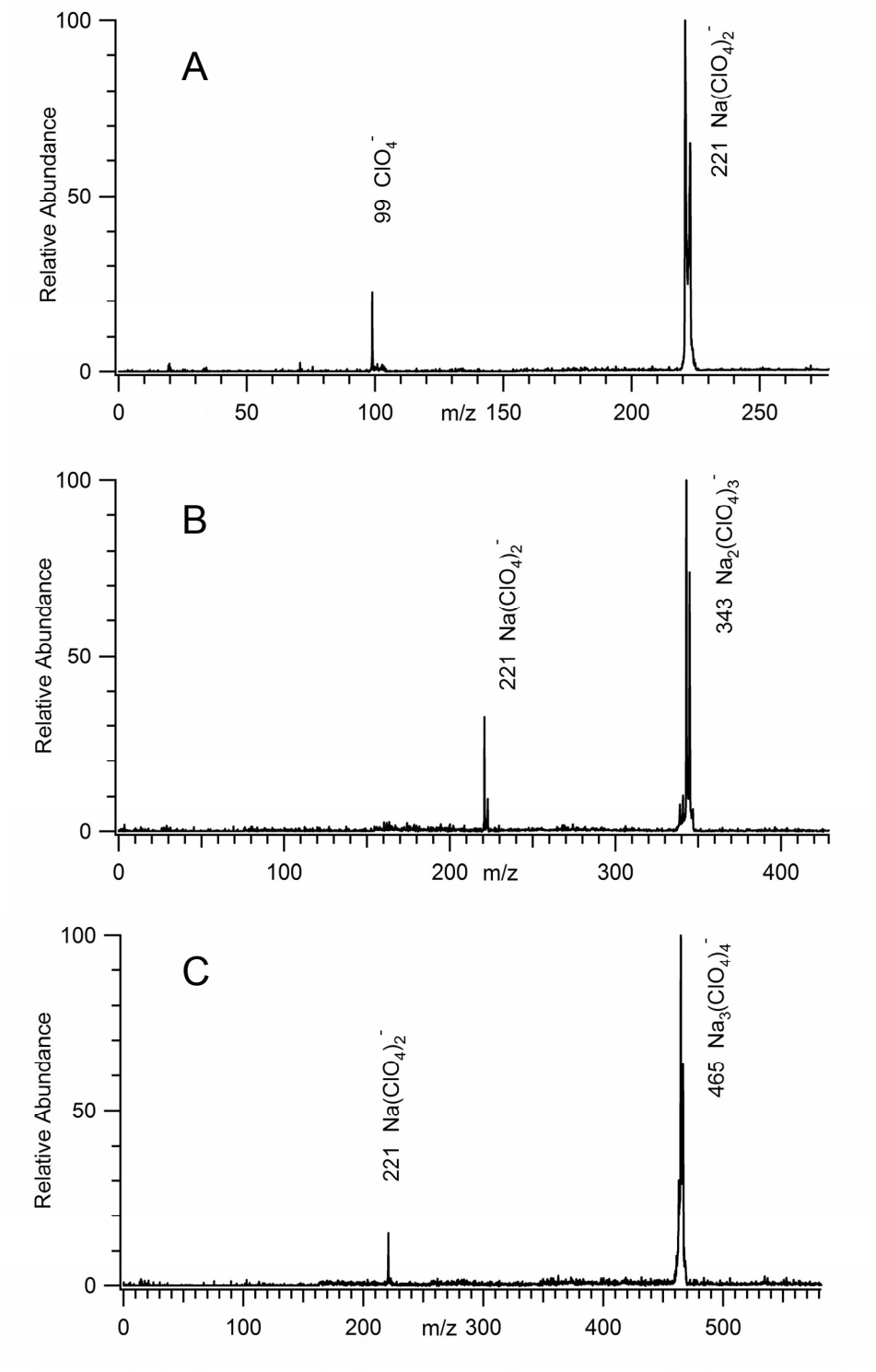

Figure 4.8. (a) PSD mass spectrum of $Na(ClO_4)_2^-$. (b) PSD mass spectrum of $Na_2(ClO_4)_3^-$. (c) PSD mass spectrum of $Na_3(ClO_4)_4$.

Figures 4.9a shows the MALDI-TOF mass spectrum of calcium perchlorate recorded with harmane as matrix in the negative-ion mode. $Ca_n(ClO_4)_{2n+1}^-$ (n = 1, 2) are detected as the predominant cluster ions. The characteristic isotopic pattern of chlorine could be seen by the ions at m/z 337, 339, 341 and 343, as well as by the ions at m/z 575, 577, 579 and 581 for calcium perchlorate, in the negative-ion mass spectrum (neglecting calcium isotopes). The relative peak intensities of m/z 99 and 101 (ClO_4^-) in the negative-ion mass spectrum are also close to 3:1.

A typical PSD mass spectrum is shown for $Ca(ClO_4)_3^-$ (m/z 337) in Figure 4.9b; perchlorate is the only product ion observed. A mass spectrum from PSD of the cluster $Ca_2(ClO_4)_5^-$ (m/z 575) is shown in Figure 4.9c. The only ionic product is $Ca(ClO_4)_3^-$ (m/z 337).

4.4 Conclusion

MALDI-MS, as a soft ionization technique, enables positive identification of the investigated inorganic oxidizers, and representative cluster ions are obtained in the negative-ion mode. The identities and fragmentation properties of the respective cluster ions are further characterized by PSD analysis. PSD analysis of selected precursor ions provides additional information on the ionic compositions. For qualitative purposes, MALDI-MS is well suited for the characterization of the inorganic oxidizers and can be used as a complementary method to ion chromatography.

Complexation with nitrate and perchlorate can stabilize metal ions allowing their detection in negative MALDI MS. Copper (II) nitrate ions can undergo internal redox processes during PSD, with conversion of Cu^{II} to Cu^{I}. Oxo ions are prominent from PSD of most transition metal nitrate complexes, as expected for “hard” metal cations. Cluster ions with more than one

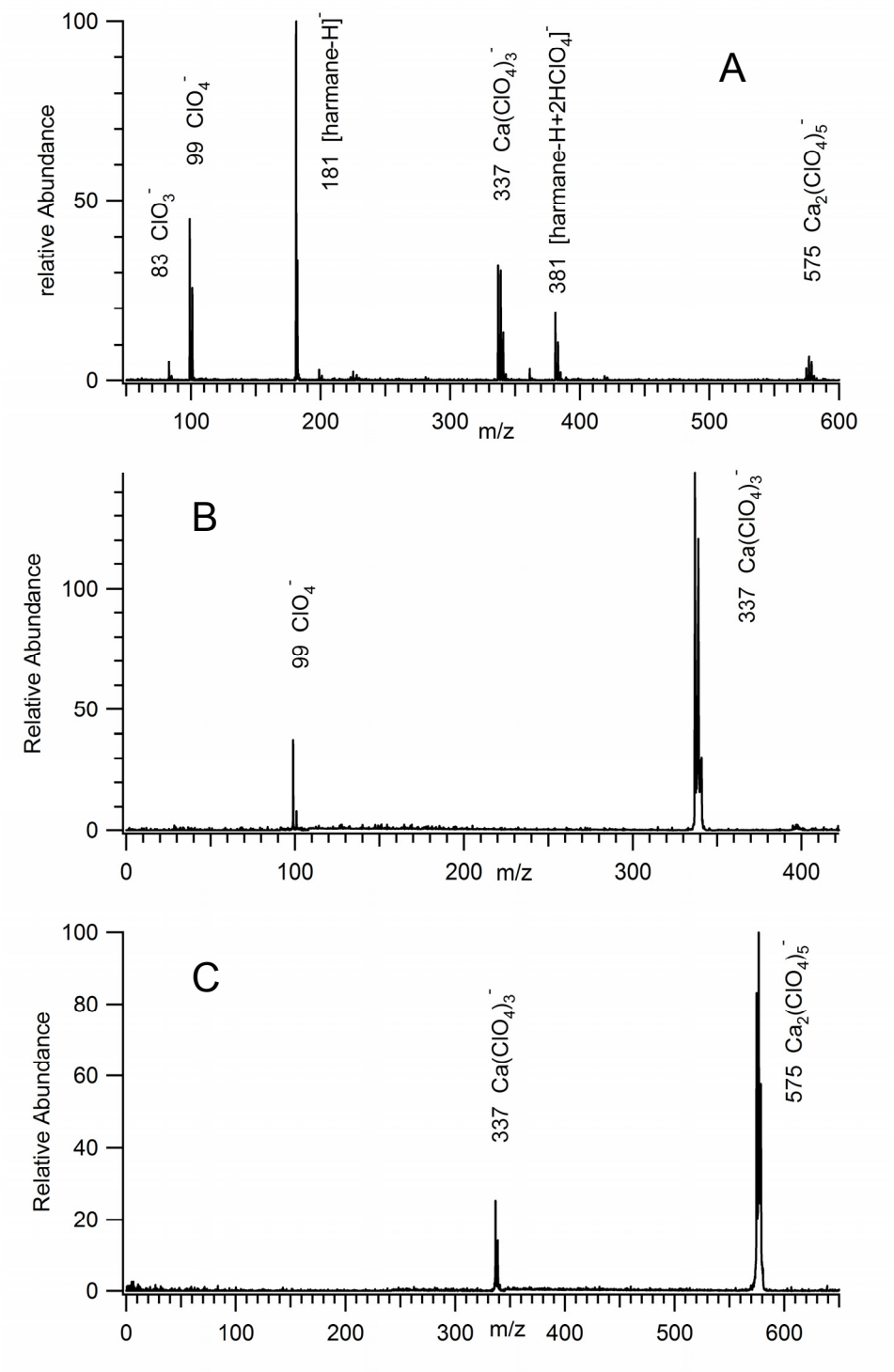

Figure 4.9. (a) MALDI mass spectrum of $Ca(ClO_4)_2$ with harmane as matrix. (b) PSD mass spectrum of $Ca(ClO_4)_3$. (c) PSD mass spectrum of $Ca_2(ClO_4)_5$.

metal atom are most evident for small metals with low charges. Cluster ions consisting of neutral inorganic salt and depronated matrix ions are also observed.

4.5 References

1. Yinon, J.; Zitrin, S., *Modern Methods and Applications in Analysis of Explosives*. John Wiley & Sons Ltd.: Chichester, 2001.
2. Mendiratta, S. K.; Dotson, R. L.; Brooker, R. T., Perchloric acid and perchlorates. In *Kirk-Othmer Encyclopedia of Chemical Technology*, John Wiley & Sons, Inc.: New York, NY, 2005; pp 157–170.
3. Yinon, J., *Advances in Analysis and Detection of Explosives. Proceedings of the International Symposium on Analysis and Detection of Explosives (4th), Held in Jerusalem, Israel on September 7-10, 1992*. Springer: New York, 1993.
4. Carre, V.; Aubriet, F.; Muller, J. F., Analysis of cigarette smoke by laser desorption mass spectrometry. *Analytica Chimica Acta* **2005,** 540, (2), 257-268.
5. Smith, C. J.; Livingston, S. D.; Doolittle, D. J., An international literature survey of "IARC Group I carcinogens" reported in mainstream cigarette smoke. *Food and Chemical Toxicology* **1997,** 35, (10-11), 1107-1130.
6. Finlayson-Pitts, B. J.; Pitts, J. N., *Chemistry of the Upper and Lower Atmosphere. Theory, Experiment, and Applications.* Academic: San Diego, 2000.
7. Viggiano, A. A.; Schlager, H.; Arnold, F., Stratospheric Negative-Ions Detailed Height Profiles. *Planetary and Space Science* **1983,** 31, (8), 813-820.
8. Kirk, A. B.; Smith, E. E.; Tian, K.; Anderson, T. A.; Dasgupta, P. K., Perchlorate in milk. *Environmental Science & Technology* **2003,** 37, (21), 4979-4981.
9. Hogue, C., Rocket-fueled river. *Chemical & Engineering News* **2003,** 81, (33), 37-46.
10. Krynitsky, A. J.; Niemann, R. A.; Nortrup, D. A., Determination of perchlorate anion in foods by ion chromatography-tandem mass spectrometry. *Analytical Chemistry* **2004,** 76, (18), 5518-5522.
11. Dasgupta, P. K.; Martinelango, P. K.; Jackson, W. A.; Anderson, T. A.; Tian, K.; Tock, R. W.; Rajagopalan, S., The origin of naturally occurring perchlorate: The role of atmospheric processes. *Environmental Science & Technology* **2005,** 39, (6), 1569-1575.
12. Kirk, A. B.; Martinelango, P. K.; Tian, K.; Dutta, A.; Smith, E. E.; Dasgupta, P. K., Perchlorate and iodide in dairy and breast milk. *Environmental Science & Technology* **2005,** 39, (7), 2011-2017.
13. Valentin-Blasini, L.; Mauldin, J. P.; Maple, D.; Blount, B. C., Analysis of perchlorate in human urine using ion chromatography and electrospray tandem mass spectrometry. *Analytical Chemistry* **2005,** 77, (8), 2475-2481.
14. Reutter, D. J.; Buechele, R. C.; Rudolph, T. L., Ion Chromatography in Bombing Investigations. *Analytical Chemistry* **1983,** 55, (14), 1468A-1472A.
15. McCord, B. R.; Hargadon, K. A.; Hall, K. E.; Burmeister, S. G., Forensic Analysis of Explosives Using Ion-Chromatographic Methods. *Analytica Chimica Acta* **1994,** 288, (1-2), 43-56.

16. Martinelango, P. K.; Anderson, J. L.; Dasgupta, P. K.; Armstrong, D. W.; Al-Horr, R. S.; Slingsby, R. W., Gas-phase ion association provides increased selectivity and sensitivity for measuring perchlorate by mass spectrometry. *Analytical Chemistry* **2005,** 77, (15), 4829-4835.
17. Kishi, T.; Nakamura, J.; Arai, H., Application of capillary electrophoresis for the determination of inorganic ions in trace explosives and explosive residues. *Electrophoresis* **1998,** 19, (1), 3-5.
18. Colton, R.; Dagostino, A.; Traeger, J. C., Electrospray mass spectrometry applied inorganic and organometallic chemistry. *Mass Spectrometry Reviews* **1995,** 14, (2), 79-106.
19. Cheng, Z. L.; Siu, K. W. M.; Guevremont, R.; Berman, S. S., Solvent-Derived Metal-Oxides in Electrospray Mass-Spectrometry of Metal Salt-Solutions. *Organic Mass Spectrometry* **1992,** 27, (12), 1370-1376.
20. Agnes, G. R.; Horlick, G., Electrospray Mass-Spectrometry as a Technique for Elemental Analysis - Preliminary-Results. *Applied Spectroscopy* **1992,** 46, (3), 401-406.
21. Stewart, II, Electrospray mass spectrometry: a tool for elemental speciation. *Spectrochimica Acta Part B-Atomic Spectroscopy* **1999,** 54, (12), 1649-1695.
22. Li, F. M.; Byers, M. A.; Houk, R. S., Tandem mass spectrometry of metal nitrate negative ions produced by electrospray ionization. *Journal of the American Society for Mass Spectrometry* **2003,** 14, (6), 671-679.
23. Mollah, S.; Pris, A. D.; Johnson, S. K.; Gwizdala, A. B.; Houk, R. S., Identification of metal cations, metal complexes, and anions by electrospray mass spectrometry in the negative ion mode. *Analytical Chemistry* **2000,** 72, (5), 985-991.
24. Zhao, X. M.; Yinon, J., Forensic identification of explosive oxidizers by electrospray ionization mass spectrometry. *Rapid Communications in Mass Spectrometry* **2002,** 16, (12), 1137-1146.
25. Hunsucker, S. W.; Watson, R. C.; Tissue, B. M., Characterization of inorganic coordination complexes by matrix-assisted laser desorption/ionization mass spectrometry. *Rapid Communications in Mass Spectrometry* **2001,** 15, (15), 1334-1340.
26. Siemsen, P.; Gubler, U.; Bosshard, C.; Gunter, P.; Diederich, F., Pt-tetraethynylethene molecular scaffolding: Synthesis and characterization of a novel class of organometallic molecular rods. *Chemistry-a European Journal* **2001,** 7, (6), 1333-1341.
27. Valerio, C.; Moulines, F.; Ruiz, J.; Blais, J. C.; Astruc, D., Regioselective chlorocarbonylation of polybenzyl cores and functionalization using dendritic and organometallic nucleophiles. *Journal of Organic Chemistry* **2000,** 65, (7), 1996-2002.
28. Ruiz, J.; Alonso, E.; Blais, J. C.; Astruc, D., Hydrosilylation of an hexa-olefin star with organometallic hydrogenosilanes: ferrocenylsilylation and desilylenation. *Journal of Organometallic Chemistry* **1999,** 582, (1), 139-141.
29. McGaff, R. W.; Hayashi, R. K.; Powell, D. R.; Treichel, P. M., Synthesis and X-ray crystal structures of new trirhenium nonachloride chalcogenide clusters. *Polyhedron* **1998,** 17, (25-26), 4425-4431.
30. Kasuya, A.; Sivamohan, R.; Barnakov, Y. A.; Dmitruk, I. M.; Nirasawa, T.; Romanyuk, V. R.; Kumar, V.; Mamykin, S. V.; Tohji, K.; Jeyadevan, B.; Shinoda, K.; Kudo, T.; Terasaki, O.; Liu, Z.; Belosludov, R. V.; Sundararajan, V.; Kawazoe, Y., Ultra-stable nanoparticles of CdSe revealed from mass spectrometry. *Nature Materials* **2004,** 3, (2), 99-102.

31. Khitrov, G. A.; Strouse, G. F., ZnS nanomaterial characterization by MALDI-TOF mass spectrometry. *Journal of the American Chemical Society* **2003,** 125, (34), 10465-10469.
32. Dopke, N. C.; Treichel, P. M.; Vestling, M. M., Matrix-assisted laser desorption/ionization time-of-flight mass spectrometry (MALDI-TOF MS) of rhenium(III) halides: A characterization tool for metal atom clusters. *Inorganic Chemistry* **1998,** 37, (6), 1272-1277.
33. Schaaff, T. G.; Shafigullin, M. N.; Khoury, J. T.; Vezmar, I.; Whetten, R. L., Properties of a ubiquitous 29 kDa Au : SR cluster compound. *Journal of Physical Chemistry B* **2001,** 105, (37), 8785-8796.
34. Whetten, R. L.; Khoury, J. T.; Alvarez, M. M.; Murthy, S.; Vezmar, I.; Wang, Z. L.; Stephens, P. W.; Cleveland, C. L.; Luedtke, W. D.; Landman, U., Nanocrystal gold molecules. *Advanced Materials* **1996,** 8, (5), 428-&.
35. Arnold, R. J.; Reilly, J. P., High-resolution time-of-flight mass spectra of alkanethiolate-coated gold nanocrystals. *Journal of the American Chemical Society* **1998,** 120, (7), 1528-1532.
36. Vezmar, I.; Alvarez, M. M.; Khoury, J. T.; Salisbury, B. E.; Shafigullin, M. N.; Whetten, R. L., Cluster beams from passivated nanocrystals. *Zeitschrift Fur Physik D-Atoms Molecules and Clusters* **1997,** 40, (1-4), 147-151.
37. Lafargue, P. E.; Gaumet, J. J.; Muller, J. F.; Labrosse, A., Laser ablation of silica: Study of induced clusters by Fourier transform ion cyclotron resonance mass spectrometry. *Journal of Mass Spectrometry* **1996,** 31, (6), 623-632.
38. Hummelen, J. C.; Knight, B.; Pavlovich, J.; Gonzalez, R.; Wudl, F., Isolation of the Heterofullerene C59n as Its Dimer (C59n)(2). *Science* **1995,** 269, (5230), 1554-1556.
39. Kubler, B.; Millon, E.; Gaumet, J. J.; Muller, J. F., Formation of high mass C-n clusters (n>100) by laser ablation/desorption coupled with mass spectrometry. *Fullerene Science and Technology* **1996,** 4, (6), 1247-1261.
40. Guan, B.; Lu, W. G.; Fang, J. Y.; Cole, R. B., Characterization of synthesized titanium oxide nanoclusters by MALDI-TOF mass spectrometry. *Journal of the American Society for Mass Spectrometry* **2007,** 18, (3), 517-524.
41. d'Avray, A. T. D.; Carpenter, E. E.; O'Connor, C. J.; Cole, R. B., Characterization of ferrite nanoparticles by laser desorption/ionization mass spectrometry. *European Mass Spectrometry* **1998,** 4, (6), 441-449.
42. Kinumi, T.; Saisu, T.; Takayama, M.; Niwa, H., Matrix-assisted laser desorption/ionization time-of-flight mass spectrometry using an inorganic particle matrix for small molecule analysis. *Journal of Mass Spectrometry* **2000,** 35, (3), 417-422.
43. Zhang, Q. C.; Zou, H. F.; Guo, Z.; Zhang, Q.; Chen, X. M.; Ni, J. Y., Matrix-assisted laser desorption/ionization mass spectrometry using porous silicon and silica gel as matrix. *Rapid Communications in Mass Spectrometry* **2001,** 15, (3), 217-223.
44. Tanaka, K.; H., W.; Y., I.; S., A.; Y., Y.; T., Y., Protein and polymer analyses up to m/z 100 000 by laser ionization time-of-flight mass spectrometry. *Rapid Communications in Mass Spectrometry* **1988,** 2, (8), 151-153.
45. Zhao, X. M.; Yinon, J., Characterization of ammonium nitrate by electrospray ionization tandem mass spectrometry. *Rapid Communications in Mass Spectrometry* **2001,** 15, (17), 1514-1519.

46. Sigman, M. E.; Armstrong, P., Analysis of oxidizer salt mixtures by electrospray ionization mass spectrometry. *Rapid Communications in Mass Spectrometry* **2006,** 20, (3), 427-432.
47. Spengler, B.; Kirsch, D.; Kaufmann, R., Metastable Decay of Peptides and Proteins in Matrix-Assisted Laser-Desorption Mass-Spectrometry. *Rapid Communications in Mass Spectrometry* **1991,** 5, (4), 198-202.
48. Spengler, B.; Kirsch, D.; Kaufmann, R.; Jaeger, E., Peptide Sequencing by Matrix-Assisted Laser-Desorption Mass-Spectrometry. *Rapid Communications in Mass Spectrometry* **1992,** 6, (2), 105-108.
49. Mark, T. D.; Castleman, A. W., Experimental Studies on Cluster Ions. *Advances in Atomic and Molecular Physics* **1985,** 20, 65-172.
50. Castleman, A. W.; Keesee, R. G., Clusters - Bridging the Gas and Condensed Phases. *Accounts of Chemical Research* **1986,** 19, (12), 413-419.
51. Karas, M.; Hillenkamp, F., Laser Desorption Ionization of Proteins with Molecular Masses Exceeding 10000 Daltons. *Analytical Chemistry* **1988,** 60, (20), 2299-2301.
52. Aubriet, F.; Maunit, B.; Muller, J. F., Studies on alkali and alkaline earth chromate by time-of-flight laser microprobe mass spectrometry and Fourier transform ion cyclotron resonance mass spectrometry. Part I: differentiation of chromate compounds. *International Journal of Mass Spectrometry* **2000,** 198, (3), 189-211.
53. Aubriet, F.; Maunit, B.; Muller, J. F., Studies on alkali and alkaline earth chromate by time-of-flight laser microprobe mass spectrometry and Fourier transform ion cyclotron resonance mass spectrometry Part II: understanding cluster ion formation. *International Journal of Mass Spectrometry* **2000,** 198, (3), 213-234.
54. Bradley, R. A.; Lanzendorf, E.; McCarthy, M. I.; Orlando, T. M.; Hess, W. P., Molecular No Desorption from Crystalline-Sodium Nitrate by Resonant Excitation of the No3- Pi-Pi-Asterisk Transition. *Journal of Physical Chemistry* **1995,** 99, (30), 11715-11721.
55. Knutsen, K.; Orlando, T. M., Photon-stimulated desorption of O(P-3) and NO((2)Pi) from NaNO3 single crystals. *Physical Review B* **1997,** 55, (19), 13246-13252.
56. Dashtiev, M.; Frankevich, V.; Zenobi, R., Signal enhancement in matrix-assisted laser desorption/ionization by doping with Cu(II) chloride. *Rapid Communications in Mass Spectrometry* **2005,** 19, (2), 289-291.
57. Zhang, J.; Frankevich, V.; Knochenmuss, R.; Friess, S. D.; Zenobi, R., Reduction of Cu(II) in matrix-assisted laser desorption/ionization mass spectrometry. *Journal of the American Society for Mass Spectrometry* **2003,** 14, (1), 42-50.

SUMMARY

Various anions can form anionic adducts with oligosaccharides in negative ion MALDI-MS. Employing negative ion MALDI with addition of these anions, weakly acidic and neutral oligosaccharides can form $[M + anion]^-$ in varying degrees of preference to $[M - H]^-$ formation. The anion attachment approach provides a simple means to simultaneously analyze neutral and acidic carbohydrates without switching the polarity.

Contrary to common opinion that relative peak intensities are not generally reliable in linear-field reflectron post-source decay (PSD), we demonstrate that even without a curved-field reflectron, the relative peak intensities of the oligosaccharide fragment peaks intentionally acquired within the same PSD segment are rather stable, even if the laser intensities vary greatly and the target crystals may vary substantially in shape and quality. Our proposed characteristic neutral losses in MALDI-PSD mass spectra of the chloride adducts of neutral oligosaccharides, and the relative ion abundances of selected diagnostic fragment pairs, allow simultaneous determination of both linkage information and anomeric configurations of the oligosaccharides.

Competitive fragmentation pathways are revealed and rationalized in PSD of chloride adducts of oligosaccharides. For specific glycosidic linkage types, PSD spectra of oligosaccharides with the same anomeric configuration show the same trend of relative ion abundance for specific diagnostic fragment peaks, independent of monosaccharide structure. This finding strongly indicates that the fragmentation pathways observed in negative ion PSD spectra are largely affected by the anomeric configuration between the monosaccharide rings for the particular linkage positions. It becomes clear that differentiating anomeric configurations of glycosidic bonds is viable by comparing relative peak intensities of diagnostic peaks in negative

ion PSD via anion attachment. The fragmentation profiles and relative peak abundances in PSD spectra are expected to present important hints in determining the glycosidic linkage types and anomeric configuration of more complex glycoconjugates. The potential usage of MALDI linear-field reflectron TOF MS in stereoisomeric chemistry thus has been greatly expanded.

We have shown that a stable TiO_2 cluster suspension is produced by the thermal solvent process, and clusters with different sizes are obtained by size-selection. XRD patterns of clusters with sizes less than 1 nm are very different from the principal peaks of the larger particles stemming from the extreme surface area-to-volume ratio. We successfully used MALDI-TOF and LDI-TOF MS to characterize ultra small (< 1 nm) nanoparticles. Peak maxima observed in MALDI-TOF and LDI-TOF mass spectra were shown to correlate with nanoparticle size. The obtained size distributions of TiO_2 nanoparticles are in good agreement with TEM measurements made on the identical samples. PSD analysis of inorganic nanomaterials has also been performed. PSD data demonstrate that MALDI-TOF and LDI-TOF peaks originating from titanium oxide nanoparticles may appear as sodium adducts. The ability to obtain detailed information concerning sub-nanometer titania nanoparticles has important implications for the continuing development of nanoparticle-based bactericidal agents.

MALDI-MS, as a soft ionization technique, enables positive identification of the investigated inorganic oxidizers, and representative cluster ions are obtained in the negative-ion mode. The identities and fragmentation properties of the respective cluster ions are further characterized by PSD analysis. PSD analysis of selected precursor ions provides additional information on the ion compositions. For qualitative purposes, MALDI-MS is well suited for the characterization of the inorganic oxidizers and can be used as a complementary method to ion chromatography.

Complexation with nitrate and perchlorate can stabilize metal ions allowing their detection in negative MALDI MS. Copper (II) nitrate ions can undergo internal redox processes during PSD, with conversion of Cu^{II} to Cu^{I}. Oxo ions are prominent from PSD of most transition metal nitrate complexes, as expected for "hard" metal cations. Cluster ions with more than one metal atom are most evident for small metals with low charges. Cluster ions consisting of neutral inorganic salt and deprotonated matrix ions are observed.

VITA

Bing Guan was born in People's Republic of China. He graduated from Nanjing University in July 1994 and received his B. S. in Chemistry. Later he obtained his M.S. in Chemistry in July 1998 from Institute of Chemistry, Chinese Academy of Sciences and another M. S. in Computer Science in December, 2000 from Loyola University Chicago. He joined Dr. Richard B. Cole's biomedical mass spectrometry research group at University of New Orleans in May, 2002. During Hurricane Katrina, he was a visiting student at Columbia University Medical School. He changed research projects after coming back to New Orleans and finished his PhD in Analytical Chemistry in summer 2007.